UiT
THE ARCTIC UNIVERSITY OF NORWAY

Faculty of Science and Technology

Department of Geology

Ore petrography and fluid evolution in the Cu-(Zn) VMS deposits at Sulitjelma, Northern Norway

—

Andre Birkeland

GEO-3900 Master's thesis in Geology

May 2018

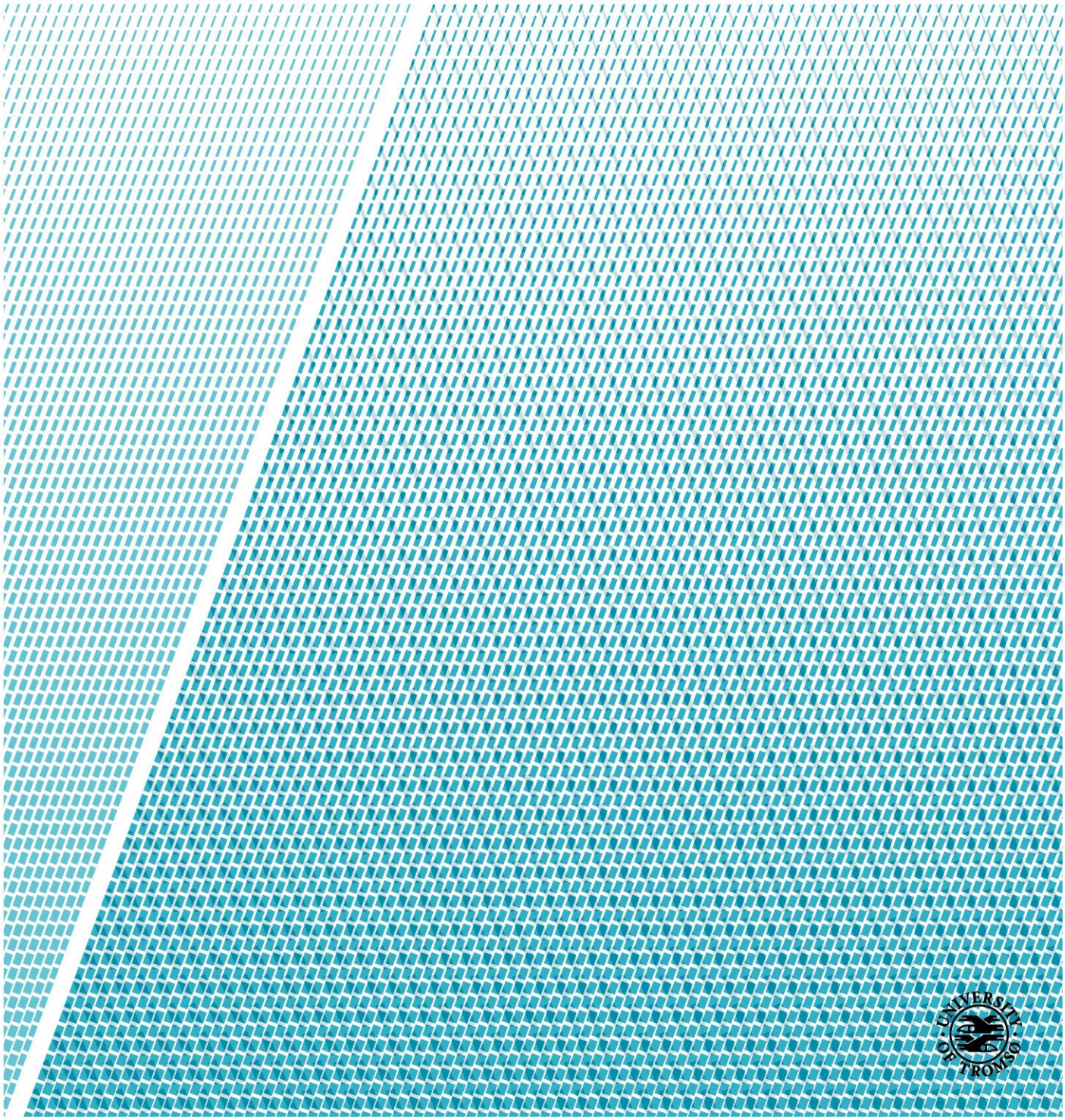

Acknowledgements

First and foremost I have to thank my supervisor Sabina Strmic Palinkas for all the help and support through this study. I would also like to thank Hanne Paulsen for all the help with field and laboratory work. I have to acknowledge all the people working in the lab, you are all great. I would also like to acknowledge the financial support from Mineralklynge and Rana Gruber. All my fellow students have been a great support in which I am grateful for. Last but not least I would like to thank my family.

Andre Birkeland

Tromsø, May 29th 2018

Abstract

The Sulitjelma deposits, Nordland, Northern Norway, with more than 20 Zn-Cu ore bodies (total tonnage excesses 35 Mt of ore at 1.84 % Cu, 0.86 % Zn, 10 g/t Ag and 0.25 g/t Au) have been described as a classic example of the Zn-Cu volcanogenic massive sulfide (VMS) mineralization.

The mineralization is spatially associated with metamorphosed mafic rocks of Ordovician age. Both, ore bodies and their host rocks, were exposed to deformation processes and recrystallization during the cycle of metamorphism and tectonic transport caused by the Scandian Orogeny. These processes affected ore textures as well as mineral chemistry of ore and gangue minerals.

The aim of this study is to estimate mineralogical, petrological and geochemical characteristics of ore mineralization and associated hydrothermal alteration products and to characterize P-T-X conditions during and after ore deposition.

The mineralization at the Sulitjelma deposits is characterized by predomination of pyrite over other sulfide minerals. The major ore-bearing phases are chalcopyrite and sphalerite. Galena occurs as a major mineral only in the Jakobsbakken ore body. Pyrrhotite predominates in the Sagmo ore body. Ag-sulfides, Fe-oxides and Ti-oxides are common accessory minerals. The major gangue mineral is quartz.

Fluid inclusion studies give an insight into P-T-X characteristics of ore-forming fluids but also revealed several generations of metamorphogenic fluids. Ore-forming conditions are estimated from primary boiling fluid inclusion assemblages indicating the formation temperature between 355 and 370ºC and formation pressure of 20-24 MPa, or 2000 – 2400 m depth assuming a bulk salinity of 7.5 wt.% NaCl and a hydrostatic regime. Secondary fluid inclusions found in Ny Sulitjelma samples reflect prograde metamorphic conditions, whereas secondary inclusions from Giken rather represented retrograde fluids. The metamorphic conditions at Giken, estimated by a combination of fluid inclusion data and the sphalerite-CuS geothermometer, suggest metamorphic P-T conditions between 570 and 610ºC and between 350 and 475 MPa, respectively.

Table of Contents

1 Introduction 1
1.1 Context of study 1
1.2 Goal of study 1
1.3 Location 1
1.4 Regional geology and geologic setting 2
1.5 VMS deposits 4
1.5.1 Tectonic settings 4
1.5.2 Fluid transportation and metal precipitation 4
1.5.3 Classification 6
2 Sample description 10
3 Methods 14
3.1 Fieldwork and sampling 14
3.2 Thin section preparation 14
3.3 Transmitted and reflected light microscopy 14
3.4 Scanning electron microscopy (SEM) 15
3.5 X-ray powder diffraction (XRD) 16
3.6 Lithogeochemistry 16
3.7 Fluid inclusion studies 16
4 Results 17
4.1 Petrography and SEM/EDS studies 17
4.1.1 Giken 17
4.1.2 Hankabakken 1 24
4.1.3 Jakobsbakken 33
4.1.4 Ny-Sulitjelma 40
4.1.5 Sagmo 45
4.1.6 Chemical analyses 49
4.2 EBSD analyses 51
4.2.1 SJ-02 51
4.3 X-ray powder diffraction (XRD) 54
4.3.1 SH1-03 54
4.3.2 SS-02 55
4.4 Lithogeochemistry 56
4.5 Fluid inclusion studies 61
4.5.1 Petrographic description 61

4.5.2 Microthermometric description 64
4.5.3 Fluid inclusions measurements 66
5 Discussion 67
6 Conclusion 74
References 75
Appendix I 77
Appendix II 79

1 Introduction

1.1 Context of study

The Sulitjelma area, Nordland, includes more than 20 Zn-Cu VMS deposits with a total tonnage in excess of 35 Mt. The average grades of the 25 Mt mined from 11 deposits between 1887 and 1991 are 1.84 % Cu and 0.86 % Zn. Contents of precious metals are 10 g/t Ag and 0.25 g/t Au (Cook, N. J., 1996; Cook, N. J. et al., 1990). Although
the Sulitjelma deposits are described as classic examples of the Zn-Cu volcanogenic massive sulfide (VMS) mineralization in Northern Norway (Vokes, 2012), they have not been a subject of detail geochemical studies. However, understanding of the ore-forming processes should increase the probability for discovery of new orebodies in the area as well as has an application in environmental risks assessment of potential mining activities.

1.2 Goal of study

The principal goals of the project are to: 1) estimate mineralogical, petrological and geochemical characteristics of host rocks, ore mineralization and alteration products and 2) to characterize P-T-X conditions during ore deposition.

1.3 Location

Sulitjelma is located in northern Norway approximately 90 kilometers eastern from Bodø, Fauske municipaly of the Nordland county (Fig. 1.1). The area hosts more than 20 Cu-(Zn) ore bodies and 6 of them were selected for this study: Giken, Hankabakken 1 and 2, Jakobsbakken, Ny-Sulitjelma and Sagmo (Table 1, Appendix 1). All the orebodies are listed with coordinates at the Norwegian Geological Survey's website after EU89-UTM Zone 33.

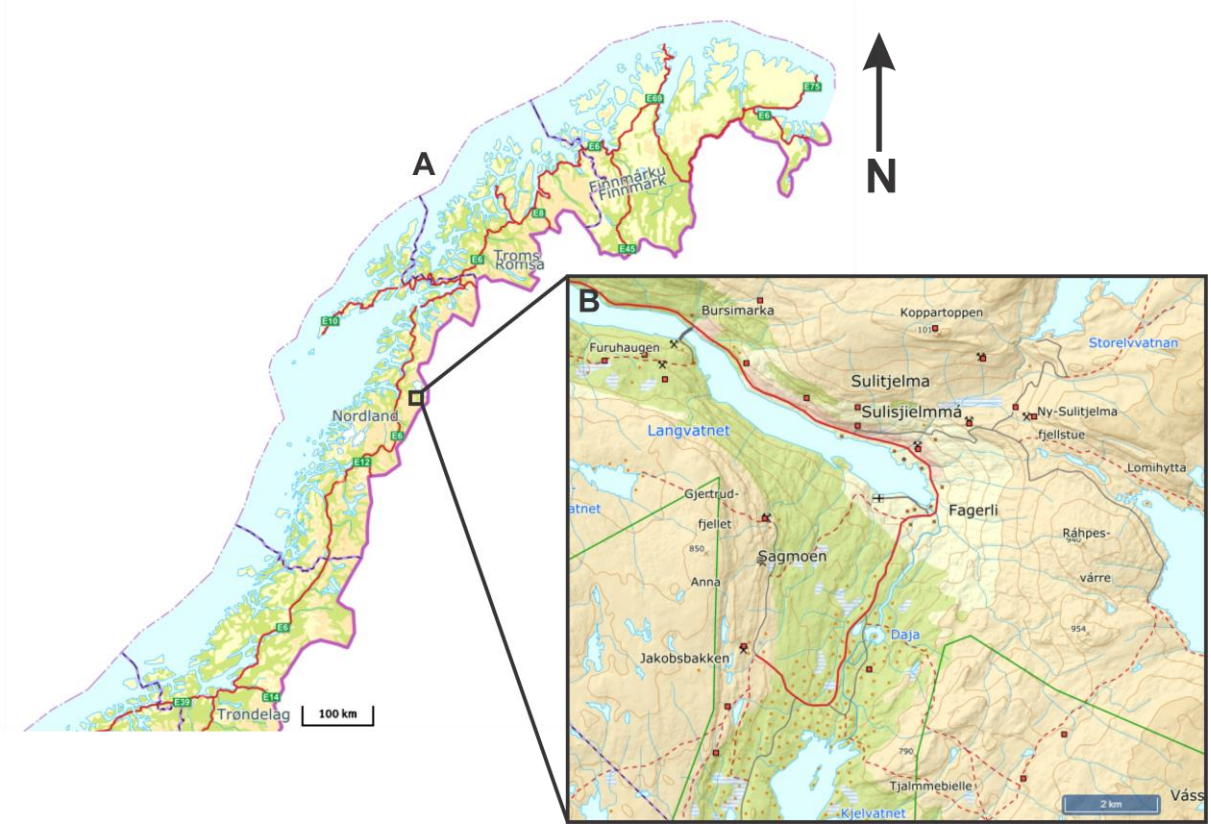

Figure 1.1: *A: Map section of Northern Norway. B: Map section of Sulitjelma study area (small red squares marks presence of metals). Modified from www.norgeskart.no (A) and www.ngu.no/emne/kartinnsyn (B).*

1.4 Regional geology and geologic setting

The Sulitjelma deposits are situated within the Scandinavian Caledonides, a mountain range that extends for about 1500 km from the Stavanger region in southern Norway to the Barents Sea region in northern Norway (Fig. 1.2). The Scandinavian Caledonides are characterized by a succession of four allochthons (the Lower Allochthon, the Middle Allochthon, the Upper Allochthon and the Uppermost Allochthon) formed in different geological environments (Gee and Sturt, 1985; Roberts and Gee, 1985) thrust upon each other both prior to and during the collision between Laurentia and Baltica in Silurian–Devonian time. The underneath basement as well as terrains eastern from the Scandinavian Caledonides consists of Archaean to Neoproterozoic rocks of the Fennoscandian shield (Fig. 1.2) that are variably affected by Caledonian deformation, metamorphism and/or thrusting (Corfu et al., 2014).

The structure and metallogeny of the Scandinavian Caledonides are the result of a plate-tectonic cycle that started in Neoproterozoic times with rifting and continental break-up (800-730 Ma; Melezhik et al., 2015), followed by the opening-up of a wide ocean (Iapetus), and ended in the Devonian subsequent to a continent-to-continent collision. The Lower Allochthon and the Middle Allochthon were formed during the rifting of Baltica whereas the Uppermost Allochthon contains sequences deposited on margins of the Laurentian plate (Roberts and Gee, 1985; Roberts et al., 2007). The Upper Allochthon represents remains of the Iapetus ocean realm (Gee et al., 2007; Roberts et al., 2007) and hosts numerous volcanogenic massive sulfide (VMS) deposits, including the Sulitjelma Cu-(Zn) deposits.

The Sulitjelma region represents a part of the Køli Nappe Complex of the Upper Allochthon (Stephens et al., 1985) and consists of: (1) a metabasic igneous complex of the Sulitjelma ophiolite (Boyle, 1980); (2) metasedimentary rocks of the Skaiti Supergroup (Boyle et al., 1985; Kollung, 1989, 1990) and (3) a sequence of metasediments and calc-alkaline volcanic rocks of the Furulund and Sjønsta Groups (Boyle, 1989). The mineralization of the Sulitjelma Cu-(Zn) VMS deposits mostly occurs along the contact of the basaltic volcanics of the Sulitjelma ophiolite and the overlying metapelites of the Furulund Group (Fig. 1.3). This contact represents the ancient oceanic floor. The sediments of the upper part of the Furulund Group contain fossils of Ordovician-Silurian age near the contact with the Sjønsta Group (Vogt, 1927; Wilson, 1971), while a gabbro pegmatite within the ophiolite has recently been dated at 437 ± 2 Ma (U/Pb zircon/titanite methods; Pedersen et al., 1991).

Three main phases of deformation are recorded in the rocks enclosing the deposits. The first deformation (Dl) was related to compression and closure of the ocean basin, and was followed by the D2 event during emplacement onto the Baltic Shield. This took place in the form of a major fold nappe (the Sulitjelma Fold Nappe, Boyle et al., 1985; Boyle, 1987). The D2 event resulted in strong penetrative simple-shear, development of sheath folds, and inversion of the metamorphic zones. The non-penetrative D3 deformation accompanied slow uplift and cooling. The Sulitjelma deposits and their country rocks were exposed to rapid initial burial and heating (8°C/Ma and 0.8 km/Ma, respectively). D2 deformation

accompanied peak metamorphism, with slow rates of cooling (4°C/Ma) and uplift (Burton & O'Nions, 1991, 1992).

The ore mineralization in the Sulitjelma Cu-(Zn) deposits occurs in forms of elongated or tabular ore bodies. Major ore minerals are pyrite, chalcopyrite, sphalerite and pyrrhotite. Galena, arsenopyrite cubanite, molybdenite, stannite, tetrahedrite and Sb-sulfides and sulfosalts are rare. Main gangue minerals are quartz, Fe and Ti oxides, and locally, anhydrite (Cook, 1996).

1.5 VMS deposits

Volcanoclastic massive sulphide deposits or simply VMS deposits, is a collective name for ore deposits consisting of sulphides chiefly with a Cu-Zn affinity. Pb, Au and Ag however, are important contributors in some deposits. VMS deposits are worldwide of high economic value and are important sources for Cu, Zn, Pb, Au and Ag. They also represent minor sources of Sn, Co, S, Se, Cd, Mn, Te, In, Bi, Ge, Ga. They form as a result from hydrothermal convection and precipitation from fluids enriched in metals close to or on the ocean floor. Their host rocks can be both volcanic and sedimentary related to stratigraphic sequences (Barrie & Hannington, 1999; Galley et al., 2007; Robb, 2005).

1.5.1 Tectonic settings

Tectonically all VMS deposits seems to be connected to an extensional regime (Barrie & Hannington, 1999; Galley et al., 2007; Ohmoto, 1996). This includes various mid-ocean ridge and rifted arc settings (Barrie & Hannington, 1999; Galley et al., 2007). Today the most preserved VMS-deposits are formed in arc settings. This is due oceanic crust which forms in relation to mid-ocean ridges often ends up being subducted at a later tectonic stage. The preserved VMS deposits related to mid-ocean ridges is a result of minor parts being obducted rather than subducted (Galley et al., 2007).

1.5.2 Fluid transportation and metal precipitation

For a hydrothermal convection system beneath an ocean floor to be able to exist, a heat source is needed (Ohmoto, 1996). This can be provided by the presence of a volcanic intrusion. As

cold near pH neutral seawater infiltrates the crust, as it move downward in the system it is gradually heated by the intrusion. This makes the water to become buoyant and rise back toward the seafloor and at the same time causes more seawater to move down in the crust (Galley et al., 2007).

Hydrothermal circulation in the oceanic crust highly depends on the porosity and permeability. The first 100 meters of the volcanic heterogeneous section of the oceanic crust, is the most porous and permeable part, due to extensive open fractures and pore space. Further down in the system towards what is referred to as the sheeted dike complex, the porosity and permeability gradually decrease as the lithology becomes more homogenous and massive. Locally, faults and/or great depth fissures can disturb this relationship causing focused fluid flow pathways. The intensity of the fluid convection does not occur in a uniform matter throughout the oceanic crust. The highest intensity is found straight above the magma chamber where the temperature is high. As the distance from the spreading centre increases, the crust become cooler and hence does the intensity of the fluid convection decrease. Naturally the temperature of the fluids correlates to the fluid convection intensity, with high temperatures close to the spreading axis (above the magma chamber) and decreases with distance from the spreading centre (Barrie & Hannington, 1999).

As seawater are moving downward in the crust and interacts with the surrounding rocks the fluid originating from seawater chemically changes. This occurs as stepwise process dependent on the temperature. First at low temperatures below 150 °C, SO_4^{2-} from the seawater forms anhydrite and gypsum. As the fluid further interacts with higher temperature rocks it becomes enriched in metals and H_2S due to leaching. When the now enriched fluid flows towards the seafloor surface, it encounters cooler rocks which results in alteration and in the precipitation of ore minerals in what is referred to as the stockwork ore zone. Further precipitation of ore minerals occurs as the enriched fluid mixes with sea water when it reaches unconsolidated sediments and further exhales on to the seafloor. This results in ore which is rich in sphalerite and galena. (Ohmoto, 1996). Over time hotter fluid arise which leads to the introduction of chalcopyrite and sphalerite and galena are being dissolved (Large, 1992).

1.5.3 Classification

VMS deposits show broad spectre of deposits with their own characteristics. Even though they all share similarities in terms of genesis they do also show a broad spectre of differences. For this reason a classification system or systems are necessary. A simple, but useful classification can be done based on the content and ratio between the three base metals; Cu, Zn and Pb. This yields the three groups Cu-Zn, Zn-Cu and Zn-Pb-Cu (Galley et al., 2007). A more comprehensive classification have been presented by Barrie and Hannington (1999). This is based on dividing into five groups of deposits based on their stratigraphic succession of host rocks. The classification also discusses other criteria in relation to the host rocks like, tectonic settings and metal content. One good example will also be presented.

Mafic Type

Defined by the stratigraphic succession of host rocks being more than 75 % mafic with less than 1 % being of felsic rocks. Usually they also contain less than 10 % ultramafic and/or siliciclastic rocks. Mafic type deposits are related to ophiolite forming conditions. This is conditions which can be observed today at ocean spreading centre, back-arc spreading centres and nascent arc settings. Mainly the basaltic country rocks origins from tholeiitic magma, but are also in some cases of boninitic origin. The mafic VMS deposits represents the lowest abundance and average tonnage compared to the others types (Barrie & Hannington, 1999; Galley et al., 2007). In terms of base metal content on the other hand when compared to the other types, they are considered to have the highest Cu content and the lowest Pb content (see figure X) (Barrie & Hannington, 1999). Among famous known deposits one good example would be the deposits found in the Troodos Massif in Cyprus (Ohmoto, 1996; Robb, 2005).

Bimodal-Mafic Type

Defined by the stratigraphic sequence of host rocks being more than 50 % mafic and more than 3 % being of felsic rocks. Siliclastic rocks does also occur, but in minor amounts. Although the amount of mafic volcanic rocks are clearly greater than felsic volcanic rocks, felsic rocks is usually acting as the host rocks. In terms of tectonic environment, the compositional make-up of host rocks reflects volcanic arcs and rifted volcanic arcs at an early stage of its formation. Mainly the mafic host rocks origins from a tholeiitic basalts, but can also shift toward a more calc-alkalic composition. The felsic volcanic rocks are usually composed of rhyolites with a high silica content, but can also shift toward calc-alkalic rhyolites. In number the bimodal-mafic type represents the most abundant among VMS

deposits. In despite of this they do not represent the highest total tonnage due their relatively low average tonnage. Only the mafic type contain a higher amount of Cu than the bimodal mafic type (see figure). Among famous known deposits one good example would be the deposits in the Noranda region in Quebec, Canada (Barrie & Hannington, 1999).

Mafic-Siliciclastic Type

Defined by containing a similar proportion of mafic volcanics/intrusives and siliciclastic turbidites in the stratigraphic sequence of host rocks. Felsic material is low or non-abundant. The main constituent in the siliclastic turbidites will always be the siliclastic one although they can contain substantial amount of carbonates. This is relatively rare deposit, but can show for a relatively high average tonnage (see figure). In base metal content this is one of the deposit types containing a high amount of Pb, but also a fair amount of Cu (see figure). Many of the known deposits are highly deformed. Among famous known deposits one good example would be the Besshi deposits in Japan (Barrie & Hannington, 1999).

Bimodal-Felsic Type

In the stratigraphic sequence of host rocks they are defined as containing over 50 % felsic volcanic rocks with less than 15 % siliciclastic rocks. The residuum rocks are dominated by mafic volcanics and mafic intrusives. In terms of tectonic environment bimodal-felsic VMS type deposits reflects a composition which favours volcanic or rifted volcanic arcs at a late stage of its formation. The composition of the felsic host rocks are in general calc-alkalic with some other cases of compositions shifting from high-silica rhyolite towards calc-alkalic. The composition of the mafic rocks are in general calc-alkalic with other cases with shifting from tholeiitic toward calc-alkalic. This is a higly abundant deposit, but have a low average tonnage. In terms of metal content, this deposit is known for the high amount of zinc and silver compared to the other deposits (Barrie & Hannington, 1999). Among famous known deposits one good example would be the Kuroko deposits of the Hukoroku region in Japan (Barrie & Hannington, 1999; Ohmoto, 1996).

Bimodal-Siliclastic Type

Defined by the stratigraphic sequence of host rocks containing relatively equal amounts volcanic and siliciclastic rocks. Among the volcanic rocks, felsic types dominates rather than mafic types. The composition of the felsic volcanic rock are usually calc-alkalic, whereas the mafic volcanic rocks are usually tholeiitic in composition. Some rare cases of mafic volcanic rocks with a moderately alkaline has also been recorded. In terms of tectonic environment,

bimodal-siliciclastic VMS deposits have been suggested to form in relation to continental arcs or rifted continental arcs. Altought their abundance is relatively low, they contain the highest average tonnage among all VMS types. In terms of metal content, they represent the lowest amount of Cu and the highest amount of Pb. Among famous known deposits one good example would be the Iberian Pyrite Belt found in Spain and Portugal (Barrie & Hannington, 1999).

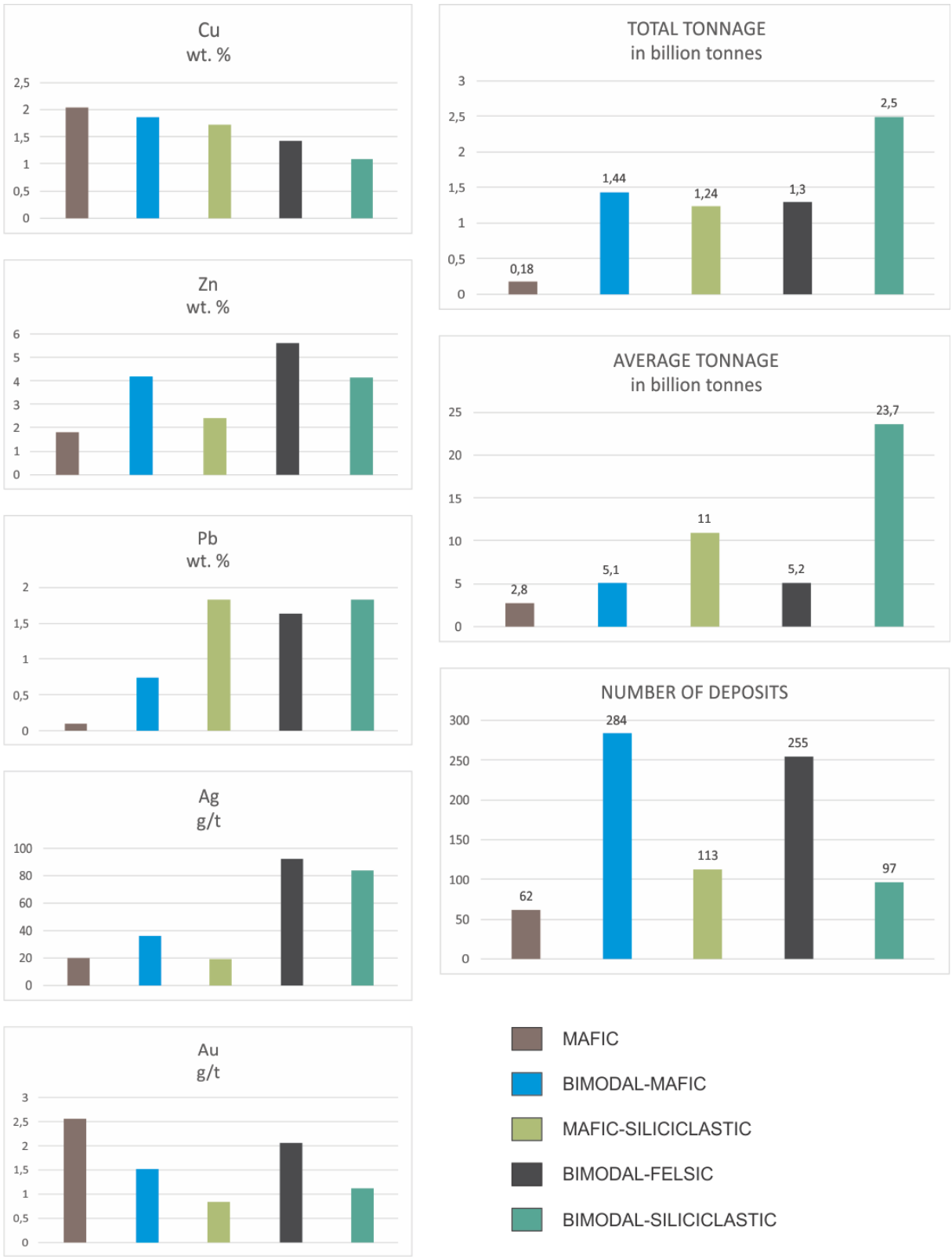

Figure 1.2: *Column charts representing different VMS types. The left row is showing average metal content. Deposits of the mafic type contains the highest amount of copper, but the lowest amount Pb. In the other end, bimodal-siliciclastic contains the lowest amount of copper, but the highest amount of Pb. The right row is showing total tonnage, average tonnage and number of deposits. Deposits of bimodal-siliciclastic holds the highest total and average tonnage. The bimodal-mafic and bimodal-felsic are the most numerous. Mafic type holds the lowest total tonnage, average tonnage and are the least abundant VMS modified from Barrie % Hannington* (1999)*; Galley et al.* (2007)*.*

2 Sample description

In this section there will be given an introduction to the samples that were chosen for further geochemical, petrographic and fluid inclusion study. Samples are listed according to locality and sample name. The samples are named after the deposits from where they were collected. These are: Giken (SG-0X), Hankabakken 1 and 2 (SH1-0X, SH2-0X), Jakobsbakken (SJ-0X), Ny Sulitjelma (SNY-0X) and Sagmo (SS-0X). For each sample, a brief macro textural description will be given as well as major mineralogy and which method they were chosen for.

Table 2.1: *A presentation of the samples from Giken*

Sample	Lithology	Major Mineralogy	Texture	Chosen for
SG-01	Massive sulphide	Pyrite, chalcopyrite, pyrrhotite, sphalerite	Coarse grained, homogenous	Microscopy, lithogeochemestry
SG-02	?	Pyrite, chalcopyrite, feldspar, mica	Coarse grained, disseminated	Microscopy, lithogeochemestry
SG-003 A	Massive sulphide	Pyrite, chalcopyrite, magnetite, sphalerite, chlorite, mica	Coarse grained with finer edges.	Microscopy, lithogeochemestry
SG-003 B	Sedimentary?	Pyrite, quartz, plagioclase, mica, chlorite	Quite fine-grained, layered/disseminated	Microscopy
SG-003 C	?	Pyrite, chalcopyrite, sphalerite, carbonate, quartz,	Layered fine grained/disseminated coarse grained	Microscopy, lithogeochemestry

Table 2.2: *A presentation of the samples from Hankabakken*

Sample	Lithology	Major Mineralogy	Texture	Chosen for
SH1-01	Quartz vein?	Pyrite, Chalcopyrite, quartz, plagioclase, mica	Fine grained, disseminated, weakly layered	Microscopy
SH1-02	Sedimentary?	Pyrite, chalocopyrite, sphalerite, magnetite, quartz, feldspar, mica	Quite fine-grained, disseminated	Microscopy, lithogeochemestry
SH1-03	Micaschist	Pyrite, magnetite, mica,	Fine grained with porphyroblastic ductile deformed pyrite	Microscopy, lithogeochemestry, SEM
SH2-01	Sedimentary	Pyrite, quartz/feldspar, mica?	Finegrained, disseminated, homogenous weathered	Lithogeochemestry

Table 2.3: *A presentation of the samples from Jakobsbakken*

Sample	Lithology	Major Mineralogy	Texture	Chosen for
SJ-01	Sedimentary+ hydrothermal?	Galena, quartz, carbonate, mica, clinozoisite	Finegrained with accumulated galena crystals	Microscopy, lithogeochemestry, SEM
SJ-02	Sedimentary+ hydrothermal?	Sphalerite, quartz, feldspar, mica	Finegrained with accumulated spahlerite crystals	Microscopy, SEM
SJ-03	Massive sulphide + sedimentary	Pyrite, chalcopyrite, sphalerite, pyrrhotite, quartz, mica, amphibole, unknown	Coarse grained part + smaller fine-grained part	Microscopy, lithogeochemstry, SEM
SJ-04	Quartzvein?	Quartz, sphalerite?, ?, ?	Coarse grained quartz next to finer grains	Fluid inclusions
SJ-05	Sedimentary/quartz vein?	Pyrite, quartz, mica	Layered, fine grained with coarser sulphides	Microscopy, lithogeochemestry

Table 2.4: *A presentation of the samples from Ny-Sulitjelma*

Sample	Lithology	Major Mineralogy	Texture	Chosen for
SNY-001	Quartz vein?	Pyrite, quartz, feldspar, chlorite	Mostly fine-grained with some larger crystals	Microscopy, SEM, fluid inclusions
SNY-002	Quartz vein/sedimentary?	Pyrite, quartz, mica	Layered fine-grained	Microscopy
SNY-003	Sedimentary, quartz vein?	Pyrite, sphalerite, quartz, mica, carbonate	Disseminated, weak layering and folding. Fine-grained.	Microscopy, lithogeochemestry
SNY-004	Quartz vein?	Pyrite, chalcopyrite, sphalerite, quartz, mica	Disseminated, fine grained, weak layering	Microscopy, lithogeochemestry

Table 2.5: *A presentation of the samples from Sagmo*

Sample	Lithology	Major Mineralogy	Texture	Chosen for
SS-01	Mineralised mica something?	Pyrrhotite, chalcopyrite, quartz, mica, weathering product	Coarse grains in fine grained matrix.	Microscopy, lithogeochemestry
SS-02	?	Pyrrhotite, chalcopyrite, sphalerite, quartz, mica, weathering product	Coarse grained, homogenous	Microscopy, lithogeochemestry
SS-04	?	Pyrrhotite, chalcopyrite, quartz, mica, weathering product	Coarse grained homogenous	Microscopy

Figure 2.1: *Pictures of selected samples after they were cut. Sample names are market the underlying (A4) paper or on the sample itself. For clarification, sample SH1-04 in the picture were not chosen for further study.*

Figure 2.2: *Pictures of selected samples after they were cut. Sample name is marked on the underlying (A4) paper or the sample itself. For clarification, sample SG-003 D in the picture were not chosen for further study.*

3 Methods

3.1 Fieldwork and sampling

Sample collection was done during two days of fieldwork in October 2016 (13.10.2016-14.10.2016). During this period, more than 20 samples were collected. The goal of the fieldwork was to collect ore samples or samples showing mineralization from different orebodies in the area. In addition to mineralization, transparent minerals such as quartz and sphalerite were of the interest due to the possibility of containing entrapments of fluid inclusion.

During the fieldwork, six orebodies were sampled. As the Sulitjelma mine has been closed for more than 20 years, the access for the ore mineralization was very limited. The most of the studied samples were collected from waste piles or close to abandon adits.

3.2 Thin section preparation

From the collected samples, 19 thin sections where made. The selected samples where first cut by a large rotary saw and then by a smaller rotary saw for finer cutting. The samples where cut into square pieces measuring approximately 30 mm x 15 mm x 20 mm. The samples where then delivered to the lab at the Department of Geosciences at UiT for further preparation. The finished thin sections where polished and approximately 30-40 µm thick.

3.3 Transmitted and reflected light microscopy

Both the transmitted and reflected polarised light microscopy technique were used. The microscope used were Leica DMLP with Leica DFC450 camera mounted on top. Both plane polarised light (PPL) and crossed polarised light (XPL) were applied. The purpose was to determine, texture, mineralogy, mineral interactions and a modal percent estimation of each mineral in the thin section. For the minerals which were difficult to determine, the optical properties where noted and later correlated with the data retrieved from SEM, EBSD and XRD analyses.

3.4 Scanning electron microscopy (SEM)

The goal of SEM studies, was to complement the lithogeochemical analysis to better understand in which mineral form some elements occur, both as major and trace elements. Also by understanding the mineral forms, an assumption of the carrier and origin of different metals could be discussed. In addition, these analysis were used to help with the determination of mineral phases which were too small for reliable determination by transmitted and/or reflected light microscopy.

The preliminary textural and semi-quantitative SEM analyses were conducted at the Hitachi TM3030 Tabletop SEM equipped with Energy-Dispersive X-Ray spectroscopy (EDS) detector provided by BRUKER, at the Department of Geoscience, UiT-The Arctic University of Norway. This instrument works in a variable vacuum condition and does not require coating of polished sections. The analyses were conducted at the working distance of 8.5 mm and accelerating voltage of 15 kV. The retrieved data were further processed in the Quantax 70 software also provided by BRUKER.

Further, more accurate SEM analyses were performed using a Zeiss Merlin VP Compact field emission scanning electron microscope (FE-SEM) in the electron microscopy laboratory at UiT-The Arctic University of Norway. This microscope is equipped with several detectors, including EDS, wavelength dispersive X-ray spectroscopy (WDS) and an electron backscattered diffraction (EBSD) detector, all provided by Oxford instruments. The analysed polished thin sections were carbon coated (20 nm) and analysed under high vacuum conditions. The analyses were conducted at the working distance of 8.5 mm for EDS/WDS, an accelerating voltage of 20 kV and an aperture of 120 µm for EDS and WDS as well as 240 µm for EBSD. The retrieved data were further processed applying the Aztec software by Oxford instruments. The EBSD technique was applied for the mineral phase identification. The method is based on the crystallographic indexing of EBSD patterns, taking in account the position and intensity of crystallographic orientation patterns (Kikuchi patterns), which are unique for a particular crystal lattice and orientation (Goehner & Michael, 1996; Nowell & Wright, 2005). The stepsize used was 5 µm applied to a measured area of 7,98 mm x 13,5 mm. The stage/specimen were tilted to 70 ° during the analysis. The identification of phases were done through AZTEC and CHANNEL 5/Tango software, also provided by Oxford instruments.

3.5 X-ray powder diffraction (XRD)

The XRD analyses were used for mineralogical phase analyses of selected hydrothermal alteration products. The analyses were conducted at the Department of Mineralogy and Petrography, Faculty of Sciences, University of Zagreb. Measurements were performed on Philips PW 3040/60 X'Pert PRO powder diffractometer (45 kV, 40 μA) with CuKα monochromatised radiation (λ=1.54056 Å) and θ-θ geometry. Area between 4 and 63 θ-θ, with 0.02° step, was measured with 0.5° primary beam divergence. Compound identifications were based on the software X'Pert High Score 1.0B and literature data.

3.6 Lithogeochemistry

Powder (10 g) of 14 selected ore samples were crushed and milled in an agate ball-mill and analysed a ActLabs laboratory (Ancaster, Canada) after lithium metaborate or tetraborate fusion using Inductively Coupled Plasma – Emission Spectrometry (ICP-ES) for the major elements. Detection limits for all analysed elements are listed in Appendix III.

3.7 Fluid inclusion studies

Fluid inclusions are tiny amounts of fluids, usually aqueous solutions, entrapped within 3D defects of individual crystals. Fluid inclusions can be classified according to phases stable at standard conditions (mono-phase, two-phase, poly-phase) or according to the timing of formation of the inclusion relative to that of the host mineral (primary, secondary, pseudosecondary). Primary fluid inclusions are entrapped during growth of their host crystal. In contrast, if a crystal fractures after it has been precipitated, some fluid may enter the fracture and become trapped as secondary fluid inclusions as the fracture heals. If fracturing occurs during growth of the crystal, pseudosecondary fluid inclusions may be trapped during continued crystal growth (Roedder, 1984; Goldstein, 2003). The temporal classification of studied fluid inclusions is critical for proper interpretation of the origin and evolution of their host minerals (e.g. Bodnar, 2003).

Fluid inclusions can be used for determination of P-T-X conditions during and after their entrapment (e.g. Roeder, 1984; Shepherd et al, 1985, Bodnar, 2003). A wide spectrum of analytical techniques may be applied in the fluid inclusion studies and the most common are: fluid inclusion petrography (Goldstein, 2003); microthermometry (Bodnar & Vityk, 1994); Raman spectrometry (Burke, 2001) and LA-ICP-MS analyses of individual inclusions (Audetat et al., 1998).

In the framework of this thesis, fluid inclusion petrography and microthermometry were performed. The analyses were conducted at the Department of Geosciences, UiT The Arctic University of Tromsø. Double polished ~0.3 mm thick, transparent quartz wafers were used. Measurements were carried out at Linkam THMS 600 stage mounted on an Olympus BX 2 microscope using 10x and 50x Olympus long-working distance objective lenses for visible light. Two synthetic fluid inclusion standards (SYN FLINC; pure H_2O and mixed H_2O-CO_2) were used to calibrate equipment. The precision of the system was ±2.0°C for homogenization temperature, and ±0.2°C in the temperature range between –60 and +10°C.

4 Results

4.1 Petrography and SEM/EDS studies

4.1.1 Giken

Thin section SG-01

Table 4.1: Estimated Modal Mineralogy

Mineral	Modal percent	Form
Pyrite	50 %	Subhedral
Chalcopyrite	30 %	Anhedral
Pyrrhotite	5 %	Anhedral
Sphalerite	10 %	Anhedral
Galena	<5 %	Anhedral
Polylithionite	<5 %	Euhedral to subhedral
Organic material	<<5 %	Anhedral
Fe-oxyhydroxides	<<5 %	Anhedral

Thin-Section Description

The thin section is from a massive sulfide sample, and hence it consists mainly of sulfides. Large pyrite grains surrounded by chalcopyrite and patches of sphalerite dominates. The pyrite grains does still show evidence of their cubic crystallographic shape, but most of them are extensively cracked and with rounded edges. They also often contain inclusions/entrapments of some of the other minerals present in the thin section e.g. chalcopyrite, sphalerite or galena. This can often be seen in relation to cracks in the mineral grains.

The chalcopyrite is found crushed in between the pyrite grains and is evenly distributed. Sphalerite also occur as infill between the pyrite grains, but in a lower amount than the chalcopyrite and unevenly distributed. Low amounts of pyrrhotite and rare grains of galena are observed as well.

Minerals with low interference colors are found in some small patches between other mineral grains and along cracks in pyrite. Analysis and comparison with other samples containing same mineral in larger quantities suggests Li-bearing mica polylithionite ($KLi_2AlSi_4O_{10}(F,OH)_2$)

A low amount of what could be organic matter is observed a few places in the thin section. It occur as small brownish light-yellow patches or along some grain borders. Also around some sulfide grain borders, a low amount of rusty weathering material composed predominantly of Fe-oxyhydrates.

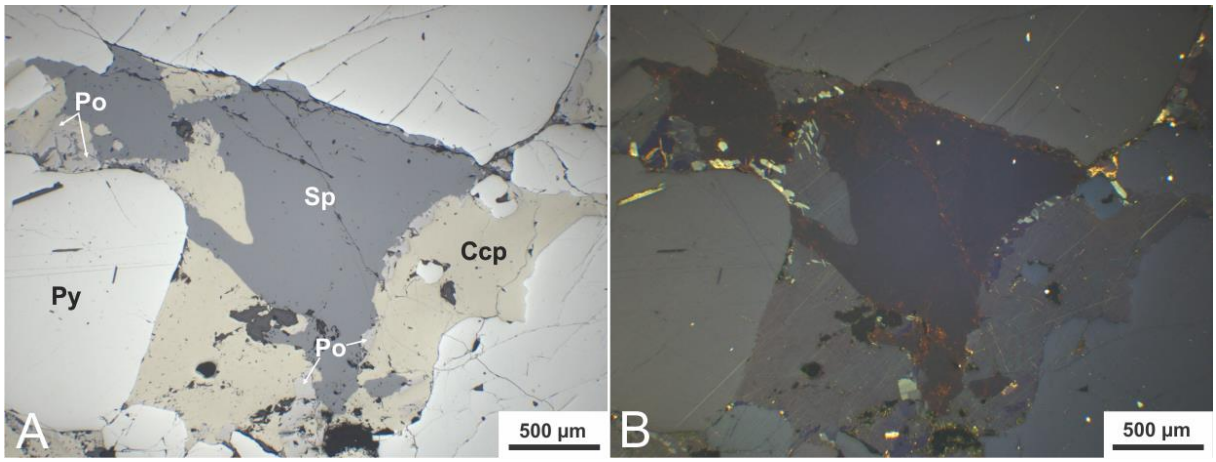

Figure 4.1: *Photomicrograph of sample SG-01 in reflected light. A: in plane polarized. B: in crossed polarized light. Showing large grains of pyrite (Py) with chalcopyrite (Ccp), sphalerite (Sp) and small grains of pyrrhotite (Po) in between. Small grains between sphalerite and chalcopyrite are pyrrhotite.*

Sample SG-02

Table 4.2 Estimated Modal Mineralogy

Mineral	Modal percent	Form
Pyrite	20 %	Subhedral to anhedral
Chalcopyrite	5 %	anhedral
Sphalerite	<5 %	anhedral
Galena	<5 %	Anhedral
Feldspar	40 %	Anhedral
Phlogopite	10 %	Subhedral
Gypsum	<5 %	Anhedral
Carbonate	<5 %	Anhedral
Organic material	<<5 %	Anhedral
Weathering material	<<5 %	Anhedral

Thin-Section Description

Disseminated sulfides within plagioclase and phlogopite rich matrix. Plagioclase is the dominating mineral in the thin section (Fig. 4.2). The SEM/EDS analysis reveals its albite composition (Table 4.22). Plagioclase grains often contain mica fragments. The highest amount is located in plagioclase grains without twinning.

Micas are disseminated as small grains in the matrix and show optical properties characteristic for phlogopite (Fig. 4.2). They are also found within plagioclase grains. Rare gypsum and carbonate grains are recorded as well.

Disseminated sulfides are dominated by large pyrite grains. Attached to or in between pyrite, crushed chalcopyrite occurs in a minor amount. The grain sizes are in general smaller than pyrite, but does also show some relatively large grains. Sphalerite and galena are observed as well, usually attached to chalcopyrite or pyrite, but also disseminated as small single grains.

A low amount of organic matter is observed some places in the thin section. They occur as small brownish light-yellow patches or rims around some mineral grains. Some sulfide grains show dark brown weathering rims.

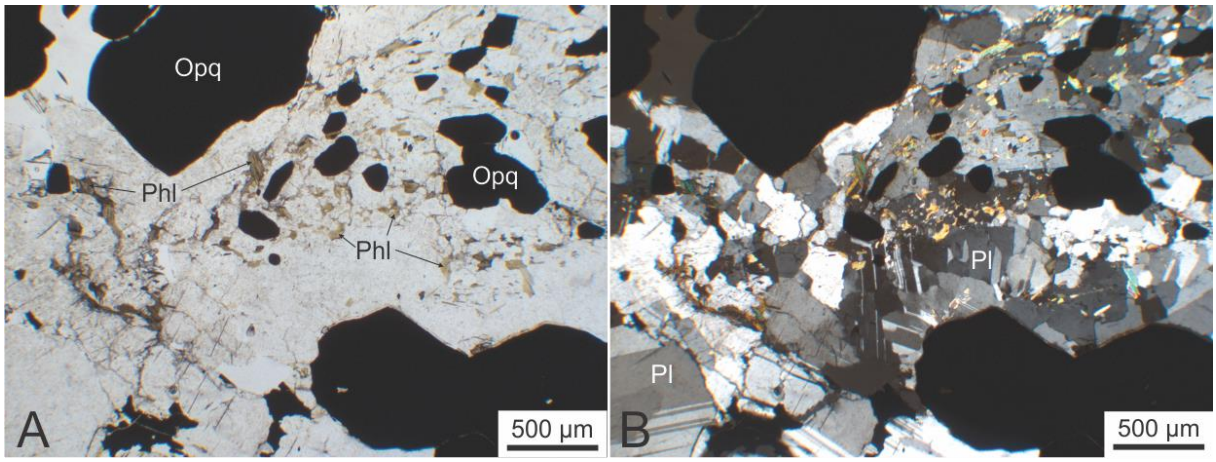

Figure 4.2: Photomicrograph of sample SG-02 in transparent light. A: In plane polarised light. B: In crossed polarised light. Showing disseminated opaque minerals (Opq) in a plagioclase (Pl) and phlogopite (Phl) matrix.

Sample SG-003A

Table 4.3: Estimated Modal Mineralogy

Mineral	Modal percent	Form
Pyrite	65 %	Subhedral to anhedral
Chalcopyrite	20 %	Anhedral
Magnetite	5 %	Anhedral
Sphalerite	5 %	Anhedral
Chlorite	10 %	Euhedral
Biotite	5 %	Subhedral
Polylithionite	5 %	Euhedral
Plagioclase	<5 %	Anhedral
Carbonate	<5 %	Anhedral
Organic material	<<5 %	Anhedral
Weathering material	<<5 %	Anhedral

Thin-Section Description

The major part of the sample consists of massive sulfides. Large pyrite grains dominate with chalcopyrite and a minor amount of sphalerite and magnetite in between (Fig. 4.3; Table 4.3). The pyrite grains are often rounded and cracked, but some grains still show evidence of cubic crystal symmetry. Chalcopyrite is crushed in between the pyrite grains and does not preserve its original crystal shape. Sphalerite and magnetite are usually crushed as well.

In between the pyrite grains there is also a substantial amount of what seems to be a mix of chlorites, biotites and polylithionites. Among these chlorite is the dominating mineral. Here one also can observe a few grains of what looks like carbonate, but could also be a different mineral. A minor amount of plagioclase is also observed with the presence of carlsbad twinning.

Small amount of organic matter occurs as brownish light-yellow patches or along a few grain borders. Many of the sulfides show a thin rim of dark brown weathering material around the grain border or as infill in cracks.

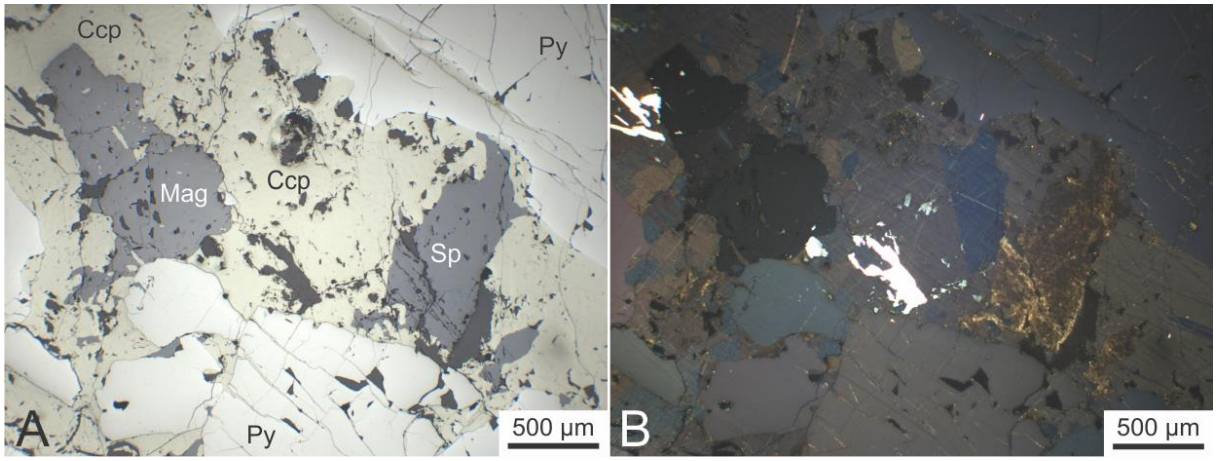

Figure 4.3: Photomicrograph of sample SG-003 A in reflected light. A: In plane polarised light. B: In crossed polarised light. Showing large pyrite grains (Py) with chalcopyrite (Ccp), magnetite (Mag) and sphalerite (Sp) in between.

Sample SG-003B

Table 4.4: Estimated Modal Mineralogy

Mineral	Modal percent	Form
Pyrite	20 %	Euhedral
Chalcopyrite	<5 %	Anhedral
Quartz	35 %	Anhedral
Plagioclase	10 %	Anhedral
Biotite	15 %	Euhedral
Chlorite	10 %	Euhedral
Muscovite	<5 %	Euhedral

The sample show a layered structure and consists of disseminated pyrite in a quartz, mica and chlorite matrix with minor amount of chalcopyrite (Table 4.4.).

Quartz is the most abundant mineral the thin section. The grains are often elongated parallel to the layering of the thin section, and many show undolose extinction. Some grains does also show weak recrystallization in a form of grain boundary migration. Some plagioclases are also observed and can be difficult to distinguish from quartz. Some of them however show albite or Carlsbad twinning. Many grains show entrapments or overprint of micas.

Biotite occurs in a substantial amount in this sample. Usually it is orientated parallel to the layering in the thin section. Biotite occurs both as single grains and in clusters. Many of the biotite grains show alteration to chlorite seen as a change from brown to light green in PPL. Small amount of muscovite was observed.

Pyrite grains are also concentrated in layers, but are mostly euhedral and seems unaffected by deformation. Also they cut other neighboring mineral grains, where the other grains seem unaffected by the interaction with pyrite. Pyrite and chalcopyrite therefore appear to be later and they overprint other minerals.

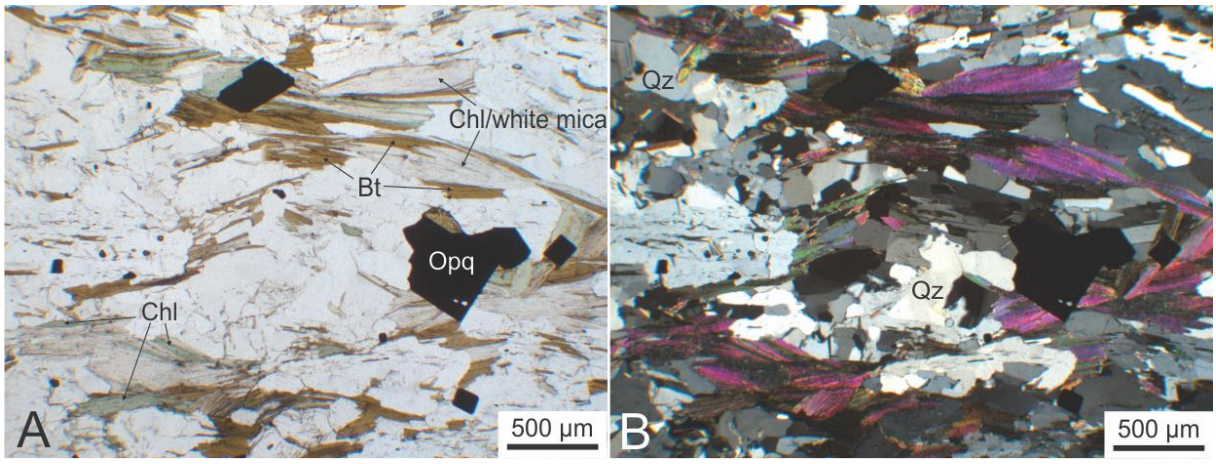

Figure 4.4: Photomicrograph of sample SG-003B in transparent light. A: In plane polarised light. B: In crossed polarised light. Showing disseminated opaque (Opq) minerals in a quartz (Qz), biotite (Bt), chlorite (Chl) and white mica matrix.

Sample SG-003C

Table 4.5: Estimated Modal Mineralogy

Mineral	Modal percent	Form

Chalcopyrite	30 %	Anhedral
Pyrite	20 %	Anhedral to subhedral
Sphalerite	5 %	Anhedral
Carbonate	10 %	Anhedral
Quartz	15 %	Anhedral
Plagioclase	<5 %	Anhedral
Biotite	5 %	Subhedral
Muscovite	<5 %	Subhedral
Polylithionite	<5 %	Euhedral to subhedral
Green mineral	10 %	Anhedral
Amphibole	10 %	Subhedral to anhedral
Organic material	<<5 %	Anhedral

The studied thin section from this sample can be subdivided into three areas where one part is dominated by a massive sulfide texture with large pyrite and chalcopyrite grains. In between the sulfide grains, isolated clusters of quartz, plagioclases, carbonates and a low amount of mica are observed. Plagioclase at contact with sulfides are crushed. The micas in this area seems to be mostly polylithionite, but rare biotite and muscovite grains are found.

The central part of the thin section shows mostly monomineralic clusters of large quartz grains accompanied by large and medium carbonate grains nearby. The quartz grains in this area shows dynamic recrystallization in the form of grain boundary migration and undolose extinction (Fig. 4.5).

The third part is located in the other outer end of the thin section as well as in between two of the monomineralic quartz clusters. This part consists of a mixure of quartz, mica, carbonates, amphiboles and some disseminated sulfides. In this area the grain size among the quartz and mica is smaller than the rest of the thin section. Many of them could to be recrystallized grains, but this is difficult to determine. The micas are dominated by biotite, but some amount could also be muscovite.

Carbonates and amphiboles on the other hand are often relatively large, and the carbonates occurs usually as in other areas in clusters. Some grain preferred orientation is observed, especially the mica.

Rare plagioclase grains occur usually as large single grains or in small fine-grained clusters.

A low amount of organic matter have been recorded.

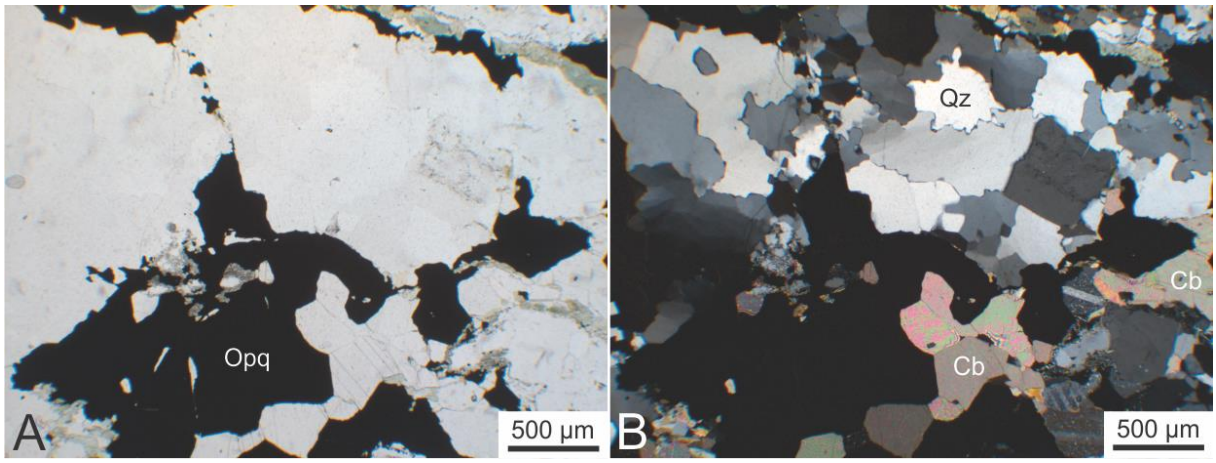

Figure 4.5: Photomicrograph of sample SG-003A in transmitted light. A: In plane polarised light. B: In crossed polarised light. Showing opaque minerals with quartz (Qz) and carbonate minerals in between. The interlobate shape of the quartz grains, suggests grain boundary migration (GMB) recrystallization.

4.1.2 Hankabakken 1

Sample SH1-01

Table 4.6: Estimated Modal Mineralogy

Mineral	Modal percent	Form
Pyrite	20 %	Euhedral to subhedral
Chalcopyrite	15 %	Anhedral
Sphalerite	<5 %	Anhedral
Quartz	30 %	Anhedral
Plagioclase	15 %	Anhedral
Muscovite	15 %	Anhedral to subhedral
Magnetite	<<5 %	Subhedral to anhedral
Organic matter	<<5 %	Anhedral

Thin-Section Description

This sample is dominated by a quartz, plagioclase and muscovite matrix, with a disseminated sulfide overprint. Quartz occurs as monomineralic clusters or with some interaction with muscovite and sulfide overprint. It also occurs as either small grains affected by subgrain rotation or medium sized grains maybe affected by annealing. The areas with smaller quartz grains, points towards a higher strain due to the higher amount of recrystallization.

Feldspars show albite and Carlsbad twinning. These grains are usually large and show mostly bulging (smaller recrystallized grains) or, locally, transition to subgrain rotation. The overall amount of recrystallized grains occur in a lower amount around plagioclase compared to quartz. Not every grain of the plagioclase show recrystallization either. They occur in clusters with a few grains each time. Entrapments of mica is also higher than compared to quartz.

According to their optical properties white micas have been identified as muscovite. They occur either in the high strain small grained quartz clusters, or disseminated throughout large parts of the thin section as small or medium sized grains without any grain preferred orientation.

Sulfides as mentioned earlier occur as a disseminated overprint. They consists of medium to small sized euhedral and subhedral pyrite grains, large to small anhedral chalcopyrite and small anhedral sphalerite grains. Some of sphalerite grains seem to consist of two minerals, thus there might be third a sulfide or oxide. Some grains which don't show internal reflections (as sphalerite) does also point to another sulfide or maybe oxide, but is difficult to determine and does only occur in a low amount. Most likely it is magnetite, as one grain seems to be cubic. In general, pyrite and chalcopyrite is most abundant among the sulfides.

A small amount of organic matter have been found as well.

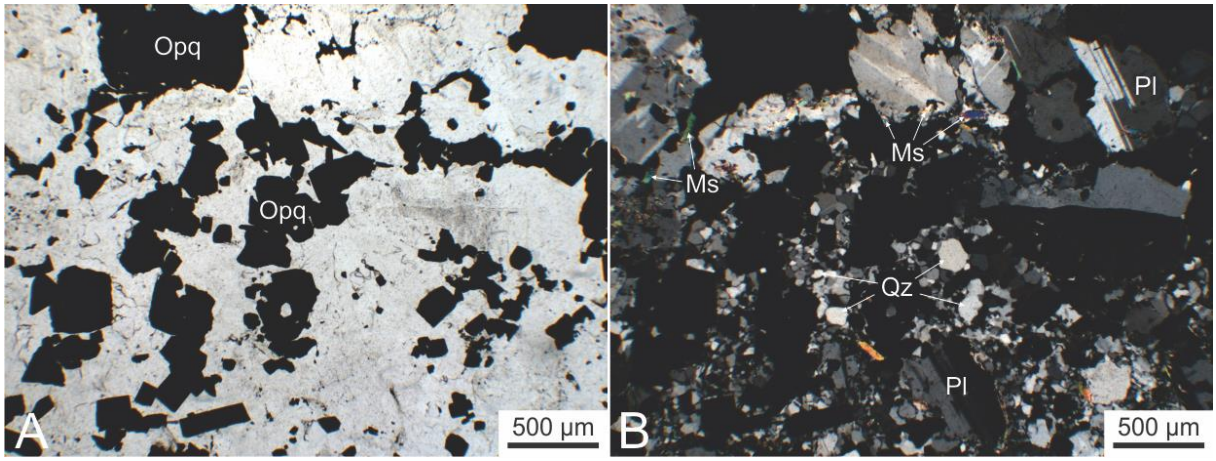

Figure 4.6: Photomicrograph of sample SH1-01 under transparent light. A: In plane polarised light. B: In crossed polarised light. Showing quartz (Qz), plagioclase and muscovite overprinted by opaque (Opq) minerals. The plagioclase grains occur in this example larger grains than quartz, and some show easy visible albite twinning.

Sample SH1-02

Table 4.7: Estimated Modal Mineralogy

Mineral	Modal percent	Form
Pyrite	25 %	Subhedral
Chalcopyrite	15 %	Anhedral
Sphalerite	5 %	Anhedral
Magnetite	15 %	Anhedral
Quartz	20 %	Anhedral
Plagioclase	15 %	Anhedral
Phlogopite	5 %	Anhedral to subhedral
Polylithionite	<5 %	Euhedral to subhedral
Organic matter	<<5 %	Anhedral

Sample consists of a quartz and feldspar matrix with some clusters of chlorite and disseminated mica, with a sulfide and oxide overprint. The sulfide and oxide overprint consists of mostly pyrite, chalcopyrite and magnetite. Minor sphalerite is recorded. Pyrite has well developed crystals with little signs of deformation. Chalcopyrite covers large areas between other opaque minerals. Magnetite can be seen by the naked eye on the sample. It occurs as black dots scattered more or less throughout the thin section.

Quartz is found throughout the thin section both in small monomineralic clusters and accompanied with other minerals. Some clusters show subgrain rotation and some show grain boundary migration. Undolose extinction is also observed in several grains. Any particular fabric is however not observed. More or less the same can be said about the feldspars, but more inclusions in the grains is observed as well as albite twinning which points towards plagioclase. It can sometimes be difficult to distinguish quartz from feldspars.

Phlogopite is the most common mica. It occurs as either clusters or disseminated grains. Locally traces of chloritization were found. A few small clusters with polylithionite are recorded as well.

A few small yellowish isotropic patches of organic matter are found.

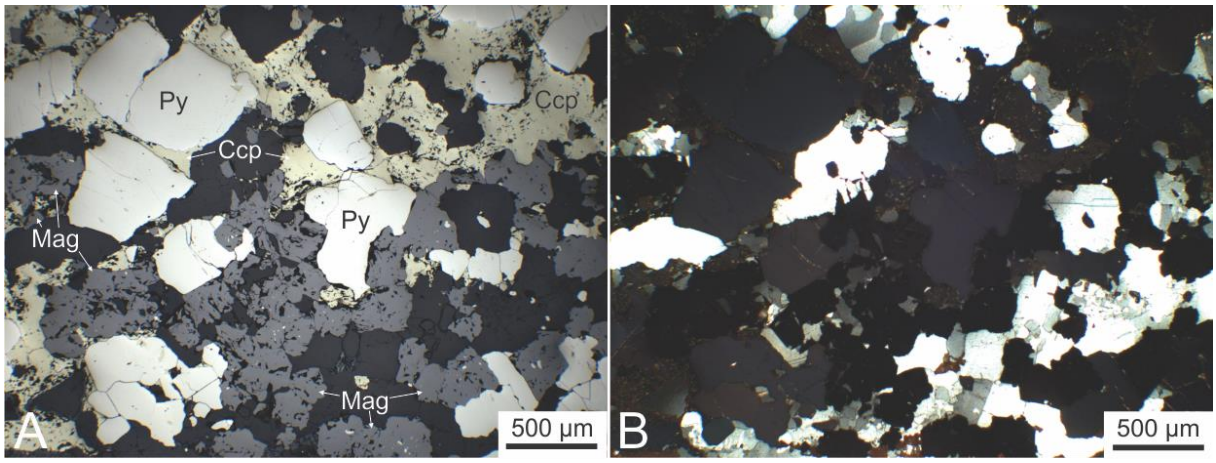

Figure 4.7: Photomicrographs of sample SH1-02 under reflected light. A: In plane polarised light. B: In crossed polarised light. Showing disseminated pyrite (Py), chalcopyrite (Ccp) and magnetite (Mag). Areas in between (dark in PPL light in XPL) are gangue minerals.

Sample SH1-03

Table 4.8: Estimated Modal Mineralogy

Mineral	Modal percent	Form
Pyrite	10 %	Anhedral
Chalcopyrite	<5 %	Anhedral
Magnetite	<10 %	Subhedral to Anhedral
Feldspar	15 %	Anhedral
Phlogopite	40 %	Euhedral
Polylithionite	20 %	Euhedral
Chlorite	<5 %	Anhedral
Mag-Ilm-Rt intergrowth	<5 %	Anhedral

The sample consists of a phlogopite and polylithionite matrix with some clusters of feldspar. Sulfides and oxides occur in layers and as disseminations.

Feldspars are mostly concentrated in large grain cluster. Some of the grains show albite or Carlsbad twinning and many show inclusions/captures of micas. Phlogopite which is the most abundant mineral in this thin section, is found throughout the sample as massive bands and in fan-like texture. They are also many cases more disseminated, but the abundance is in general quite dense. Polylithionite and another white micas, occur as long elongated grains disseminated in between the phlogopite grains. Minor chlorite is observed in a few places and seems to replace some of micas.

Pyrite occurs mostly as large elongated grains overprinting the other minerals. They also seems to follow the general layering of the thin section. The same can be said for magnetite, but some of these grains show better preserved cubic shapes. Chalcopyrite is usually found as medium sized grains attached to some of larger pyrite grains.

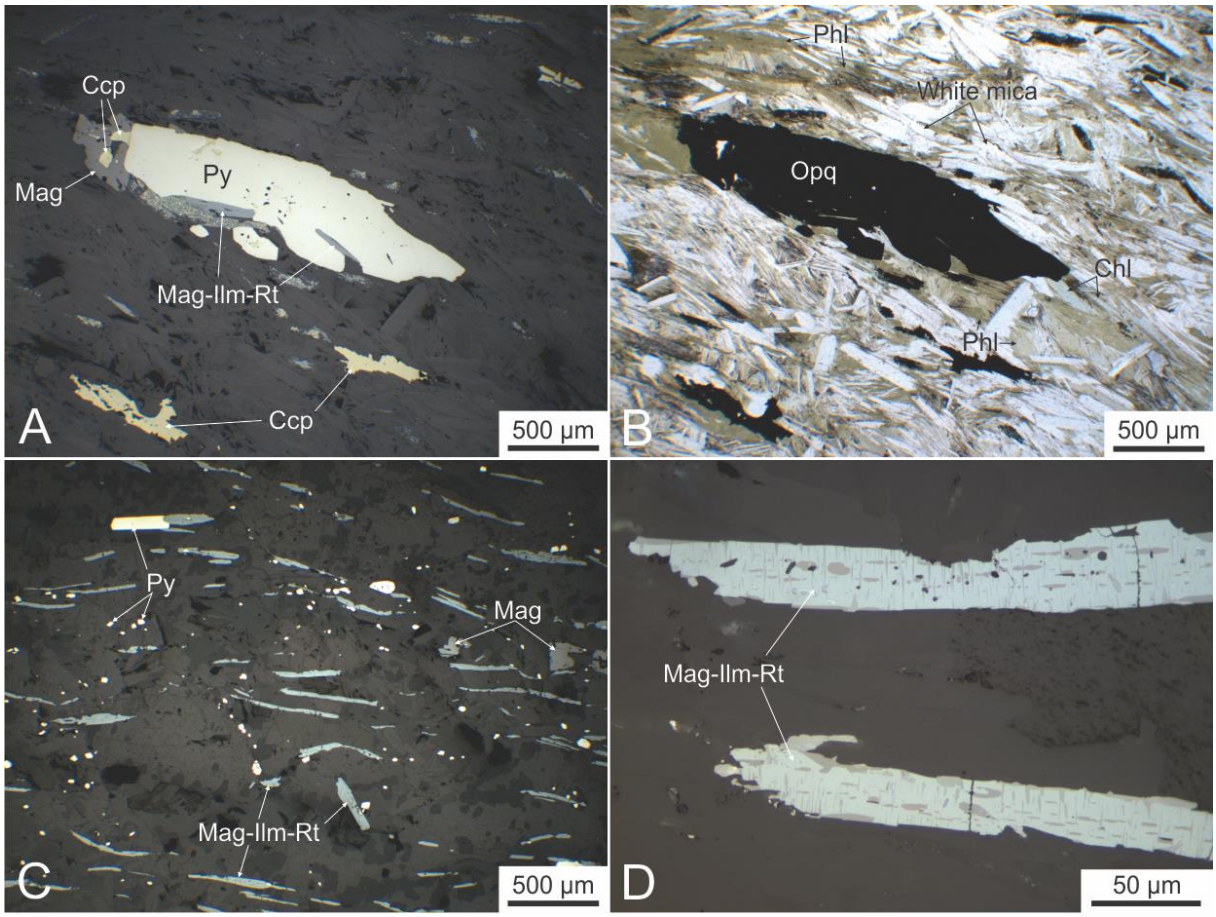

Figure 4.8: Photomicrographs of sample SH1-03. A, C and D are under reflected light. B: Under transparent light. A and B showing elongated pyrite grain with chalcopyrite (Ccp), magnetite (Mag) and Magnetite-Ilmenite-Rutile intergrowth grains attached, in a matrix of phlogopite (Phl), white mica and chlorite (Chl) matrix. C and D shows magnetite-ilmenite-rutile (Mag-Ilm-Rt) intergrowth minerals with disseminated pyrite.

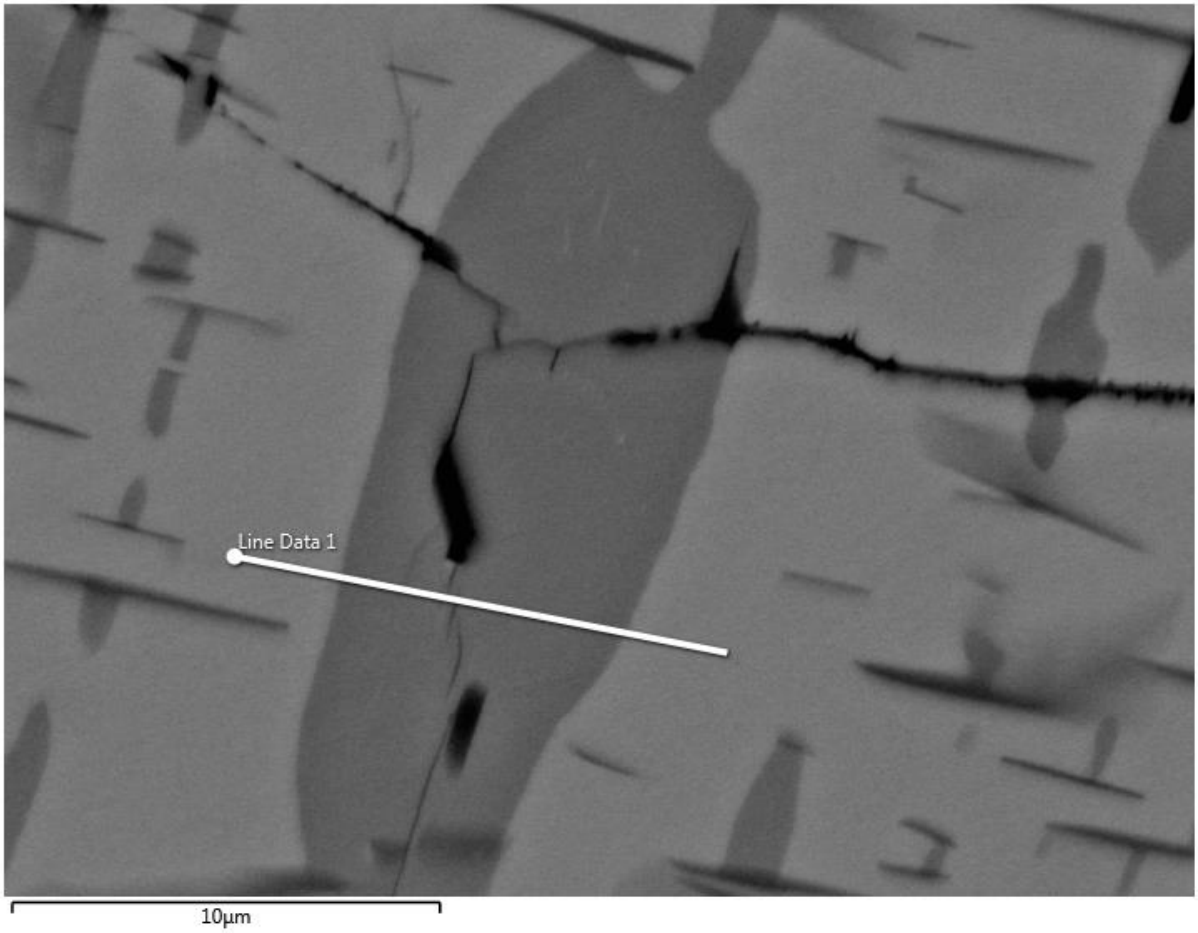

Figure 4.9: Electron backscatter image of sample SH1-03. The image is zoomed in on a magnetite-ilmenite-rutile intergrowth grain. Line data 1 is crossing an ilmenite grain and lighter "matrix" of the grain consists of magnetite whereas the thin perpendicular lines crosscutting ilmenite is rutile.

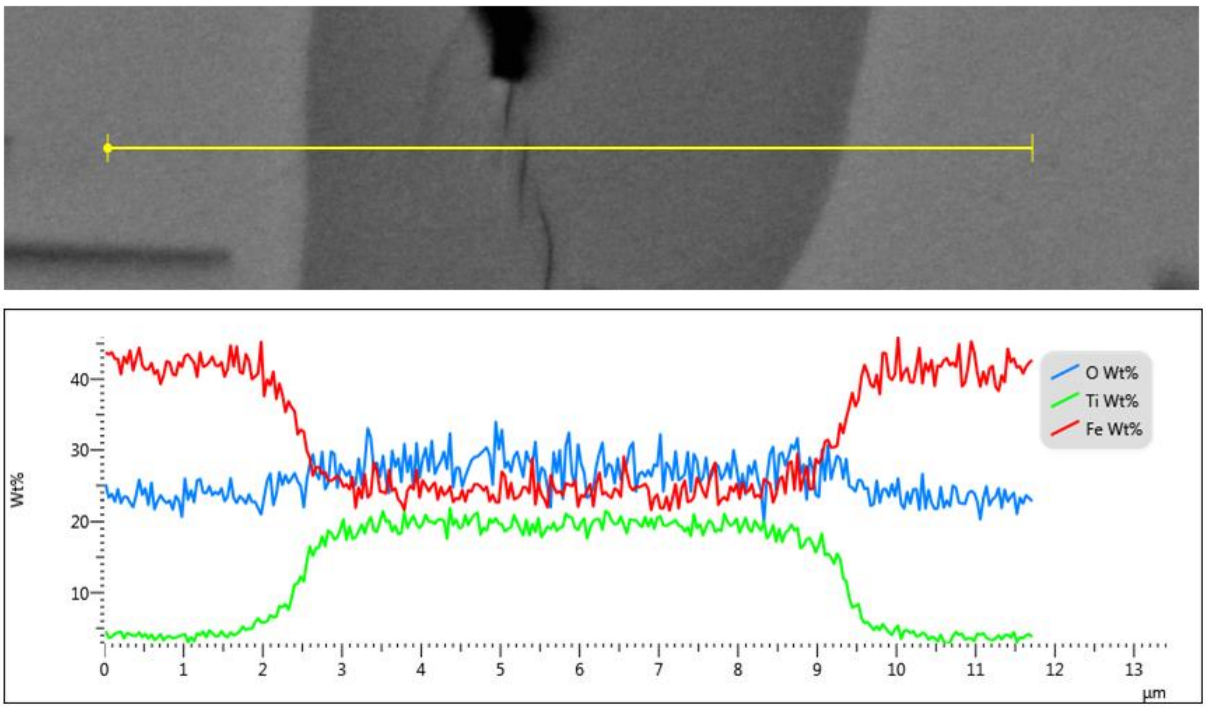

Figure 4.10: Line measurement (Line Data 1) of sample SH1-01 in weight %. Goes from magnetite to ilmenite and back to magnetite. The graph suggests some diffusion between the mineral borders as they are not very steep

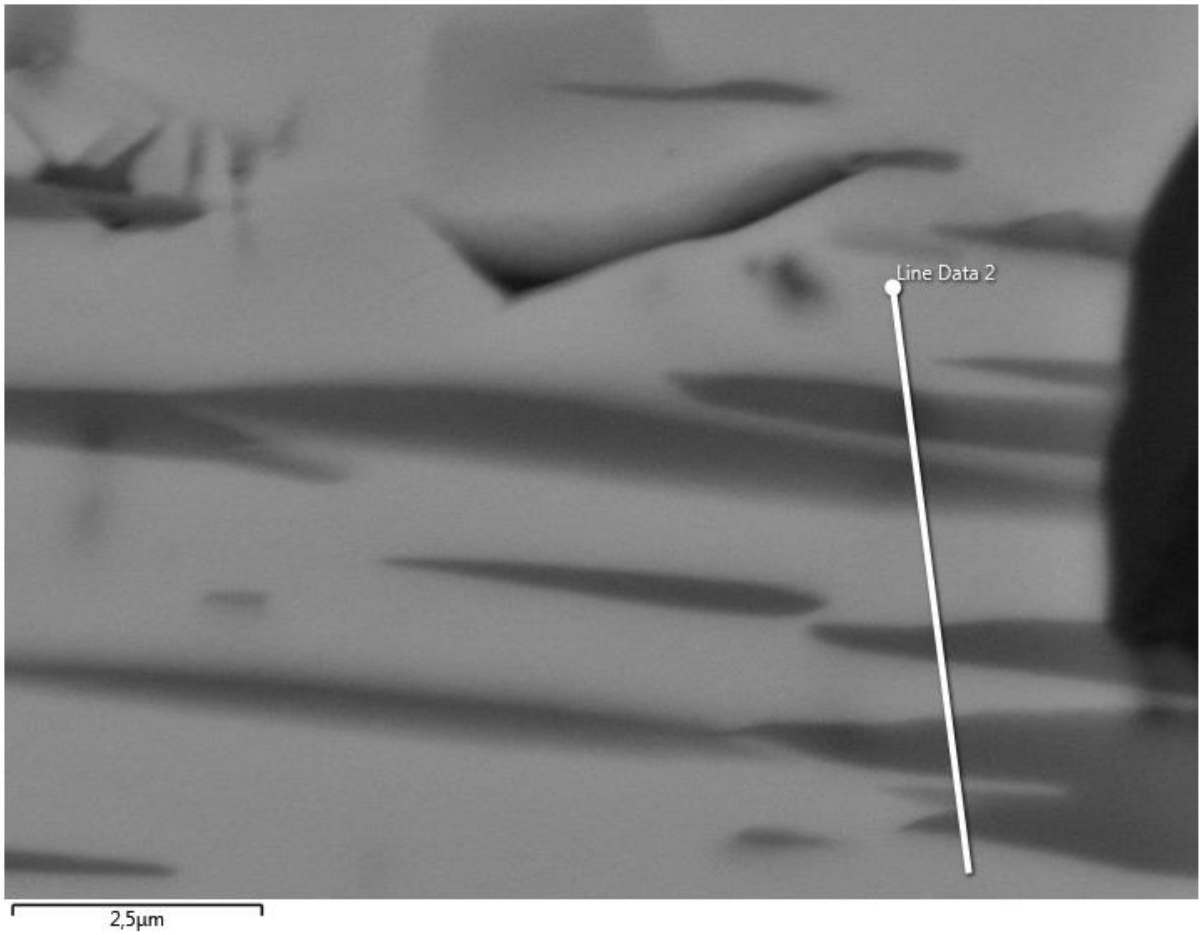

Figure 4.11: Electron backscatter image of sample SH1-03 showing magnetite with rutile lines. Line Data 2 marks line measurement crosscutting rutile lines.

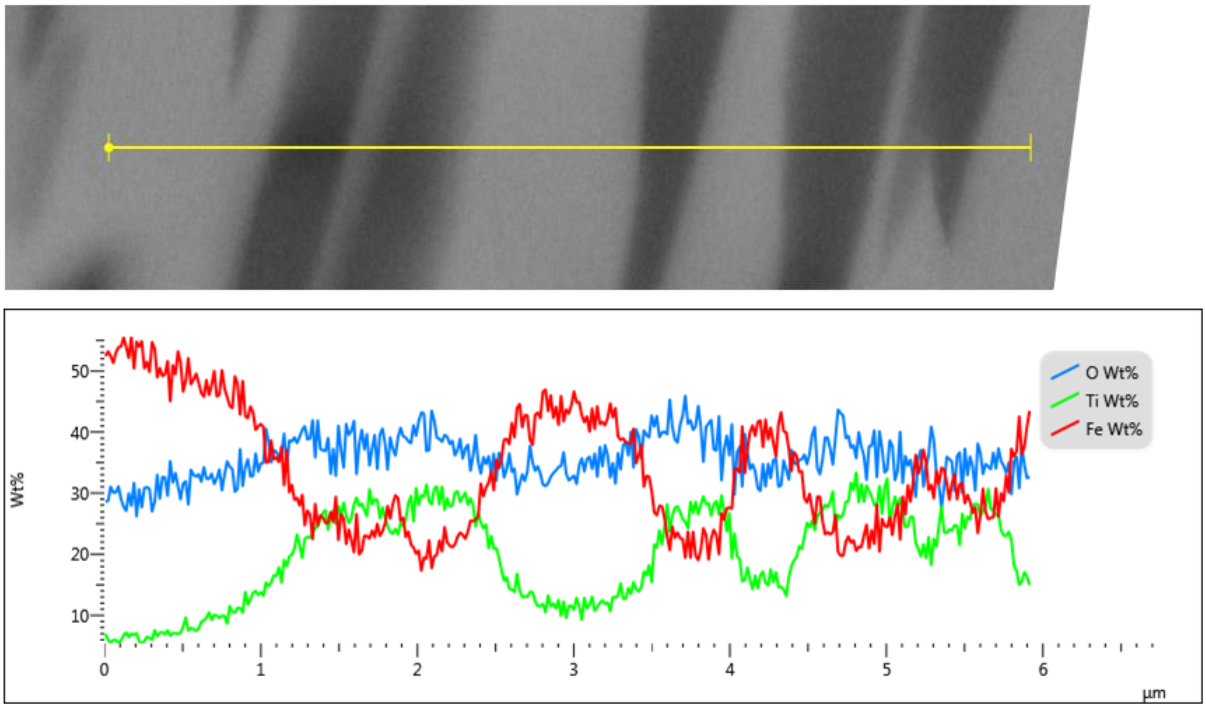

Figure 4.12: Line measurement of sample SH1-03, Line Data 2 (Figure 4.11). Diffusion is likely to have occur as the line graph transition smoothly over the rutile lines.

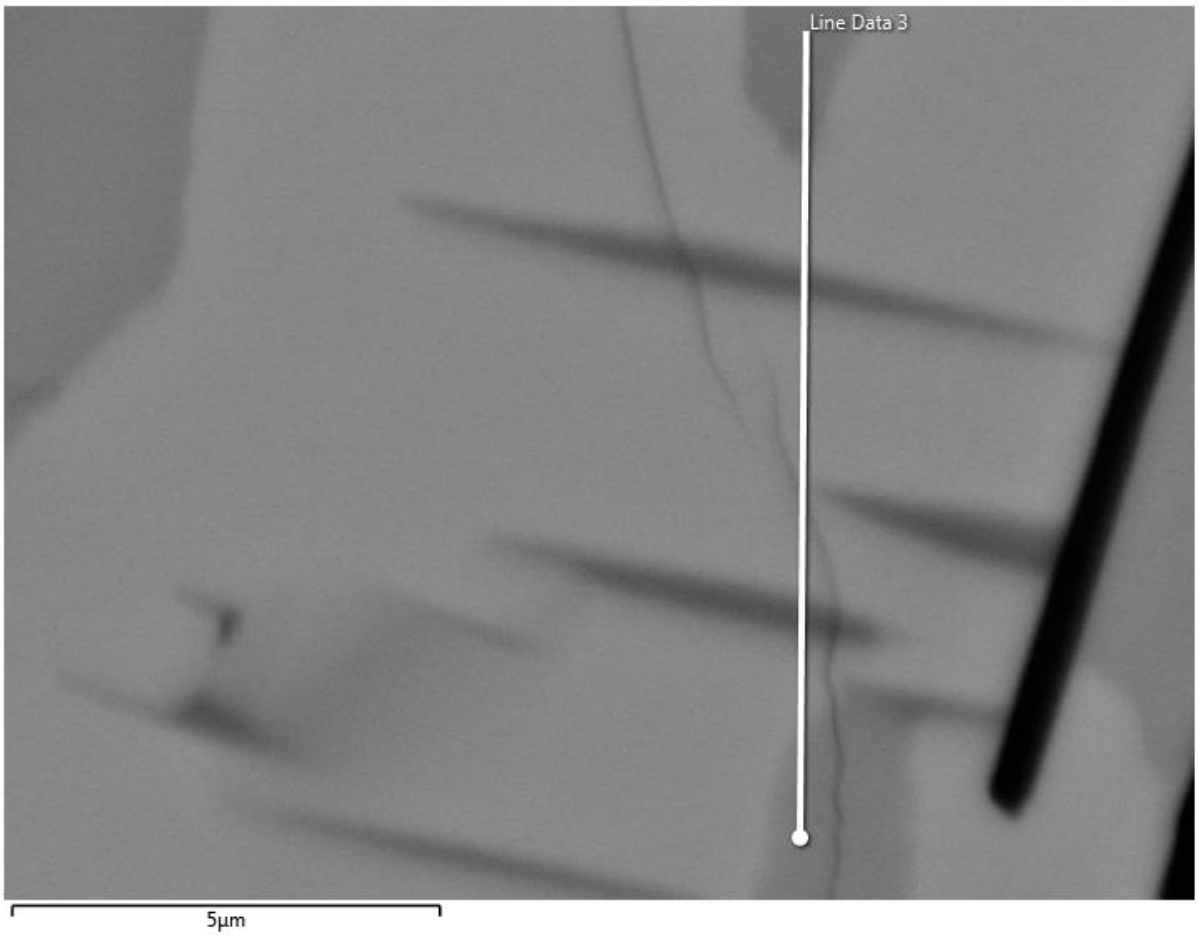

Figure 4.13: Electron backscatter image of SH1-03. Line Data 3 marks a line measurement going through Ilmenite, magnetite and rutile.

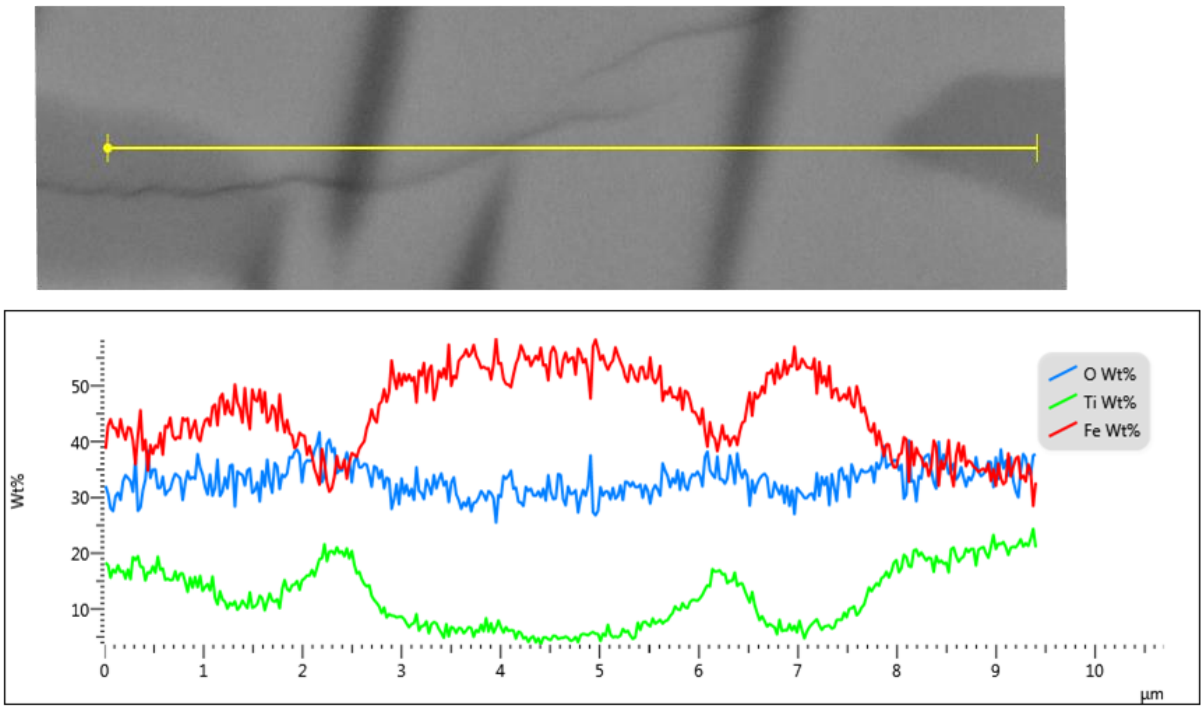

Figure 4.14: Line measurement of sample SH1- 03 of Line Data 3 (Figure 4.13). As for the other line measurements, a diffusion between the different minerals is likely due to smooth transition of the graph over mineral borders.

4.1.3 Jakobsbakken

Sample SJ-01

Table 4.9: Estimated Modal Mineralogy

Mineral	Modal percent	Form
Galena	10 %	Euhedral to anhedral
Pyrrhotite	<5 %	Anhedral
Chalcopyrite?	<<5 %	Anhedral
Quartz	40 %	Anhedral
Carbonate	20 %	Anhedral
Polylithionite	15 %	Euhedral to subhedral
Muscovite	<<5 %	Euhedral to subhedral
Clinozoisite	5-10 %	Anhedral
Organic matter	<5 %	Anhedral

Sample consists of a quartz, carbonate, mica and clinozoisite matrix where quartz is the most abundant mineral. The amount of carbonate is also relatively high compared to the other samples. Quartz appear as both disseminated with small and medium grain sizes, and with larger grains in a monomineralic quartz vein. The same can be said about the carbonate,

but occur in lower amount than quartz. Quartz also show some dynamic recrystallization were subgrain rotation is the dominant process. The grains are slightly elongated and show a grain preferred orientation parallel to micas.

Micas are evenly disseminated throughout the thin section and appear as elongated medium and small sized grains. Most of these grains show an equal orientated

fabric. Clinozoisite is disseminated as small grains, and is similar to the quartz grains in shape, but distinctly separates with grey-bluish and light yellow interference colors.

Galena is found in monomineralic accumulations and disseminated in the matrix. Pyrrhotite and very find-grain chalcopyrite are found disseminated in the matrix.

Organic matter can also be seen in several areas in the thin section, and seems often accumulate around micas or occur as small yellowish patches.

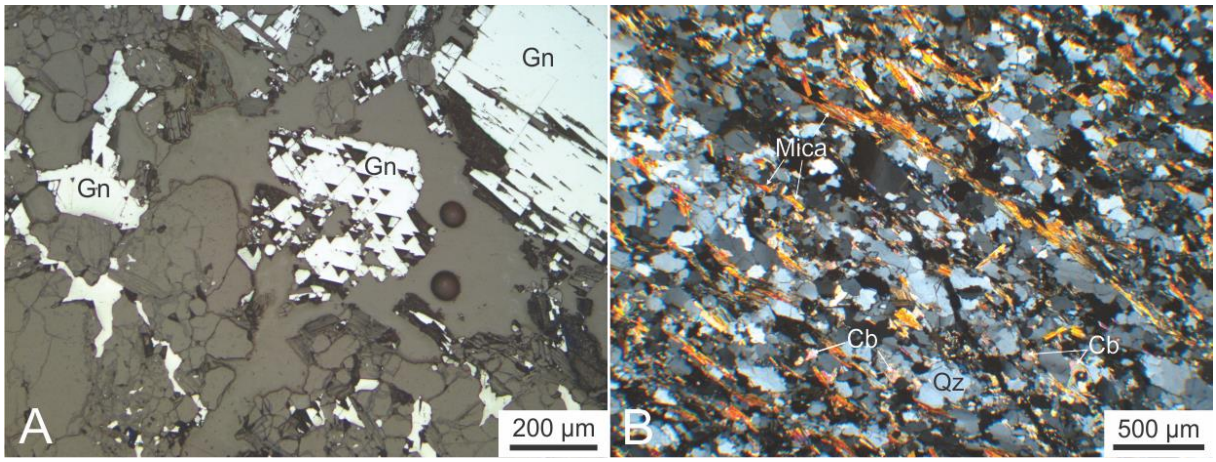

Figure 4.15: Photomicrograph of sample SJ-01. A: Under reflected light in plane polarised light. Showing accumulated galena (Gn) crystals with distinctive polish triangles. B: Under transparent light in XPL. Showing a fine grained layered part with disseminated and thin mica bands and disseminated quartz (Qz) and carbonate (Cb) grains.

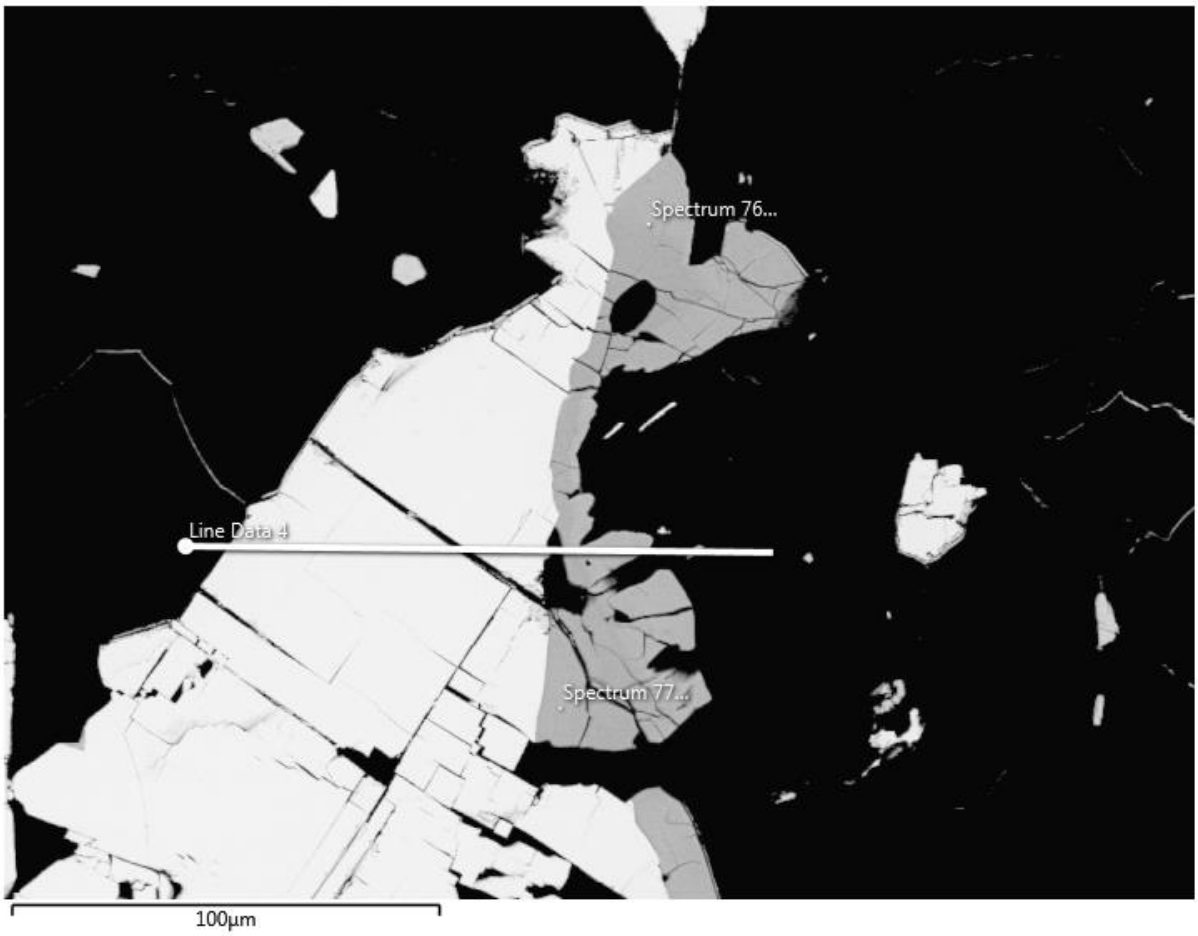

Figure 4.16: Electron backscatter image of sample SJ-01. Line Data 4 shows line measurement of galena (bright gray) and through silver-rich mineral (dark grey). Black areas are other minerals and occur due to contrast settings and are not considered as the focus is on the shift from galena to silver mineral.

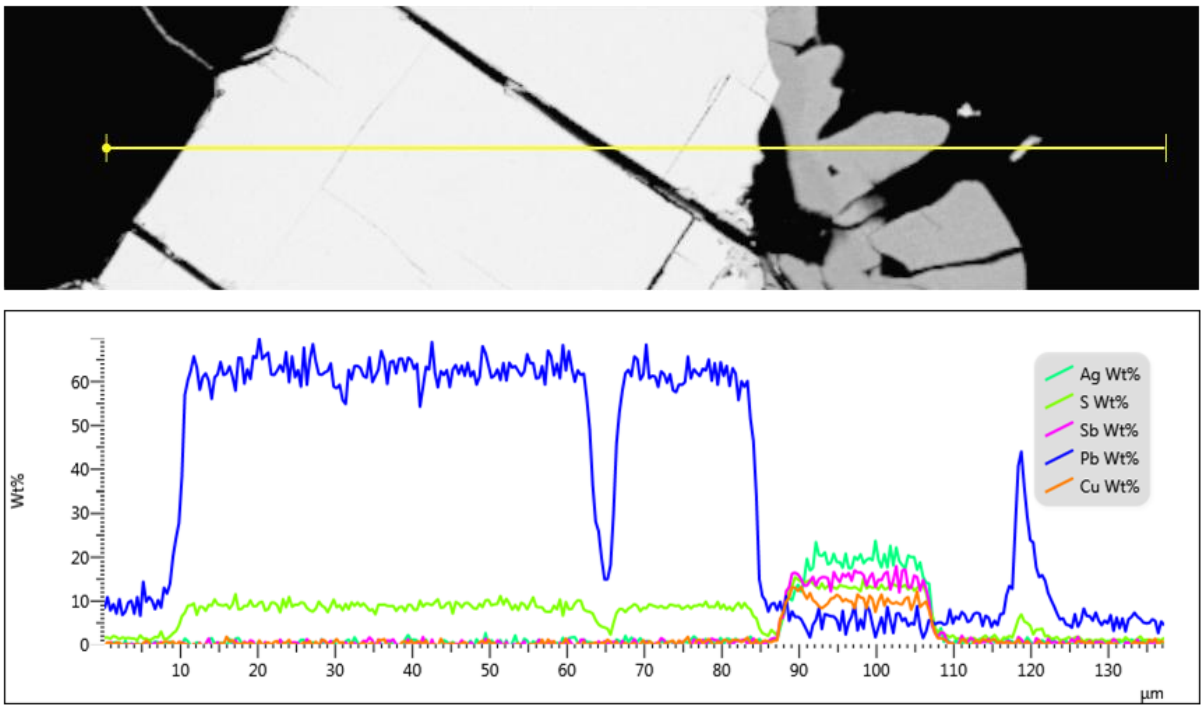

Figure 4.17: Line measurement of sample SJ-01 showing Line Data 4 (Figure 4.17). The graph show negligible amount of silver in galena which could indicate that the silver where removed from galena due to diifusion (mark smooth graph line) and can explain why the silver mineral is attached to galena.

Sample SJ-02

Table 4.10: Estimated Modal Mineralogy

Mineral	Modal percent	Form
Sphalerite	20 %	Anhedral to subhedral
Chalcopyrite	~5 %	Anhedral
Pyrrhotite	<5 %	Anhedral
Quartz	25 %	Anhedral
Plagioclase	15 %	Anhedral to subhedral
Polylithionite	15 %	Euhedral to anhedral
Muscovite?	10 %	Euhedral to anhedral
Rutile	<5 %	Anhedral
Titanite	<5 %	Subhedral
Organic matter	5 %	Anhedral

Sample consists of large amounts of sphalerite, and by far holds the highest amount of sphalerite compared to the other samples. They occur as large clustered grains or disseminated in other areas in the thin section, both along other mineral grain borders or as inclusions inside other grains.

Another dominating mineral is quartz. It occurs as large grains in monomineralic clusters or in the matrix as smaller grains sometimes showing what resembles an annealing texture. Quartz is also found many places in the thin section occurring as areas with smaller grainsizes interacting with micas. The quartz does show undolose extinction and in some cases in the monomineralic clusters, grain boundary migration.

Plagioclase does occur in the thin section as quartz. It can be therefore be difficult to distinguish these two minerals in the thin section, especially in the areas with smaller grainsizes. The plagioclases however does in some rare cases show albite and Carlsbad twinning. The larger grains does also contains many entrapments of other minerals in the thin section, typically sphalerite and mica.

Micas, mostly polylithionite, occur in a substantial amount both as inclusions in plagioclase or overprinting the quartz and plagioclase. Sometimes the mica overprint has random orientated grains, but often they occur in bands with the same orientation. Rare rutile and titanite grains have been identified.

Organic matter is observed several areas in the thin section. It occur as yellowish rims around minerals or as small patches.

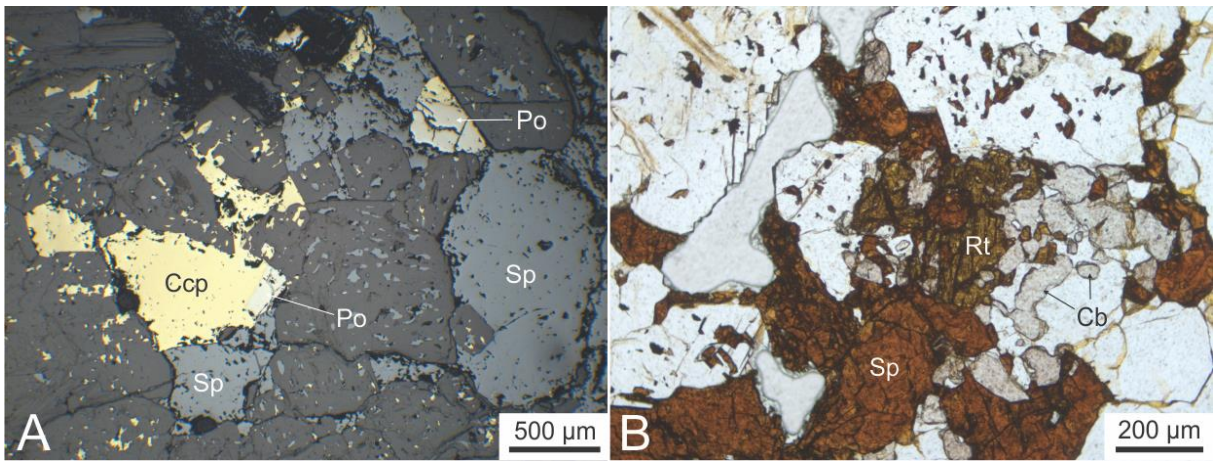

Figure 4.18: Photomicrograph of sample SJ-02. A: Under reflected light in PPL. Showing chalcopyrite (Ccp), sphalerite (Sp) and pyrrhotite (Po). B: Under transparent light in PPL. Showing sphalerite (Sp), rutile (Rt) and carbonate (Cb).

Sample SJ-03

Table 4.11: Estimated Modal Mineralogy

Mineral	Modal percent	Form
Pyrite	30 %	Anhedral
Chalcopyrite	15 %	Anhedral
Sphalerite	10 %	Anhedral
Galena	<<5 %	Anhedral
Pyrrhotite	5 %	Anhedral
Quartz	15 %	Anhedral
Amphibole	5 %	Anhedral
Biotite	10 %	Euhedral
Polylithonite	5 %	Euhedral to subhedral
Muscovite?	<5 %	Euhedral to subhedral
Clinozoisite	<5 %	Anhedral
Carbonate	<5 %	Anhedral
Organic material	<<5 %	Yellowish

Massive sulfide sample consists of large pyrite grains associated with chalcopyrite, sphalerite, pyrrhotite and gangue minerals, mostly quartz and micas. A small amount of galena has been observed within pyrite.

Biotite and polylithionite are observed. Polylithionite occurs both in preferred orientation parallel to biotite, and as larger grains between massive sulfides.

Minor clinozoisite and amphiboles have been observe. Clinozoistite occurs between massive sulfides, but occurs more often disseminated between biotite and polylithionite. Amphiboles are mostly disseminated. Organic matter have been found in irregular patches.

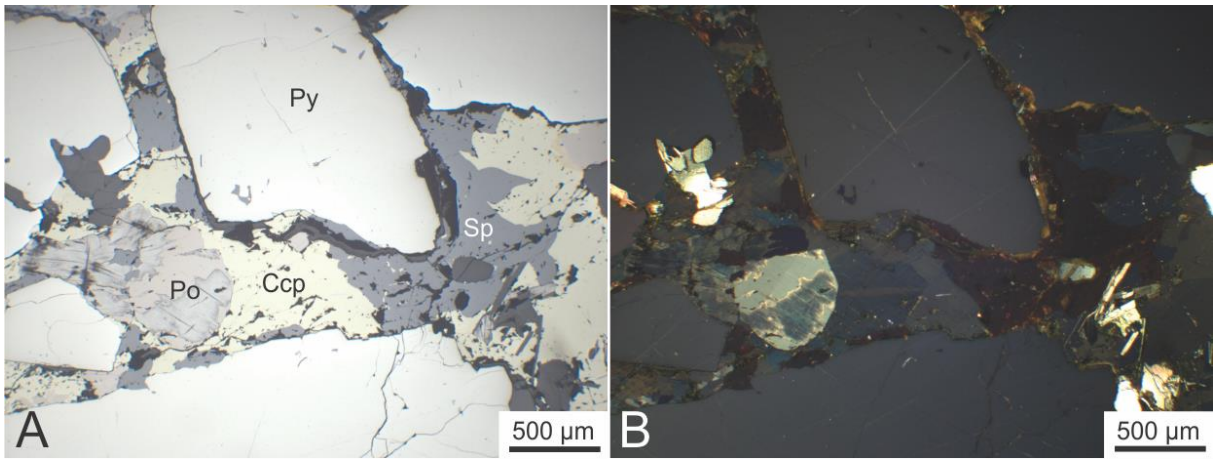

Figure 4.19: Photomicrograph of sample SJ-03 under reflected light. A: In planepolarised light. B: In cross polarised light. Showing large pyrite grains with pyrrhotite (Po), chalcopyrite (Ccp) and sphalerite in between.

Sample SJ-05

Table 4.12: Estimated Modal Mineralogy

Mineral	Modal percent	Form
Pyrite	10 %	Anhedral
Chalcopyrite	<5 %	Anhedral
Sphalerite	<5 %	Anhedral
Quartz	60 %	Anhedral
Muscovite	30 %	Subhedral
Organic material	<<5 %	Anhedral

Sample consists of a quartz and mica matrix with disseminated sulfides. All minerals in the thin section are organized in layers which seems to be caused by deformation. Quartz grains show both undolose extinction and dynamic recrystallization as a good evidence towards deformation. The grains are also often slightly elongated and orientated according to the orientation of the layers in the thin section. The "original" grains occur in general as either large mineral grain clusters or as medium mineral grain clusters. The medium sized grains dominate, but they both show recrystallization. The dominating recrystallization process seems to be subgrain rotation and some involvement of grain boundary rotation. The presence of recrystallized grains in the thin section are clear, but the overall amount is not very high. Some areas with quartz show dense cracking.

Muscovite is sometimes bent around other more competent grains (quartz, pyrite), but in general they are orientated along the layers in the thin section as single grains or as banded. They occur mostly as medium sized, but also as small grains. The interference colors are in parts of the thin section very low and possibly too low to actually be muscovite. Some presence of other mica should be considered, possibly poliylithionite.

Disseminated sulfides are dominated by pyrite with minor amounts of chalcopyrite and sphalerite. As the rest of the minerals, the orientation and distribution of the sulfides follow the general layering in the thin section. Pyrite grains are often elongated, but some grains are a bit more preserved. In these more preserved areas, chalcopyrite is observed in low amounts between and attached to pyrite grains. Some pyrite grains with dense cracks are also observed. Sphalerite occurs as small grains distributed in the matrix, but does very often seem to be incorporated in mica bands. Small patches organic matter are recorded as well.

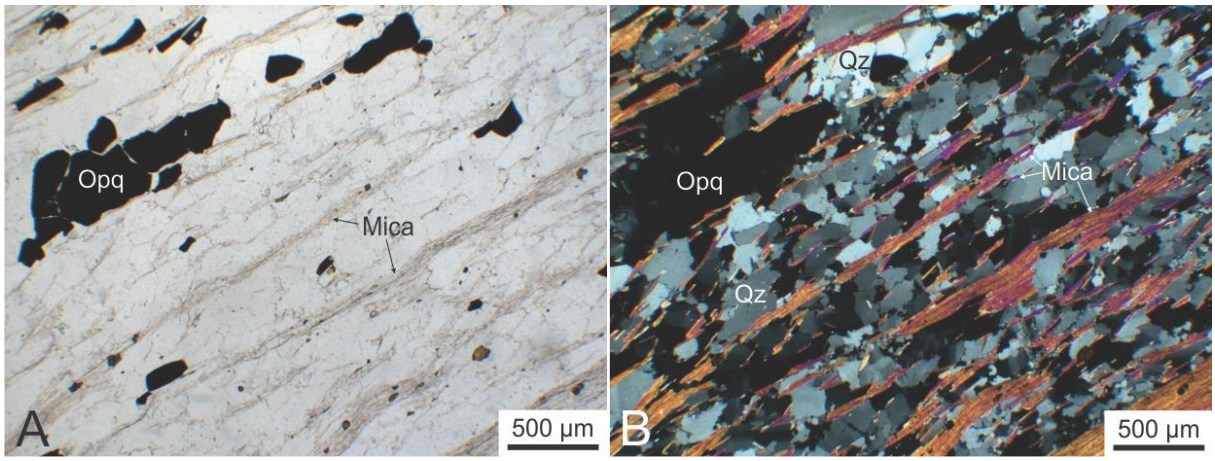

Figure 4.20: Photomicrograph of sample SJ-05. A: In plane polarised light. B: In crossed polarised light. Showing disseminated opaque (Opq) minerals in a quartz (Qz) and mica matrix, all with the same grain preferred orientation.

4.1.4 Ny-Sulitjelma

Sample SNY-001

Table 4.13: Estimated Modal Mineralogy

Mineral	Modal percent	Form
Pyrite	20 %	Euhedral to anhedral
Sphalerite	<5 %	Anhedral
Magnetite?	<5 %	Anhedral
Quartz	40 %	Anhedral
Plagioclase	25 %	Anhedral
Chlorite	20 %	Subhedral
Clinozoisite	<5 %	Anhedral
Organic material	<5 %	Anhedral

Thin-Section Description

This sample consists of a quartz, plagioclase and chlorite matrixThere is a substantial amount of pyrite disseminated within the matrix. Pyrite seems to be mostly deformed and is accumulated in layers probably as a result of the deformation. Some grains is disseminated randomly in the thin section where some of these grains which in general has a smaller grainsize, has preserved a cubic crystal shape. Some minor amounts of sphalerite and magnetite are also observed.

Quartz is sometimes accumulated in clusters or veins as larger grains, but most of the areas is dominated by a mix of quartz, plagioclase and chlorite. In these areas distinguishing these

three minerals from one another is challenging. There is also in these areas a high amount recrystallized grains due to bulging and subgrain rotation.

This sample also contains traces of organic matter.

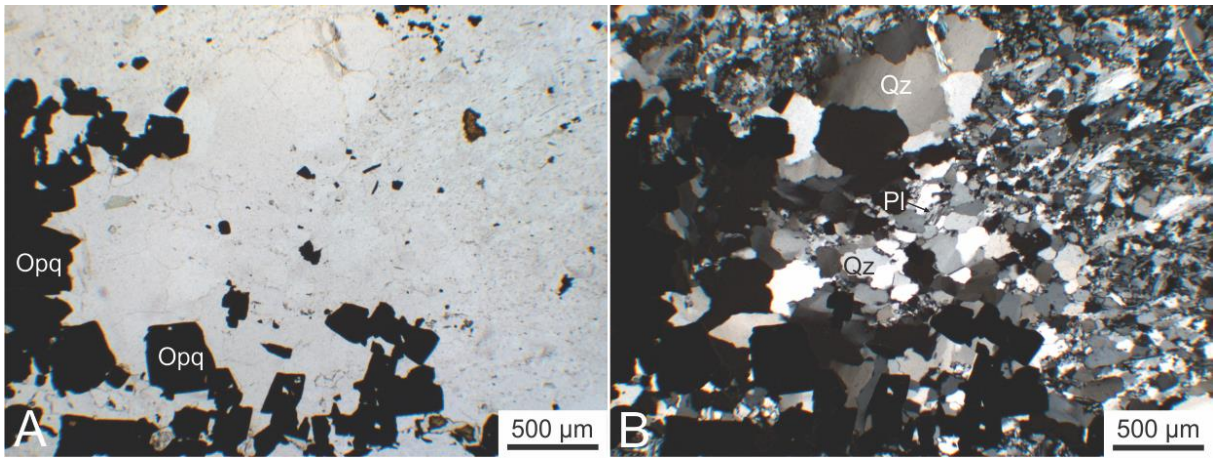

Figure 4.21: Photomicrograph of sample SNY-001 under transparent light. A: In plane polarised light. B: In cross polarised light. Showing disseminated opaque (Opq) minerals in a quartz (Qz) and plagioclase (Pl) matrix.

Sample SNY-002

Table 4.14: Estimated Modal Mineralogy

Mineral	Modal percent	Form
Pyrite	25 %	Anhedral to subhedral
Chalcopyrite	<5 %	Anhedral
Sphalerite	<<5 %	Anhedral
Quartz	55 %	Anhedral
Muscovite	15 %	Subhedral
Organic matter	<5 %	Anhedral

Thin-Section Description

The thin section is dominated by a quartz and muscovite matrix with layers of pyrite possibly overprinted. The sample is heavily affected by deformation and in general all of the minerals are organized in layers with the same shape preferred orientation. Quartz which is the most abundant mineral in the thin section is affected by substantial recrystallization dominated by subgrain rotation. The “original” grains are elongated and surrounded by small recrystallized rounded grains. There are also some quartz veins with larger grains, but these also follow the orientation of the layers as the other grains do. Most of the quartz grains also show undolose extinction.

Muscovite occur mostly as small single grains evenly disseminated throughout the thin section, but some areas typically close to pyrite grains, the muscovite grains are larger and appear more bent around pyrite grains.

The pyrite grains appear as quartz heavily deformed, with elongated grains. Some however does show remnants of their cubic crystal system. In between pyrite grains in some places, low amounts of chalcopyrite and even lower amounts of sphalerite is observed.

Brownish light-yellow material which appear as organic matter is observed many places in the sample as small patches or rims along grain borders.

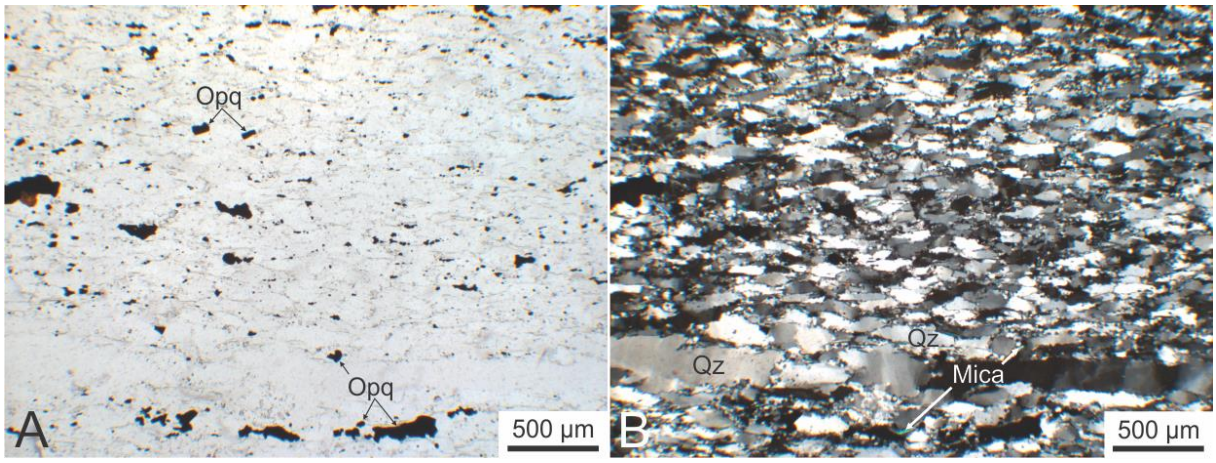

Figure 4.22: Photomicrograph of sample SNY-002 under transparent light. A: In plane polarised light. B: In crossed polarised light. Showing disseminated opaque (Opq) minerals in a quartz (Qz) and mica matrix. Around the quartz grains there are small recrystallized grains.

Sample SNY-003

Table 4.15: Estimated Modal Mineralogy

Mineral	Modal percent	Form
Pyrite	10 %	Subhedral to anhedral
Chalcopyrite	<5 %	Anhedral
Sphalerite	5 %	Anhedral
Quartz	40 %	Anhedral
Biotite	20 %	subhedral
Carbonate	15 %	Anhedral
Chlorite	<5 %	Anhedral

Thin-Section Description

The thin section consists of a quartz, mica and carbonate matrix with disseminated pyrite and sphalerite. Quartz is the most abundant mineral in the thin section. The grains are generally small, but there is some variation in sizes. This variation is evenly spread as a homogeneous texture throughout the thin section. The grains also have a rather random shape, but could seem to show some grain boundary migration texture?

The mica seems be mostly biotite where some is altered to chlorite. The biotite is evenly disseminated throughout the thin section with weak grain preferred orientations. There seem to be some small/very small grains of muscovite, but they are difficult to spot.

Carbonates occur in one vein as medium sized grains, but in general they are disseminated throughout the thin section as small grains. They show however often a slightly larger size than the mica and quartz grains.

Pyrite and sphalerite are also disseminated throughout the thin section. Of these, pyrite is the most occurring. The pyrite shows medium to small sizes with subhedral to anhedral shapes. The sphalerite is much less abundant with a smaller and anhedral grainsize.

Some grains of what seems to be alteration from biotite to chlorite is observed.

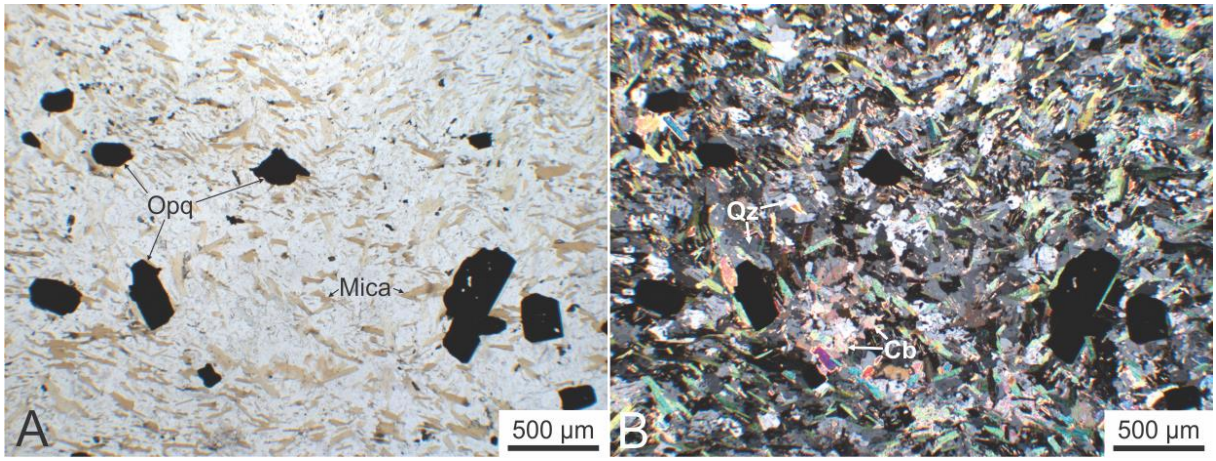

Figure 4.23: Photomicrograph of sample SNY-003 under transparent light. A: In plane polarised light. B: In crossed polarised light. Showing disseminated opaque minerals in a quartz (Qz), carbonate (Cb) and mica matrix.

Sample SNY-004

Table 4.16: Estimated Modal Mineralogy

Mineral	Modal percent	Form
Pyrite	10 %	Anhedral to subhedral
Chalcopyrite	5 %	Anhedral
Sphalerite	5 %	Anhedral
Quartz	50 %	Anhedral
Muscovite	30 %	Subhedral
Organic matter	<5 %	Light brown

Thin-Section Description

The thin section consists of a layered quartz and muscovite matrix with disseminated sulfides. Quartz is the most abundant mineral and wary in grainsize. The largest grains are accumulated in clusters or veins orientated according to the layers in the thin section. These grains are often slightly elongated and does usually show undolose extinction. The smaller grains are more evenly disseminated in the thin section and does often show a more random or annealed texture. Some recrystallization does

occur related to both of the quartz “categories” which seems to be subgrain rotation, but this is poorly developed.

Muscovite occurs in large quanta as massive bands or as small evenly disseminated grains. The bands show a general orientation along the layers in the thin section, but are also folded and bent around quartz grains.

Among the sulfides, pyrite is the most abundant mineral. The pyrite grains are disseminated throughout the thin section, but are also to some degree accumulated in poorly developed layers, which follow the general layering in the thin section. Chalcopyrite is found some areas close to pyrite grains, mostly along the top layer. Some of the smaller sulfide grains from pyrite, chalcopyrite and sphalerite are found incorporated muscovite bands.

The sphalerite is also disseminated. The larger ones are usually found close to or attached to pyrite grains. The smaller ones on the other hand is often found incorporated into the muscovite bands (maybe some remobilization of sphalerite?).

A small amount of organic matter is observed some places in the thin section either as patches or surrounding or in between of mineral grains.

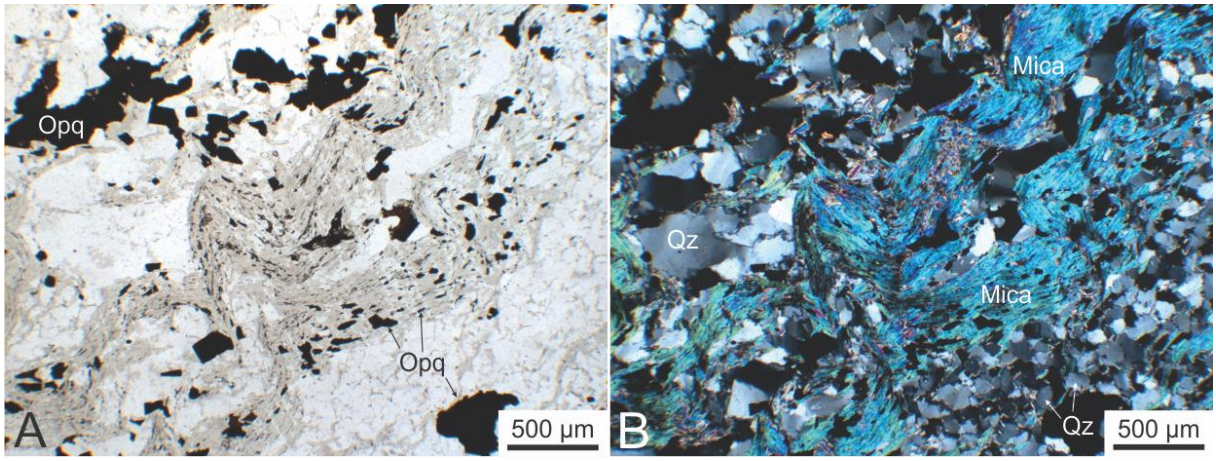

Figure 4.24: Photomicrograph of sample SNY-004 under transparent light. A: In plane polarised light. B: In cross polarised light. Showing disseminated opaque (Opq) minerals, massive mica bands and a quartz matrix.

4.1.5 Sagmo

Sample SS-01

Table 4.17: Estimated Modal Mineralogy

Mineral	Modal percent	Form
Pyrrhotite	20 %	Anhedral
Chalcopyrite	15 %	Anhedral
Sphalerite	<5 %	Anhedral
Quartz	30 %	Anhedral
Polylithionite	15 %	Subhedral
Muscovite?	5 %	Subhedral
Plagioclase	5 %	Anhedral
Weathering product	15 %	Anhedral
Carbonate	<5 %	Anhedral
Clinosoizite	<5 %	Anhedral
Organic matter	5 %?	Anhedral
Amphibole?	<<5 %	Subhedral
???	<<5 %	Anhedral

Thin-Section Description

The thin section consist of a quartz and mica matrix where large parts are weathered (seen as brown areas consisting of?). Large parts of the thin section are layered, but some parts does also show a more random grain distribution and orientation.

There is also a substantial amount of sulfides, where pyrrhotite and chalcopyrite dominates. These the grains are often large. A low amount of sphalerite is observed which seems to be more random disseminated, but is also often observed together with mica.

Quartz which is the most abundant mineral in the thin section, occur in all sizes from large to small. In some areas they show recrystallization with subgrain rotation being the dominant process. In the more layered parts of the thin section, the grains are often elongated and orientated parallel to the layering. Some single random disseminated plagioclases with albite twinning are also observed. The amount could be higher than described, since distinguishing quartz from plagioclase can be challenging if they don’t show any twinning.

The mica grains vary from typical muscovite interference colors, to grains with much lower order of colors (often first order gray and yellow). It is uncertain how many types of mica that occur in the thin section, but based on XRD from the similar sample SS-02, it is possible that everything is polylithionite.

Many areas show a light yellowish brown color which could be organic matter. It can be difficult to distinguish from weathering product, so the amount is uncertain.

One unidentified mineral which could be amphibole (due to cleavage) is observed. Show low interference colors (first order gray with yellowish tint). Another with deep blue interference colors is also observed (seen in other thin sections, but still unidentified).

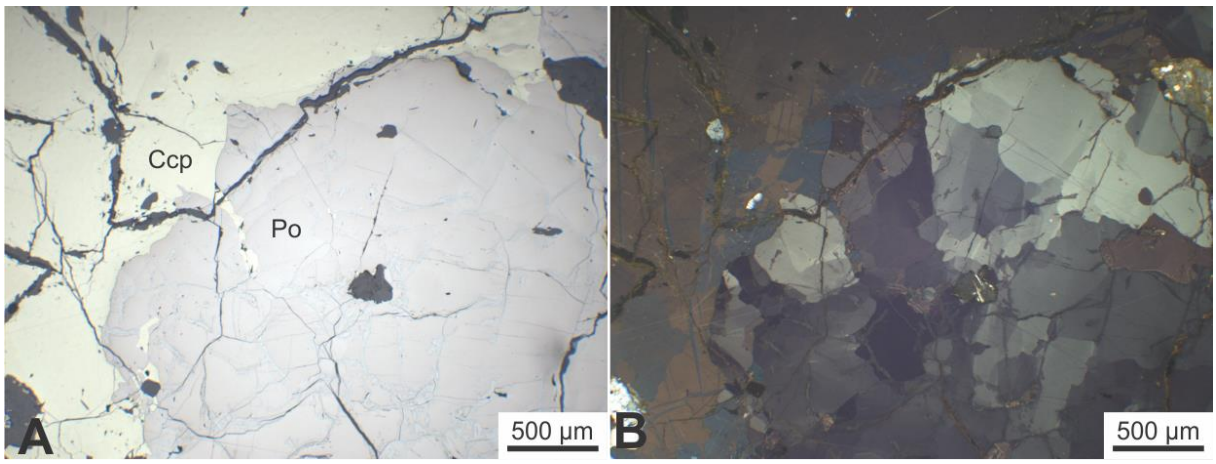

Figure 4.25: Photomicrograph of sample SS-01 under reflected light. A: In plane polarised light. B: In cross polarised light. Showing pyrrhotite (Po) next to chalcopyrite (Ccp).

Sample SS-02

Table 4.18: Estimated Modal Mineralogy

Mineral	Modal percent	Form
Chalcopyrite	20 %	Anhedral
Pyrrhotite	20 %	Anhedral
Sphalerite	5 %	Anhedral
Quartz	25 %	Anhedral
Polylithionite	25 %	Euhedral
Carbonate	<<5 %	Euhedral
Weathering product	5 %	Anhedral
Organic matter	5 %	Anhdral

Thin-Section Description

The thin section consists of a quartz and mica matrix with disseminated sulfides. Quartz occur in different grainsizes and mica are overprinting the quartz. The quartz grains are highly heterogeneous, where they show different sizes and some show undolose extinction. They also show dynamic recrystallization with seems to be both grain boundary migration and subgrain rotation. Some of the grains seems to be annealed as well. These are typically smaller grains and seems to possibly first occur as recrystallized grains before they were are annealed.

The mica has low interference colors and is often banded. The orientation is to some degree following a layered pattern, but seems also to be folded and often completely random. XRD analysis show that this could be the lithium rich mica; polylithionite. However for clarification, polylithionite is one among other overlapping possibilities from the XRD results. Based on interference colors however,

polylthionite is a plausible match. Polylithionite is the Li-high endmember of lepidolite and in terms of paragenisis, they are usually associated with granite pegmatites which doesn't really fit well with the location. On the other hand there are also examples from high temperature hydrothermal veins, aplites and granites. When adding that one of the general theory's for the origin of most leidolites is due to metasomatic replacement of muscovite or biotite, the occurence of polylithionite in this and many of the other samples could be a fair suggestion (Deer et al., 1992).

Among the sulfides, pyrrhotite and chalcopyrite dominates. They show a very large grainsize and covers large parts of the thin section. There seems also to be sphalerite as small disseminated grains found in some places in the thin section. They are often accumulated within mica bands. Surrounding some of the small sphalerite grains, a low amount of could be carbonate is observed. These possible carbonate grains are also observed as small grains "alone".

Many brown areas in the thin section seem to be a weathering product. There is also patches of a lighter brownish yellow color, which seems to be organic matter.

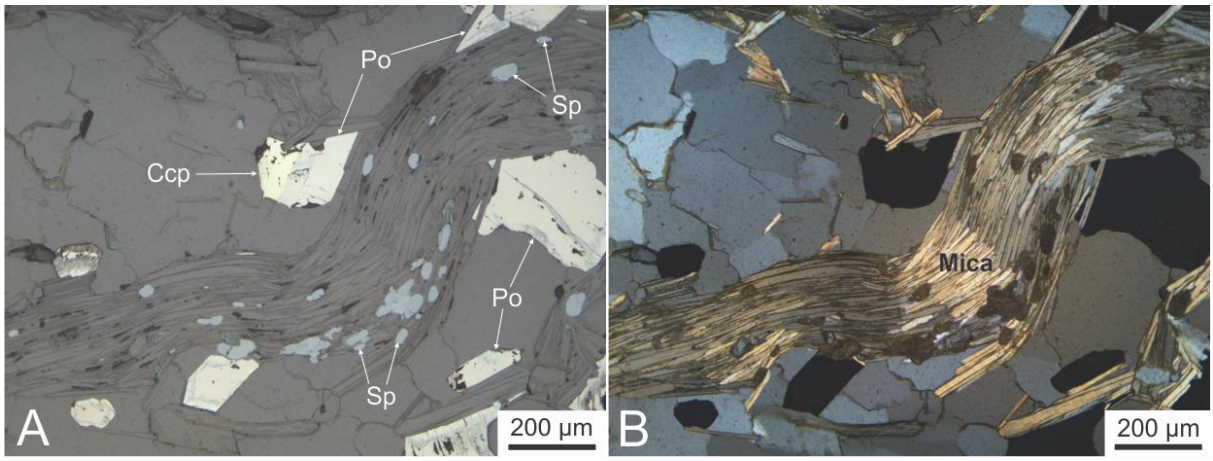

Figure 4.26: Photomicrograph of sample SS-02 under reflected light. A: In plan polarised light. B: In crossed polarised light. Showing small sphalerite (Sp) grains incorporated within mica band. Pyrrhotite (Po) and chalcopyrite (Ccp) are disseminated in other areas of the picture in a gangue matrix.

Sample SS-04

Table 4.19: Estimated Modal Mineralogy

Mineral	Modal percent	Form
Pyrrhotite	15 %	Anhedral
Chalcopyrite	5-10 %	Anhedral
Sphalerite	<5 %	Anhedral
Quartz	30 %	Anhedral
Polylithionite	20 %	Euhedral
Muscovite?	<5 %	Euhedral
Weathering product	5 %	Anhedral
Organic matter	5 %	Anhedral
Carbonate?	<<5 %	Anhedral

Thin-Section Description

Almost identical to SS-02, but some mica grains show muscovite interference colors like SS-01 and there is one area with cracked quartz.

The major part of the thin section consists of quartz and polylithionite with a substantial amount of sulfides. There is also some amount of weathering product and organic material either as medium small patches or surrounding mineral grains. These can be difficult to distinguish from each other.

Quartz grains are found throughout the thin section and occur in various grainsizes. Many grains does show undolose extinction and some also weak grain boundary migration. It is uncertain if the smaller grains are formed due to recrystallization because the grainsize among the smaller grains also vary, but some influence of subgrain rotation is not unlikely.

The pyrrhotite and chalcopyrite occur unevenly distributed in the thin section. These to minerals are usually accumulated and attached together in anhedral patches of large grains. The grain shapes are random and to distinguish cracks from grain borders are difficult. They also occur as more disseminated and smaller grains.

Small grains of sphalerite is also observed in a low amount. They are spread randomly around the thin section or seems to be incorporated in mica bands.

Polylithionite is found in large amounts throughout the thin section. They are typically accumulated in massive bands were the grains follow the same orientation. They are however also found as more disseminated grains with random orientations. Some of the grains show higher interference colors and it is uncertain if these grains are actually muscovite.

A low amount of what seems to be carbonate is observed. The grains is small and it is difficult to be sure that it actually is carbonate. In one case it is seen surrounding two sphalerite grains.

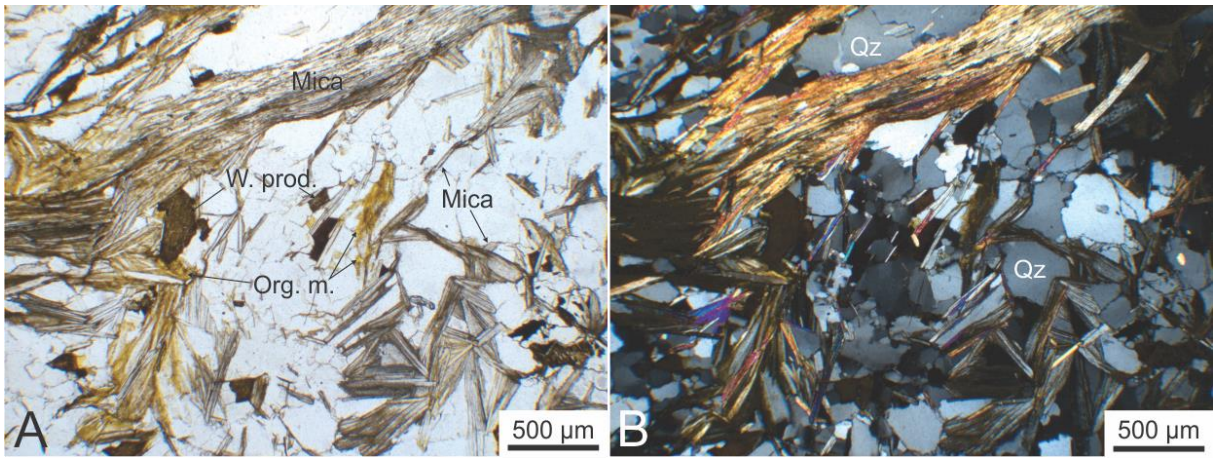

Figure 4.27: Photomicrograph of sample SS-04 under transparent light. A: In plane polarised light. B: In crossed polarised light. Showing banded and disseminated mica in a quartz (Qz) matrix with the presence of weathering product (W. prod.) and organic matter (Org. m.).

4.1.6 Chemical analyses

4.1.6.1 Hitachi TM3030 Tabletop SEM

Table 4.20: *Sulfides*

Sample	Mineralogy	Measurement	S	Fe	Cu	Zn	Pb
			Mass-% (norm.)	Mass-% (norm.)	Mass-% (norm.)	Mass-% (norm.)	Mass-% (norm.)
SH1-03	Pyrite	1	58,67	41,33	0,00	0,00	0,00
SH1-03	Pyrite	2	51,02	48,98	0,00	0,00	0,00
SH1-03	Pyrite	3	47,81	52,19	0,00	0,00	0,00
SJ-01	Pyrrhotite	4	37,69	62,31	0,00	0,00	0,00
SJ-02	Galena	5	12,50	0,00	0,00	0,00	87,50
SJ-01	Sphalerite	6	36,99	8,63	0,00	54,38	0,00
SJ-01	Sphalerite	7	32,54	9,67	0,00	57,79	0,00
SJ-01	Galena	8	9,30	0,00	0,00	0,00	90,70
SJ-01	Sphalerite	9	32,77	10,03	0,00	57,20	0,00
SJ-03	Pyrite	10	48,43	51,57	0,00	0,00	0,00
SG-01	Galena	11	19,02	0,00	0,00	0,00	80,98
SG-01	Sphalerite	12	36,68	13,21	0,00	50,11	0,00
SG-01	Pyrite	13	52,25	47,75	0,00	0,00	0,00
SG-01	Chalcopyrite	14	40,11	31,80	28,09	0,00	0,00
SG-01	Pyrite	15	48,88	51,12	0,00	0,00	0,00
SG-01	Sphalerite	16	36,57	10,42	0,00	53,01	0,00
SG-01	Galena?	17	20,32	15,18	0,00	0,00	64,50

Table 4.21: *Oxides*

Sample	Mineralogy	Measurement	O	Ti	V	Cr	Mn	Fe
			Mass-% (norm.)	Mass-% (norm.)	Mass-% (norm.)	Mass-% (norm.)	Mass-% (norm.)	Mass-% (norm.)
SNY-001	Rutile	1	51,26	45,70	0,00	0,00	0,00	3,04
SNY-001	Rutile	2	48,96	44,96	0,00	0,00	0,00	6,08
SNY-001	Rutile	3	56,03	43,97	0,00	0,00	0,00	0,00
SH1-03	Iron oxide/hydroxide	4	67,85	0,00	0,00	0,00	0,00	32,15
SH1-03	Titanomagnetite	5	39,18	12,35	0,00	0,00	0,00	48,47
SH1-03	Magnetite	6	28,41	0,00	0,00	0,00	0,00	71,59
SJ-02	Rutile	7	43,23	56,77	0,00	0,00	0,00	0,00
SJ-02	Rutile	8	51,41	48,59	0,00	0,00	0,00	0,00
SG-02	Rutile	9	53,64	45,42	0,00	0,00	0,00	0,94
SG-02	Rutile	10	56,43	42,91	0,00	0,00	0,00	0,66

Table 4.22: *Silcates*

Sample	Mineralogy	Measurement	O	Na	Mg	Al	Si	K	Ca	Ti	Fe	Zr
			Mass-% (norm.)	Mass-% (norm.)	Mass-% (norm.)	Mass-% (norm.)	Mass-% (norm.)	Mass-% (norm.)	Mass-% (norm.)	Mass-% (norm.)	Mass-% (norm.)	Mass-% (norm.)
SNY-001	Titanite	1	43,80	0,00	0,70	1,87	12,20	0,00	17,07	18,87	5,48	0,00
SH1-03	Biotite	2	44,68	0,00	7,33	8,91	18,33	6,88	0,00	1,57	12,29	0,00
SH1-03	Paragonite	3	46,43	7,81	1,26	10,28	29,00	1,03	0,00	0,00	4,20	0,00
SJ-01	Chlorite	4	53,52	0,00	5,44	6,75	27,28	0,92	3,00	0,00	3,09	0,00
SJ-01	Muscovite	5	50,55	0,00	2,05	12,62	28,14	3,39	1,91	0,00	1,34	0,00
SJ-01	Clinozoisite	6	50,05	0,00	1,09	10,51	24,87	0,00	10,26	0,00	3,22	0,00
SJ-02	Titanite	7	46,10	0,00	0,00	0,00	14,39	0,00	18,17	21,34	0,00	0,00
SJ-02	Titanite	8	38,90	6,49	0,00	2,22	14,21	0,00	16,53	18,29	3,36	0,00
SJ-03	Titanite	9	46,66	0,00	0,00	2,45	16,48	0,00	15,46	18,94	0,00	0,00
SG-02	Albite	10	49,26	9,00	0,00	10,12	30,02	0,00	0,00	0,00	1,61	0,00
SG-02	Albite	11	49,77	9,03	0,00	10,35	30,85	0,00	0,00	0,00	0,00	0,00
SG-02	Albite	12	49,76	9,07	0,00	10,13	31,05	0,00	0,00	0,00	0,00	0,00
SG-02	Biotite	13	46,86	2,75	7,42	7,59	20,82	5,42	0,00	1,07	8,08	0,00
SG-02	Zircon	14	40,39	2,79	0,00	3,05	18,83	0,00	0,00	0,93	0,00	34,00

Table 4.23: *Carbonates*

Sample	Mineralogy	Measurement	C	O	Ca	Fe
			Mass-% (norm.)	Mass-% (norm.)	Mass-% (norm.)	Mass-% (norm.)
SJ-01	Carbonate	1	19,30	41,66	39,04	0,00
SJ-01	Carbonate	2	18,32	43,04	38,64	0,00
SJ-01	Carbonate	3	18,05	44,49	37,46	0,00
SG-02	Carbonate	4	16,87	51,37	30,31	1,45

Table 4.24: *Sulfates*

Sample	Mineralogy	Measurement	O	S	Ca	Ba
			Mass-% (norm.)	Mass-% (norm.)	Mass-% (norm.)	Mass-% (norm.)
SG-02	Baryte	1	37,29	16,82	5,11	40,78
SG-02	Gypsum	2	53,84	21,27	24,89	0,00
SG-02	Baryte	3	37,21	16,05	0,00	46,74

4.1.6.2 Zeiss Merlin FE-SEM

Table 4.25: *Sulfides*

Sample	Mineralogy	Measurement	S	Ti	Mn	Fe	Co	Cu	Zn	As	Mo	Ag	Sb	Pb
			Wt% (norm.)	Wt% (norm.)	Wt% (norm.)	Wt% (norm.)	Wt% (norm.)	Wt% (norm.)	Wt% (norm.)	Wt% (norm.)	Wt% (norm.)	Wt% (norm.)	Wt% (norm.)	Wt% (norm.)
SG-01	Sphalerite	Spectrum 2	32,77	0,01	0,06	9,75	0,12	0,34	54,09	0,01	2,00	0,00	0,02	0,00
SG-01	Sphalerite	Spectrum 3	34,67	0,00	0,00	9,72	0,00	0,36	55,26	0,00	0,00	0,00	0,00	0,00
SG-01	Sphalerite	Spectrum 4	34,41	0,00	0,03	10,07	0,00	0,41	55,08	0,00	0,00	0,00	0,00	0,00
SG-01	Sphalerite	Spectrum 5	34,30	0,00	0,04	10,05	0,00	0,59	55,02	0,00	0,00	0,00	0,00	0,00
SG-01	Sphalerite	Spectrum 6	34,61	0,00	0,06	9,89	0,00	0,00	55,44	0,00	0,00	0,00	0,00	0,00
SG-01	Sphalerite	Spectrum 7	34,38	0,04	0,00	9,89	0,00	0,42	55,27	0,00	0,00	0,00	0,00	0,00
SG-01	Sphalerite	Spectrum 8	34,16	0,05	0,08	9,88	0,00	0,50	55,32	0,00	0,00	0,00	0,00	0,00
SG-01	Sphalerite	Spectrum 9	34,18	0,00	0,13	10,16	0,00	0,67	54,86	0,00	0,00	0,00	0,00	0,00
SG-01	Sphalerite	Spectrum 10	34,32	0,00	0,11	9,76	0,00	0,00	55,68	0,12	0,00	0,00	0,00	0,00
SG-01	Sphalerite	Spectrum 11	34,19	0,04	0,04	9,74	0,00	0,51	55,47	0,00	0,00	0,00	0,00	0,00
SG-01	Sphalerite	Spectrum 12	34,05	0,01	0,06	10,01	0,00	0,60	55,27	0,00	0,00	0,00	0,00	0,00
SG-01	Sphalerite	Spectrum 13	34,40	0,00	0,05	9,98	0,00	0,65	54,82	0,09	0,00	0,00	0,00	0,00
SG-01	Galena	Spectrum 14	19,66	0,00	0,00	8,02	0,00	0,00	0,00	0,00	0,00	0,00	0,00	72,32
SG-01	Galena	Spectrum 15	26,72	0,01	0,00	22,73	0,00	3,38	1,16	0,00	0,00	1,63	0,00	43,53
SG-01	Pyrite	Spectrum 16	53,04	0,00	0,00	46,46	0,29	0,00	0,00	0,12	0,00	0,00	0,09	0,00
SG-01	Pyrite	Spectrum 17	53,36	0,01	0,00	46,63	0,00	0,00	0,00	0,00	0,00	0,00	0,00	0,00
SG-01	Pyrite	Spectrum 18	53,47	0,02	0,00	46,51	0,00	0,00	0,00	0,00	0,00	0,00	0,00	0,00
SG-01	Pyrite	Spectrum 19	53,57	0,00	0,04	46,38	0,00	0,00	0,00	0,00	0,00	0,00	0,00	0,00
SG-01	Pyrite	Spectrum 20	53,28	0,00	0,02	46,34	0,36	0,00	0,00	0,00	0,00	0,00	0,00	0,00
SG-01	Pyrite	Spectrum 21	53,59	0,00	0,00	46,41	0,00	0,00	0,00	0,00	0,00	0,00	0,00	0,00
SG-01	Pyrite	Spectrum 22	53,40	0,00	0,09	46,51	0,00	0,00	0,00	0,00	0,00	0,00	0,00	0,00
SG-01	Pyrite	Spectrum 23	53,38	0,02	0,00	46,17	0,43	0,00	0,00	0,00	0,00	0,00	0,00	0,00
SG-01	Pyrite	Spectrum 24	53,53	0,01	0,05	46,40	0,00	0,00	0,00	0,00	0,00	0,00	0,00	0,00
SG-01	Chalcopyrite	Spectrum 25	36,30	0,00	0,07	31,36	0,00	31,62	0,64	0,00	0,00	0,00	0,00	0,00
SG-01	Sphalerite	Spectrum 26	37,09	0,00	0,11	14,30	0,00	0,06	48,44	0,00	0,00	0,00	0,00	0,00
SG-01	Sphalerite	Spectrum 27	36,59	0,02	0,15	13,29	0,00	0,00	49,95	0,00	0,00	0,00	0,00	0,00
SG-01	Chalcopyrite	Spectrum 28	37,04	0,03	0,02	32,24	0,00	30,67	0,00	0,00	0,00	0,00	0,00	0,00
SG-01	Chalcopyrite	Spectrum 29	39,42	0,00	0,00	34,38	0,00	26,19	0,00	0,00	0,00	0,00	0,00	0,00
SG-01	Galena	Spectrum 30	44,33	0,00	0,00	34,96	0,00	0,00	0,00	0,00	0,00	0,00	0,00	20,39
SH1-03	Pyrite	Spectrum 31	51,03	1,52	0,03	46,67	0,76	0,00	0,00	0,00	0,00	0,00	0,00	0,00
SH1-03	Chalcopyrite	Spectrum 57	35,25	0,12	0,04	34,08	0,00	30,51	0,00	0,00	0,00	0,00	0,00	0,00
SH1-03	Pyrite	Spectrum 58	52,54	0,06	0,07	46,95	0,39	0,00	0,00	0,00	0,00	0,00	0,00	0,00
SH1-03	Chalcopyrite	Spectrum 66	35,23	0,16	0,05	32,85	0,00	31,72	0,00	0,00	0,00	0,00	0,00	0,00
SH1-03	Chalcopyrite	Spectrum 68	36,74	0,08	0,04	32,39	0,00	30,75	0,00	0,00	0,00	0,00	0,00	0,00
SH1-03	Chalcopyrite	Spectrum 69	37,68	0,10	0,04	33,07	0,00	29,12	0,00	0,00	0,00	0,00	0,00	0,00
SH1-03	Pyrite	Spectrum 70	53,41	0,08	0,00	46,15	0,00	0,36	0,00	0,00	0,00	0,00	0,00	0,00

Table 4.26: *Oxides*

Sample	Mineralogy	Measurement	O	F	P	Sc	Ti	V	Mn	Fe	Co	Mo
			Wt% (norm.)	Wt% (norm.)	Wt% (norm.)	Wt% (norm.)	Wt% (norm.)	Wt% (norm.)	Wt% (norm.)	Wt% (norm.)	Wt% (norm.)	Wt% (norm.)
SH1-03	Ilmenite	Spectrum 32	37,18	0,00	0,04	0,00	27,60	0,00	1,74	33,44	0,00	0,00
SH1-03	Magnetite	Spectrum 33	33,26	0,00	0,03	0,00	5,88	0,00	0,08	60,15	0,39	0,21
SH1-03	Ilmenite	Spectrum 35	37,66	0,00	0,04	0,00	27,38	0,00	1,50	33,42	0,00	0,00
SH1-03	Magnetite	Spectrum 36	33,79	0,00	0,06	0,00	5,39	0,00	0,09	60,68	0,00	0,00
SH1-03	Ilmenite	Spectrum 37	37,56	0,00	0,04	0,00	27,36	0,00	1,50	33,53	0,00	0,00
SH1-03	Magnetite	Spectrum 38	34,45	0,00	0,00	0,00	7,42	0,21	0,16	57,77	0,00	0,00
SH1-03	Ilmenite	Spectrum 39	36,77	0,00	0,00	0,00	26,63	0,00	1,37	35,23	0,00	0,00
SH1-03	Ilmenite	Spectrum 40	54,82	0,00	0,05	0,00	0,00	0,00	1,85	43,28	0,00	0,00
SH1-03	Magnetite	Spectrum 41	33,24	0,00	0,00	0,00	5,61	0,00	0,10	61,05	0,00	0,00
SH1-03	Magnetite	Spectrum 42	33,63	0,00	0,00	0,00	5,07	0,00	0,05	61,25	0,00	0,00
SH1-03	Ilmenite	Spectrum 43	36,96	0,00	0,02	0,00	27,64	0,00	1,64	33,74	0,00	0,00
SH1-03	Ilmenite	Spectrum 44	36,02	0,00	0,03	0,00	26,39	0,00	1,51	36,05	0,00	0,00
SH1-03	Magnetite	Spectrum 45	32,99	0,00	0,03	0,00	5,15	0,00	0,01	61,82	0,00	0,00
SH1-03	Ilmenite	Spectrum 46	39,48	0,00	0,00	0,00	27,85	0,00	0,01	32,66	0,00	0,00
SH1-03	Ilmenite	Spectrum 47	41,97	0,00	0,00	0,00	30,18	0,00	0,08	27,77	0,00	0,00
SH1-03	Ilmenite	Spectrum 48	35,45	0,00	0,03	0,00	21,21	0,00	1,17	42,14	0,00	0,00
SH1-03	Magnetite	Spectrum 49	34,30	0,00	0,00	0,00	6,36	0,00	0,04	59,30	0,00	0,00
SH1-03	Rutile?	Spectrum 50	45,44	0,00	0,03	0,00	34,80	0,00	0,00	19,74	0,00	0,00
SH1-03	Ilmenite	Spectrum 51	37,92	0,00	0,00	0,00	27,49	0,00	2,08	32,51	0,00	0,00
SH1-03	Rutile	Spectrum 52	46,21	0,00	0,00	0,00	49,57	0,00	0,09	4,14	0,00	0,00
SH1-03	Rutile?	Spectrum 54	48,75	0,00	0,03	0,00	38,28	0,00	0,06	12,88	0,00	0,00
SH1-03	Rutile?	Spectrum 55	46,36	0,00	0,03	0,00	32,38	0,00	0,03	21,19	0,00	0,00
SH1-03	Magnetite	Spectrum 59	27,56	0,00	0,06	0,00	0,16	0,00	0,02	72,20	0,00	0,00
SH1-03	Magnetite	Spectrum 74	27,06	0,00	0,01	0,00	0,14	0,00	0,01	72,79	0,00	0,00

Table 4.27: *Silicates*

Sample	Mineralogy	Measurement	O	Na	Mg	Al	Si	P	Cl	K	Ca	Ti	Mn	Fe
			Wt% (norm.)	Wt% (norm.)	Wt% (norm.)	Wt% (norm.)	Wt% (norm.)	Wt% (norm.)	Wt% (norm.)	Wt% (norm.)	Wt% (norm.)	Wt% (norm.)	Wt% (norm.)	Wt% (norm.)
SH1-03	Mica	Spectrum 34	41,93	1,30	0,83	15,60	20,86	0,03	0,00	7,54	0,18	2,24	0,07	9,41
	Mica	Spectrum 56	38,26	0,48	7,40	9,17	17,61	0,00	0,00	8,52	0,10	1,18	0,17	17,12
	Mica	Spectrum 60	39,50	0,28	7,19	8,93	16,51	0,01	0,00	8,29	0,03	1,06	0,16	18,04
	Mica	Spectrum 61	43,54	0,60	1,21	16,17	19,79	0,00	0,00	7,81	0,09	0,69	0,10	10,02
	Mica	Spectrum 62	39,32	0,18	7,48	8,33	16,33	0,00	0,00	7,95	0,02	1,09	0,05	19,23
	Mica	Spectrum 63	33,45	0,95	2,82	4,15	16,63	0,00	0,72	1,63	0,27	0,36	0,00	39,02
	Mica	Spectrum 67	39,29	0,25	7,31	8,41	17,34	0,00	0,00	7,80	0,06	1,28	0,08	18,17
	Mica	Spectrum 71	45,78	8,06	0,55	10,78	31,51	0,00	0,00	0,77	0,22	0,07	0,05	2,21
	Mica	Spectrum 72	44,79	1,18	1,28	17,10	21,49	0,00	0,00	7,85	0,05	0,45	0,09	5,73

Table 4.28: *Ag-rich mineral*

Sample	Mineralogy	Measurement	S	Mn	Fe	Cu	Zn	Ag	Sb	Pb
			Wt% (norm.)	Wt% (norm.)	Wt% (norm.)	Wt% (norm.)	Wt% (norm.)	Wt% (norm.)	Wt% (norm.)	Wt% (norm.)
SJ-01	Ag-rich	Spectrum 76	20,47	0,02	5,00	16,72	0,00	25,99	24,10	7,69
SJ-01	Ag-rich	Spectrum 77	20,89	0,07	5,01	20,52	0,73	18,21	24,51	10,06

4.2 EBSD analyses

4.2.1 SJ-02

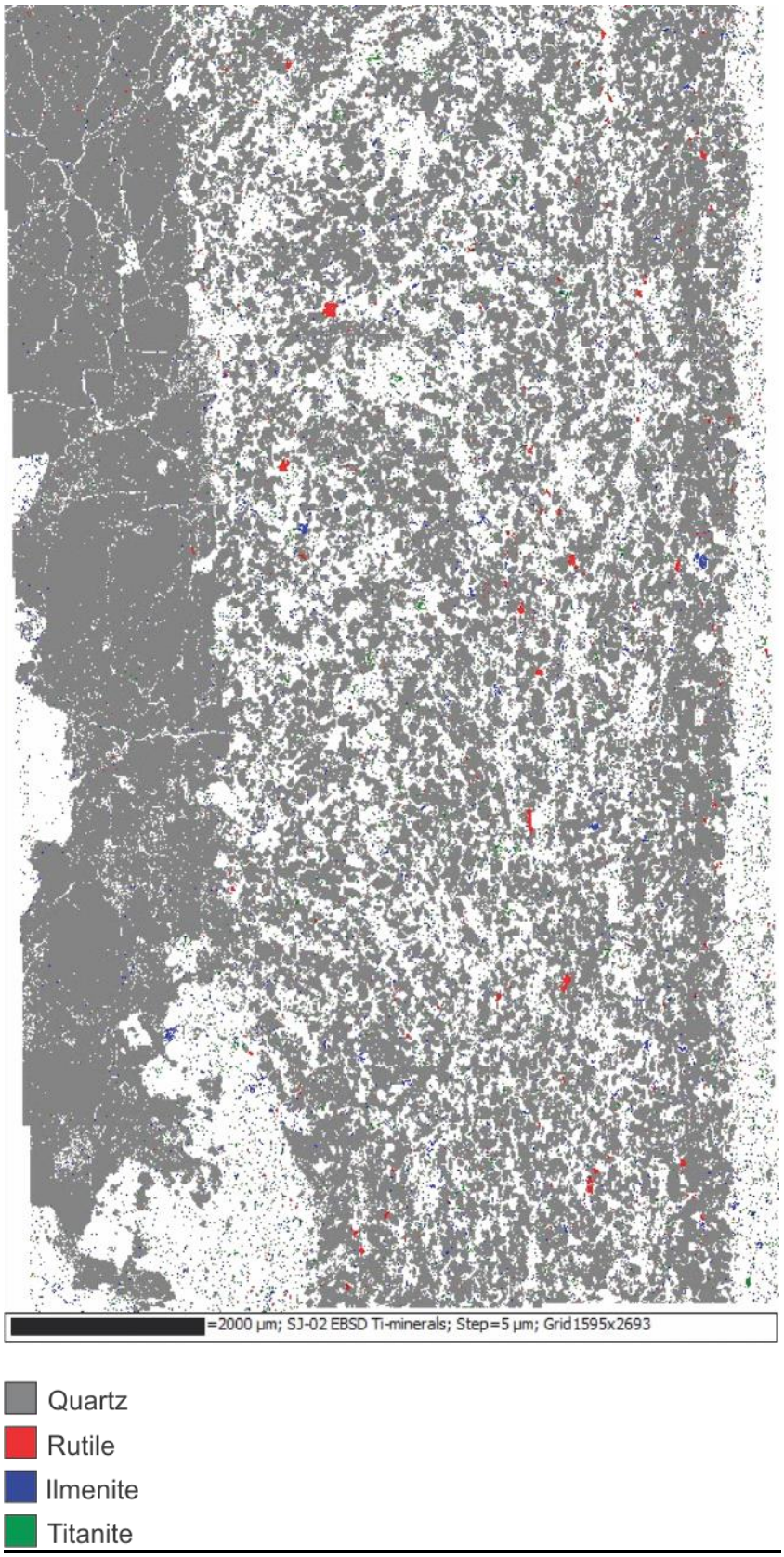

Figure 4.28: EBSD map of a square section of the fine grained part of sample SJ-02. Shows the presence and distribution of the Ti-phases; Rutile (red), Ilmenite (blue), titanite (green). Quartz (grey) is added to give texture to the image.

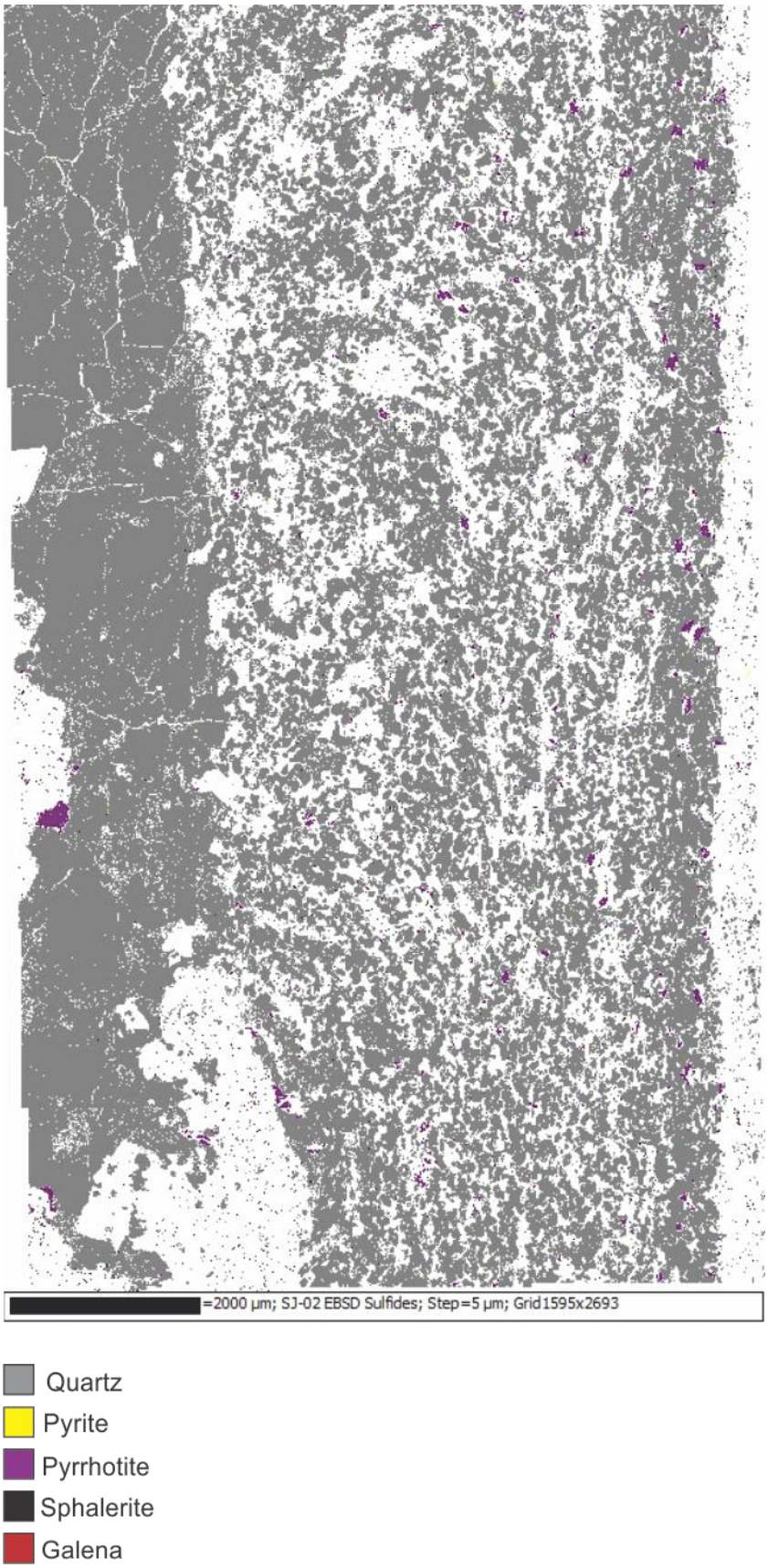

Figure 4.29: EBSD map of sample SJ-02. Showing a section from the fine grained area. In this map; the presence and distribution of pyrite (yellow), Pyrrhotite (purple), sphalerite (black) and galena (dark red). Quartz is added for texture.

4.3 X-ray powder diffraction (XRD)

4.3.1 SH1-03

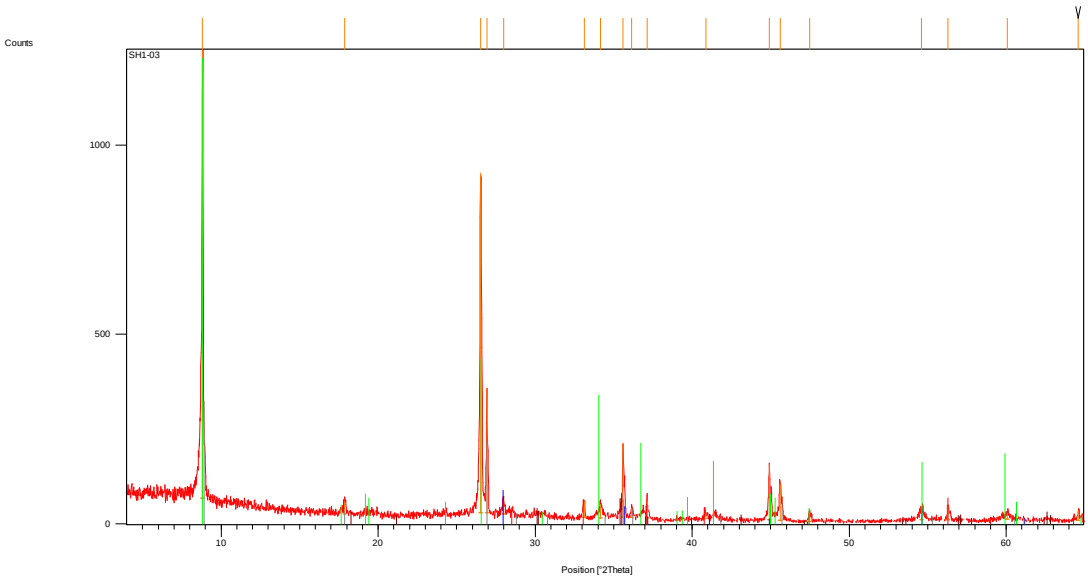

Figure 4.30: *XRD-analysis patterns of sample SH1-03*

Table 4.29: *List of identified XRD patterns in sample SH1-03*

Visible	Ref. Code	Score	Compound Name	Displacement [°2Th.]	Scale Factor	Chemical Formula
*	00-026-0801	45	Pyrite, syn	0,000	0,043	Fe S2
*	01-082-0514	31	Rutile	0,000	0,048	Ti O2
*	00-042-1437	31	Phlogopite-1\ITM\RG, ferroan	0,000	0,872	K (Mg , Fe)3 (Al , Fe) Si3 O10 (O H , F)2
*	00-042-1399	32	Polylithionite-1\ITM\RG, ferroan	0,000	0,193	K (Al Fe Li) (Si3 Al) O10 (O H) F
*	01-075-1609	12	Iron diiron(III) oxide - LT	0,000	0,047	Fe3 O4

4.3.2 SS-02

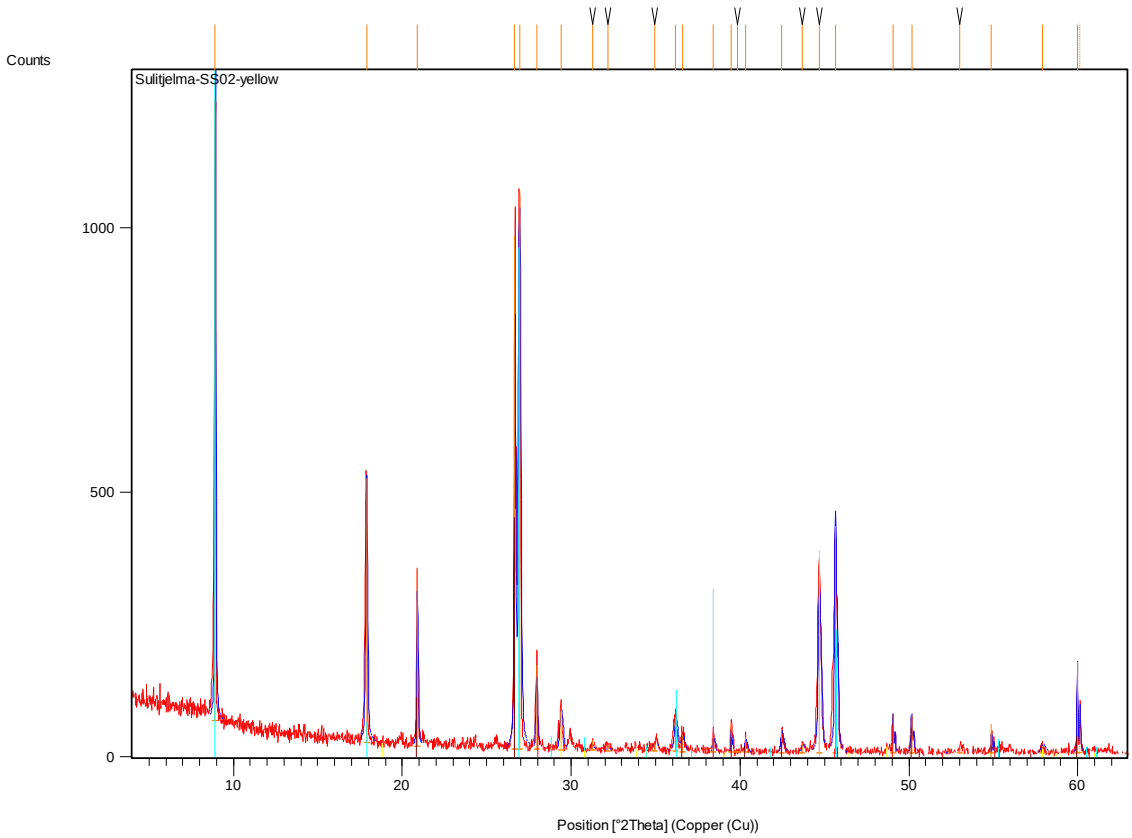

Figure 4.31: *XRD analysis patterns of sample SS-02*

Table 4.30: *List of identified XRD patterns in sample SS-02*

Visible	Ref. Code	Score	Compound Name	Displacement [°2Th.]	Scale Factor	Chemical Formula
*	01-086-1560	67	Quartz	0.012	0.337	Si O2
*	00-042-1399	54	Polylithionite-1\ITM\RG, ferroan	-0.005	1.044	K (Al Fe Li) (Si3 Al) O10 (O H) F
*	00-037-0471	32	Chalcopyrite	0.045	0.056	Cu Fe S2
*	00-001-0774	28	Bohmite	-0.208	0.049	Al2 O3 ! H2 O

4.4 Lithogeochemistry

Table 4.31: Major elements (%)

Sample	SiO2	Al2O3	Fe2O3(T)	MnO	MgO	CaO	Na2O	K2O	TiO2	P2O5	LOI	Total
	%	%	%	%	%	%	%	%	%	%	%	%
SG – 01	0,62	0,18	60,21	0,011	< 0.01	0,02	0,02	0,01	0,003	< 0.01	27,24	88,3
SG – 02	21,73	4,54	41,16	0,011	0,29	2,03	2,67	0,08	0,018	0,09	23,87	96,48
SG – 003A$_1$	1,44	0,51	58,92	0,009	0,06	0,06	0,14	0,05	0,024	< 0.01	28,21	89,42
SG – 003A$_2$	4,39	2,27	56,52	0,03	2,06	0,07	0,16	0,13	0,21	0,01	26,76	92,61
SG – 003C	15,46	0,73	46,78	0,029	< 0.01	1,61	0,32	0,04	0,01	< 0.01	21,58	86,57
SH1 – 02	23,16	2,4	51,16	0,012	0,08	0,06	1,35	0,08	0,12	0,02	16,76	95,2
SH1 – 03	37,91	15,35	21,87	0,091	8,02	0,08	1,68	7,06	2,031	0,02	4,49	98,59
SH2 – 01	37,31	8,47	30	0,024	2,92	0,65	4,82	0,33	0,605	< 0.01	12,77	97,89
SJ - 01	21,25	2,57	1,47	0,019	0,44	1,43	0,55	0,28	0,13	0,02	2,9	31,05
SJ – 03	7,32	1,13	51,91	0,031	0,19	0,34	0,05	0,21	0,105	< 0.01	27,3	88,58
SNY - 03	39,47	8,08	12,61	0,155	1,96	4,32	3,35	1,21	0,426	0,08	9,19	80,85
SNY – 04	72,35	7,39	9,49	0,007	0,16	0,04	0,33	1,83	0,618	0,03	6,01	98,26
SS – 01	23,48	8,15	45,73	0,042	3,73	0,57	1,37	1,14	0,486	0,02	10,13	94,86
SS – 02	32,76	6,58	37,97	0,021	1,61	0,25	0,5	1,43	0,444	0,02	12,33	93,92

Table 4.32: Trace elements (ppm)

Sample	Be	V	Cr	Co	Ni	Cu	Zn	Ga	Ge	As
	ppm	ppm	ppm	ppm	ppm	ppm	ppm	ppm	ppm	ppm
SG – 01	< 1	10	< 20	301	20	71200	14600	8	< 0.5	423
SG – 02	< 1	< 5	< 20	252	30	7260	640	10	< 0.5	339
SG – 003A$_1$	< 1	15	< 20	232	< 20	75300	8990	2	< 0.5	90
SG – 003A$_2$	< 1	28	< 20	220	< 20	59100	4700	6	< 0.5	129
SG – 003C	< 1	10	< 20	195	< 20	11100	1950	3	< 0.5	277
SH1 – 02	< 1	202	20	272	50	43800	1010	8	< 0.5	40
SH1 – 03	2	223	60	158	30	2980	910	25	2,3	10
SH2 – 01	< 1	84	80	291	40	17500	70	10	0,9	61
SJ - 01	< 1	17	< 20	2	< 20	220	3410	3	0,6	28
SJ – 03	< 1	17	< 20	904	< 20	36200	33200	9	0,6	848
SNY - 03	1	45	80	25	40	22700	104000	23	1	46
SNY – 04	< 1	99	90	28	20	8500	4680	12	0,8	102
SS – 01	< 1	83	90	197	50	35500	450	14	< 0.5	8
SS – 02	< 1	76	120	238	30	56900	500	10	< 0.5	6

Table 4.33: Trace elements (ppm) (continued)

Sample	Rb	Sr	Zr	Nb	Mo	Ag	In	Sn	Sb	Cs
	ppm	ppm	ppm	ppm	ppm	ppm	ppm	ppm	ppm	ppm
SG – 01	< 1	< 2	1	< 0.2	39	5,2	4,5	25	18,6	< 0.1
SG – 02	3	1445	6	< 0.2	17	9	0,4	< 1	6,9	0,2
SG – 003A_1	2	6	5	< 0.2	> 100	5,8	2	8	1,5	0,1
SG – 003A_2	6	4	47	1,1	57	8,5	1,4	7	0,8	1,2
SG – 003C	2	240	2	< 0.2	20	20,2	2,3	6	0,7	< 0.1
SH1 – 02	3	42	71	0,4	5	3,7	0,5	2	0,9	0,4
SH1 – 03	266	95	280	6,6	< 2	2,2	< 0.1	2	0,5	50,4
SH2 – 01	12	84	86	2,3	4	1,4	0,2	2	0,4	4,5
SJ - 01	9	43	59	1,5	< 2	1180	0,4	62	1300	0,1
SJ – 03	6	6	16	0,6	18	43,7	1,8	5	27,8	0,4
SNY - 03	64	130	108	8,1	15	13,4	21,1	20	2,4	6,5
SNY – 04	41	37	84	1,7	13	9,3	0,5	2	3,8	0,9
SS – 01	30	61	83	2	32	26,7	0,9	7	6,8	1,1
SS – 02	27	20	48	1	34	24,7	0,5	9	5,8	0,4

Table 4.34: Trace elements (ppm) (continued)

Sample	Ba	Hf	Ta	W	Tl	Pb	Bi	Th	U
	ppm	ppm	ppm	ppm	ppm	ppm	ppm	ppm	ppm
SG – 01	< 2	< 0.1	< 0.01	< 0.5	0,53	348	7,9	< 0.05	0,26
SG – 02	4911	0,2	< 0.01	< 0.5	0,33	3090	9,9	2,64	0,65
SG – 003A_1	6	0,1	0,01	< 0.5	< 0.05	132	4,8	0,14	0,56
SG – 003A_2	6	1,1	0,04	1,5	0,06	90	4,6	0,49	1,09
SG – 003C	416	< 0.1	< 0.01	< 0.5	< 0.05	241	4,2	0,72	0,48
SH1 – 02	97	1,6	< 0.01	1,4	0,15	17	2,6	0,72	0,76
SH1 – 03	1397	6,5	0,39	2,5	3,05	24	0,3	1,91	2,22
SH2 – 01	21	1,9	0,2	4,2	0,33	31	1,7	0,57	0,53
SJ - 01	1267	1,3	0,15	0,7	149	603000	142	2,13	0,52
SJ – 03	2421	0,4	0,07	3,4	6,08	2380	18,9	0,37	0,8
SNY - 03	137	2,9	0,55	4,2	1,58	147	1,4	5,69	1,8
SNY – 04	240	1,7	0,16	4,8	4,62	192	1,2	0,5	2,37
SS – 01	250	1,9	0,15	4,7	2,52	465	5,1	1,02	0,99
SS – 02	306	1,1	0,08	0,8	1,42	50	2,8	0,21	0,34

Table 4.35: Rare Earth elements (REE) compared to chondrite from McDounough & Sun (1995)

Sample	Sc	Y	La	Ce	Pr	Nd	Sm	Eu
	ppm	ppm	ppm	ppm	ppm	ppm	ppm	ppm
Chondrite	5,92	1,57	0,237	0,613	0,0928	0,457	0,148	0,0563
SG – 01	< 1	< 0.5	0,54	0,27	0,05	0,15	0,09	0,034
SG – 02	2	2,3	2,72	4,21	0,48	2,04	0,39	0,151
SG – 003A_1	< 1	0,7	1,55	2,16	0,28	1,13	0,25	0,099
SG – 003A_2	2	9	4,25	8,63	1,19	5,06	1,31	0,483
SG – 003C	< 1	0,9	2,01	2,2	0,26	0,95	0,2	0,091
SH1 – 02	3	17,6	4,63	9,27	1,27	5,8	1,67	0,994
SH1 – 03	32	55,1	12,9	28,2	3,81	18,7	5,91	1,7
SH2 – 01	16	18	6,64	14,3	1,83	8,65	2,29	0,774
SJ - 01	2	5,7	8,35	14,6	1,57	5,78	1,22	0,218
SJ – 03	2	2,7	1,88	3,11	0,37	1,51	0,44	0,077
SNY - 03	7	14	20,5	40,8	4,81	17,9	3,44	0,608
SNY – 04	12	22,4	4,26	8,23	1,06	5,03	1,75	1,07
SS – 01	11	16,4	6,54	14	1,93	8,38	2,39	0,931
SS – 02	10	13,1	4,02	8,36	1,22	5,87	1,78	0,777

Table 4.36: Rare Earth elements (REE) compared to chondrite (continued) from McDounough & Sun (1995)

Sample	Gd	Tb	Dy	Ho	Er	Tm	Yb	Lu
	ppm	ppm	ppm	ppm	ppm	ppm	ppm	ppm
Chondrite	0,199	0,0361	0,246	0,0546	0,16	0,0247	0,161	0,0246
SG – 01	0,03	< 0.01	0,04	< 0.01	0,02	< 0.005	0,02	0,003
SG – 02	0,41	0,07	0,43	0,08	0,22	0,026	0,15	0,024
SG – 003A_1	0,16	0,02	0,13	0,02	0,07	0,01	0,06	0,008
SG – 003A_2	1,33	0,26	1,66	0,33	1	0,152	0,98	0,157
SG – 003C	0,16	0,02	0,14	0,02	0,07	0,01	0,07	0,01
SH1 – 02	2	0,41	2,74	0,64	1,92	0,294	1,88	0,296
SH1 – 03	7,17	1,31	9,09	1,96	5,65	0,899	5,8	0,91
SH2 – 01	2,48	0,46	2,91	0,64	1,95	0,288	1,77	0,266
SJ - 01	1,14	0,16	0,95	0,2	0,58	0,082	0,52	0,076
SJ – 03	0,41	0,08	0,51	0,1	0,3	0,042	0,28	0,048
SNY - 03	2,74	0,4	2,43	0,49	1,54	0,246	1,94	0,333
SNY – 04	2,6	0,55	3,78	0,78	2,31	0,334	2,21	0,32
SS – 01	2,51	0,45	2,91	0,59	1,75	0,266	1,66	0,241
SS – 02	1,86	0,35	2,26	0,45	1,37	0,191	1,19	0,198

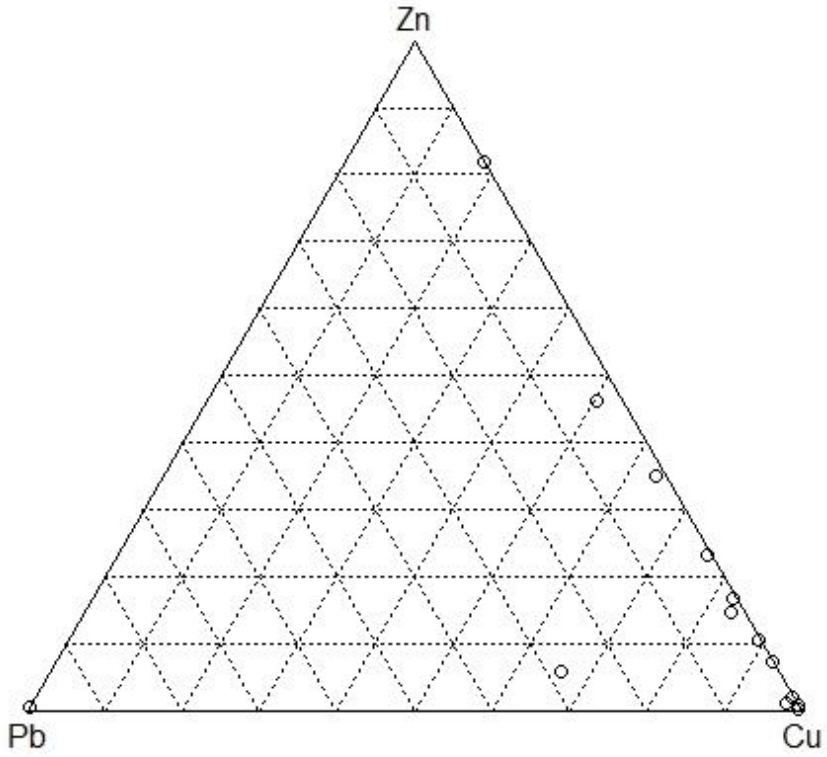

Figure 4.32: *Pb-Cu-Zn plot of the ore samples collected from Sulitjelma. Showing a clear copper affinity in most samples with some influence of zinc. One sample however is dominated in zinc. Pb (exept for two of the samples), only occur in a minor amount.*

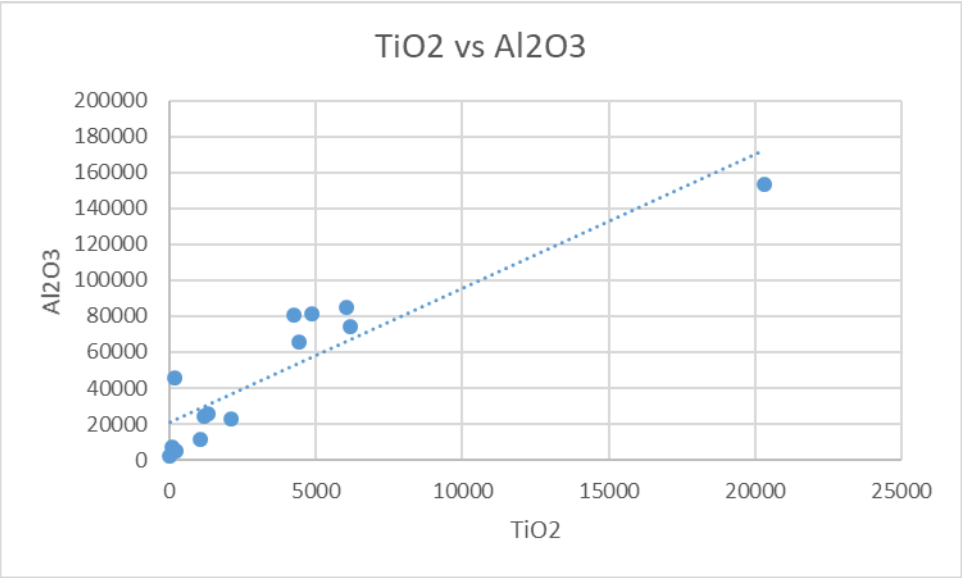

Figure 4.33: *Titanium verses aluminium plot.*

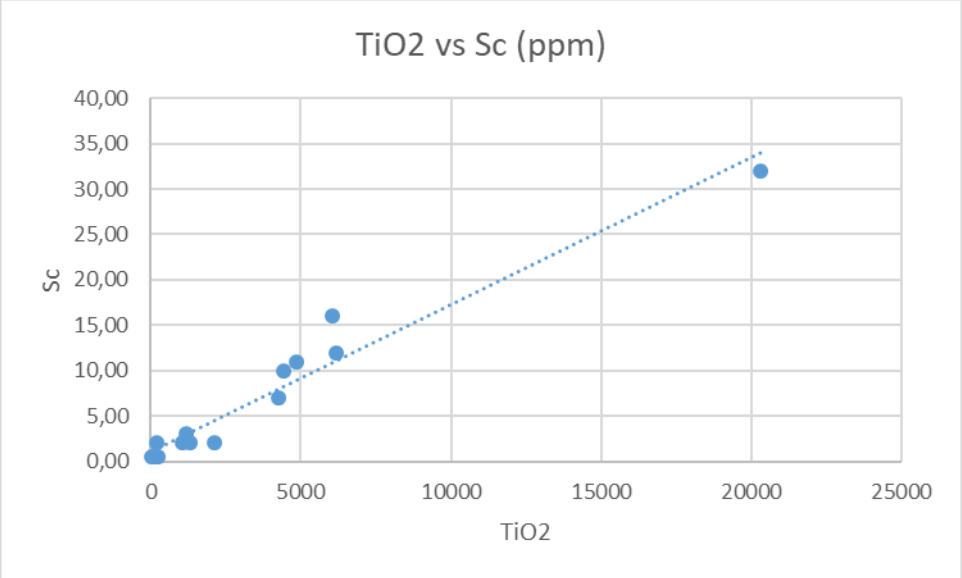

Figure 4.34: *Titanium verses scandium plot.*

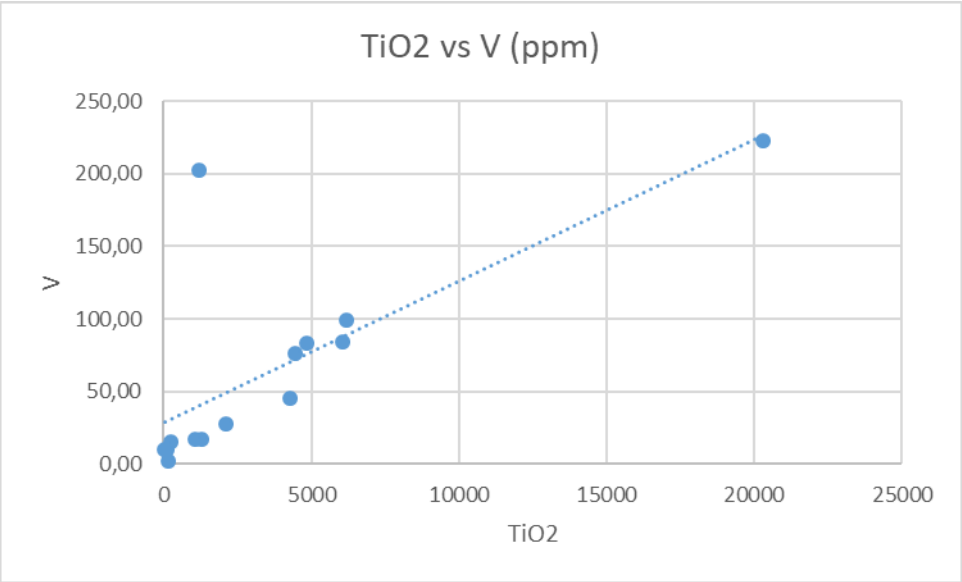

Figure 4.35: *Titanium verses vanadium plot.*

4.5 Fluid inclusion studies

Fluid inclusions from three different locations; Ny-Sulitjelma, Giken and Jakobsbakken, were measured. This revealed what occur as various generations of entrapped ore-forming and post-ore fluids hosted in gangue quartz. In general, five different types were recognised.

4.5.1 Petrographic description

Ny-Sulitjelma

Measured fluid inclusions from this location show examples of all five different types.

Type 1:

Primary two phase of liquid and vapour (L+V) aqueous fluid inclusions with a uniform degree of fill (F) of 0,7-0.8. They usually show a rounded and elongated morphology. Their sizes vary up to 30 µm and occur both as single inclusions and in three dimensional clusters.

Type 2:

Rare primary polyphase fluid inclusions of liquid, vapour and solid (L+V+S) containing halite crystals. The inclusions show mostly rounded to sub-rounded morphology and occur in clusters. Uniform L:V:S ratios could suggest entrapment of single phase fluids rather than an accidental entrapment of solid phases.

Type 3:

Consists of primary fluid inclusion assemblages composed of coexisting L-rich and V-rich inclusions.

Type 4:

Consists of primary two phase (L+V) fluid inclusions enriched in CH_4. The inclusions are characterized by irregular star-like morphologies.

Type 5:
Consists of secondary two phase (L+V) fluid inclusions with a degree of filling around 0,9. They show rounded and elongated morphologies, they vary in size up to 15 µm and are occurring along healed fractures.

Giken
Measured fluid inclusions from this location show examples of three different types.

Type 1:
Corresponds to type 1 inclusions from Ny-Sulitjelma.

Type 2:
Corresponds to type 2 inclusions from Ny-Sulitjelma

Type 5:
Consists of secondary three phase (L_1+L_2+V) fluidinclusions.

Jakobsbakken
Measured fluidinclusions from this location show examples of only one type.

Type 5:
Consists of pseudosecondary or secondary two phase (L+V) fluid inclusions.

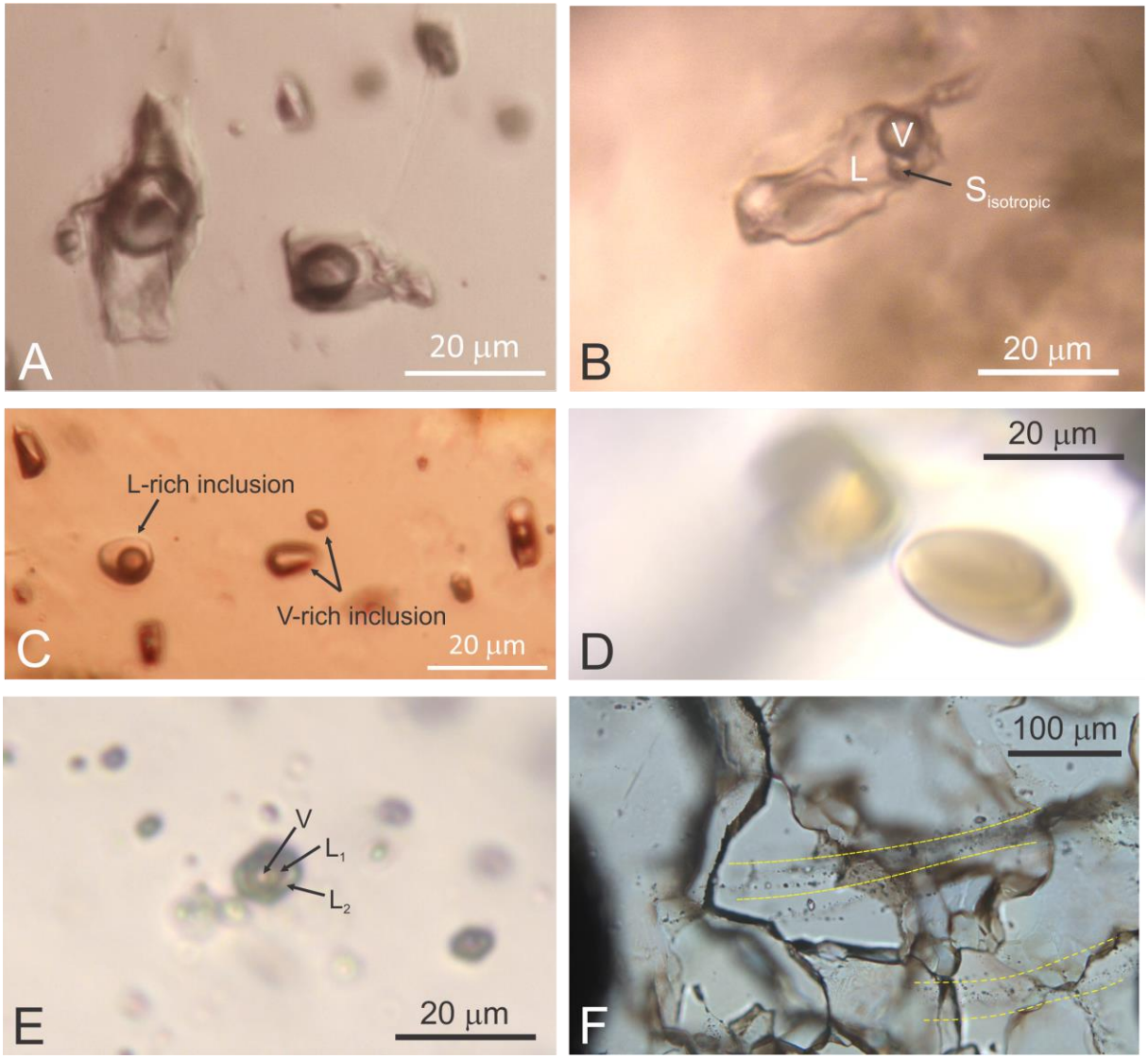

Figure 4.36: *Showing representative micrographs of the five observed fluid inclusion types. A: Primary two phase (L+V) fluid inclusions from quartz vein in Ny-Sulitjelma. B: Primary three phase (L+V+S) fluid inclusion from quartz vein in Ny-Sulitjelma, containing halite crystal which is isotropic under crossed polars. C: Fluid inclusion assemblage which indicates boiling due to heterogeneous L/V ratio. Hosted in quartz crystal from Ny-Sulitjelma. D: Hydrocarbon bearing fluid inclusions showing a brownish color. Evidence for organic matter is supported from several thin sections. Inclusions hosted in quartz crystal from Giken. E: Secondary or pseudosecondary CO_2 bearing fluid inclusions. Three phase inclusions with vapour, liquid CO_2 and aqueous solution ($V+L_1+L_2$) hosted in quartz crystal from Giken. F: Trails of very late fluids (between yellow stapled lines) crosscut the grain boundaries. Fluid inclusions are hosted in quartz from Giken.*

4.5.2 Microthermometric description

Ny-Sulitjelma

Type 1:

The eutectic temperatures (T_E) that were measured, showed values of -52 and -54 °C which could indicate the presence of divalent cations (e.g., Ca^{2+}, Mg^{2+}). The final ice melting temperature ($T_M$ice) were in the range from -3,5 to -5,5 °C corresponds to salinity between 5,7 and 8,1 wt. % NaCl equivalent. The homogenization temperature (T_H) showed values ranging from 290 to 315 °C. This is the most common type of primary fluid inclusions and could represent seawater that was modified by water-rock interactions during the deep convective circulation through the oceanic crust.

Type 2:

The T_E show the values -50 and -54 °C. The halite melting temperature (T_S) which showed values between 250 and 285 °C corresponds to salinities ranging from 34,7 to 37,0 wt.% NaCl equivalent. The total homogenization into the liquid phase were recorded in the temperature interval between 295 and 330 °C. This type of inclusions could reflect the episodic incursion of magmatic fluids.

Type 3:

The $T_M$ice values measured are ranging from -4,0 to -5,8 °C, and corresponds to salinity between 6,4 and 8,9 wt. % NaCl equivalent. The homogenization temperatures measured are ranging from 355 to 370 °C, and are in many cases overlapping. The relationship between $T_M$ice and T_H could reflect entrapment of boiling fluids.

Type 4:

To uncertain data.

Type 5:

The $T_M$ice values measured are ranging from -0,8 to -1,2 corresponding to low salinities of 1,4 to 2,1 wt. % NaCl equivalent. The homogenization temperatures measured are ranging from 125 to 145 °C and contain traces of CO_2 which could suggest entrapment of post-ore metamorphogenic fluids.

Giken

Type 1:

The eutectic temperature (T_E) measured, showed a value of -52 °C. The final ice melting temperature ($T_M$ice) were in the range from -4,8 to -8,8 °C corresponds to salinity between 7,6 and 12,6 wt. % NaCl equivalent. The homogenization temperature (T_H) showed values ranging from 202 to 357 °C.

Type 2:

The T_E showed the value of -54 °C. The halite melting temperature (T_S) which showed values between

370 and 380 °C corresponds to salinities ranging from 44,3 to 45,3 wt.% NaCl equivalent. The total homogenization into the liquid phase were recorded in the temperature interval between 360 and 365 °C.

Type 5:
The final clathrate melting temperature ($T_M$clath) values measured are ranging from 8,9 to 9,5 °C corresponding to low salinities of 0,9 to 1,9 wt. % NaCl equivalent. The partial homogenization temperature of CO_2 (T_HCO_2) shows values of 30,0 to 31,0 °C. The homogenization temperatures measured are ranging from 260 to 265 °C were many of the values are overlapping.

<u>Jakobsbakken</u>

Type 5:
The final ice melting temperature values are ranging from -0,2 to -0,7 °C which corresponds to salinities of 0,4 to 1,2 wt. % NaCl equivalent. T_HCO_2 shows values of 30,0 to 31,0 °C. The homogenization temperatures measured are ranging from 340 to 360 °C.

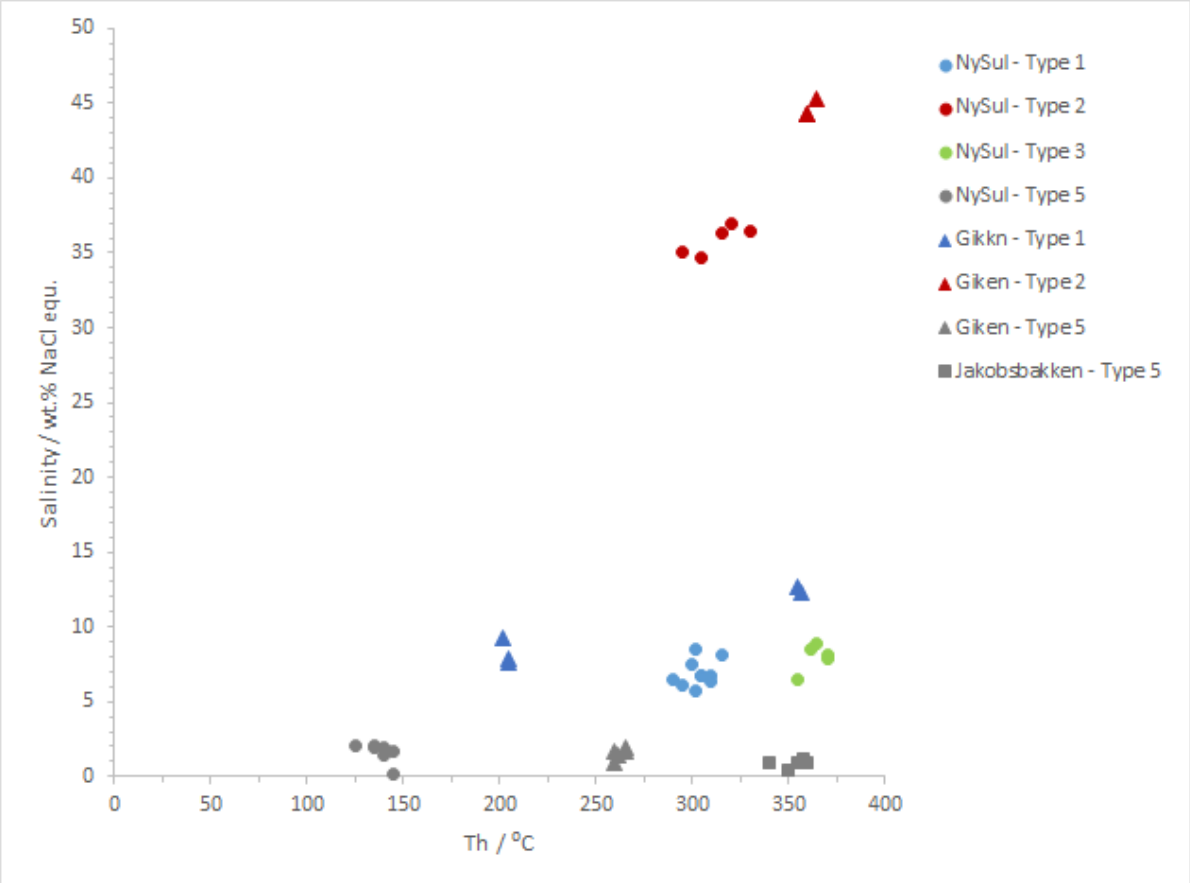

Figure 4.37: Showing fluidinclusion plots

4.5.3 Fluid inclusions measurements

Table 4.37: Fluid inclusion measuerments results from Ny-sulitjelma

Sample	Type		F	Te °C	Tm ice °C	Tm clath °C	Th CO2 °C	Tm s °C	Th °C	salinity wt% NaCl equ.
Ny Sulitjelma										
Type 1										
FI1	P	L+V	0,7-0,8	-52	-3,5				302	5,7
FI2	P	L+V	0,7-0,8		-4,0				290	6,4
FI3	P	L+V	0,7-0,8		-5,5				302	8,5
FI4	P	L+V	0,7-0,8		-5,2				315	8,1
FI5	P	L+V	0,7-0,8		-4,2				310	6,7
FI6	P	L+V	0,7-0,8	-54	-4,2				305	6,7
FI7	P	L+V	0,7-0,8		-4,7				300	7,4
FI8	P	L+V	0,7-0,8		-3,8				295	6,2
FI9	P	L+V	0,7-0,8		-4,2				305	6,7
FI10	P	L+V	0,7-0,8	-52	-3,9				310	6,3
Type 2										
FI11	P	L+V+S		-54				285	320	37,0
FI12	P	L+V+S		-50				252	295	35,0
FI13	P	L+V+S						250	305	34,7
FI14	P	L+V+S						275	315	36,3
FI15	P	L+V+S						278	330	36,4
Type 3 (boiling FIAs)										
FI16	P	L+V	0,8		-5,8				365	8,9
FI17	P	L+V	0,85		-4,0				355	6,4
FI18	P	L+V	0,75		-5,0				370	7,9
FI19	P	L+V	0,85		-5,5				362	8,5
FI20	P	L+V	0,7		-5,2				370	8,1
FI21	P	L+V	0,3						365	
FI22	P	L+V	0,2						360	
FI23	P	L+V	0,2						360	
Type 4 (organic matter bearing fluid inclusions)										
Type 5 (metamorphogenic fluids?)										
FI24	S	L+V	0,9		-1,0				145	1,7
FI25	S	L+V	0,9		-1,2				125	2,1
FI26	S	L+V	0,9		-1,1				135	1,9
FI27	S	L+V	0,9		-0,8				140	1,4
FI28	S	L+V	0,9		-0,1				145	0,2
FI29	S	L+V	0,9		-1,1				140	1,9
FI30	S	L+V	0,9		-1,2				135	2,1

Table 4.38: Fluid inclusion measuerments results from Giken and Jakobsbakken

Sample	Type		F	Te °C	Tm ice °C	Tm clath °C	Th CO2 °C	Tm s °C	Th °C	salinity wt% NaCl equ.
Giken										
Type 1										
FI31	P	L+V	0,7-0,8	-52	-6,0				202	9,2
FI32	P	L+V	0,7-0,8		-4,8				205	7,6
FI33	P	L+V	0,7-0,8		-5,0				205	7,9
FI34	P	L+V	0,7-0,8		-8,8				355	12,6
FI35	P	L+V	0,7-0,8		-8,5				357	12,3
Type 2										
FI36	P	L+V+S		-52				380	365	45,3
FI37	P	L+V+S						375	360	44,3
FI38	P	L+V+S						370	360	44,3
Type 5 (metamorphogenic fluids)										
FI39	PS/S	L1+L2+V				9	31		265	1,7
FI40	PS/S	L1+L2+V				9,5	30,5		260	0,9
FI41	PS/S	L1+L2+V				8,9			265	1,9
FI42	PS/S	L1+L2+V				9,2			262	1,4
FI43	PS/S	L1+L2+V				9	30		260	1,7
Jakobsbakken										
Type 5 (metamorphogenic fluids)										
FI43	PS/S	L+V			-0,5				340	0,9
FI44	PS/S	L+V			-0,2				350	0,4
FI45	PS/S	L+V			-0,7				358	1,2
FI46	PS/S	L+V			-0,5				360	0,9
FI47+K47/	PS/S	L+V			-0,5				355	0,9

5 Discussion

The VMS mineralization at the Sulitjelma deposits are spatially associated with metamorphosed mafic rocks of Ordovician age (Boyle, A. P. et al., 1985; Cook, N. J. et al., 1990; Pedersen et al., 1991). Both, ore bodies and their host rocks, were exposed to deformation processes and recrystallization during the cycle of metamorphism and tectonic transport caused by the Scandian Orogeny (Cook, N. J., 1993; Cook, N. J., 1996).

The mineralization at the Sulitjelma deposits is characterized by predomination of pyrite over other sulfide minerals. The major ore-bearing phases are chalcopyrite and sphalerite. Galena occurs as a major mineral only in the Jakobsbakken ore body. Pyrrhotite predominates in the Sagmo ore body. Ag-sulfides, Fe-oxides and Ti-oxides are common accessory minerals. The major gangue mineral is quartz.

The presence of Fe-sulfides (pyrite and pyrrhotite) and Fe-oxides (magnetite) suggest fluctuations in sulfur and oxygen fugacity during the ore deposition (Figure 5.1):

$FeS + ½\ S_2 \leftrightarrow FeS_2$ $\qquad K_{eq} = (fS_2)^{1/2}$

$3\ FeS + 2\ O_2 \leftrightarrow Fe_3O_4 + 3/2\ S_2$ $\qquad K_{eq} = \frac{(fS_2)^{3/2}}{(fO)^2}$

$3\ FeS_2 + 2\ O_2 \leftrightarrow Fe_3O_4 + 3\ S_2$ $\qquad K_{eq} = \frac{(fS_2)^3}{(fO)^2}$

In addition, the log fS_2 vs. log fO_2 diagrams constructed for a range of pressures and temperatures revealed that stability of coexisting pyrite, pyrrhotite and magnetite is especially sensitive for temperature changes and may indicate that variations in Fe-sulfide and Fe-oxide content within different ore bodies may be a result of post-ore metamorphic conditions. The stability field of pyrrhotite is extending toward both higher oxygen and sulfur fugacities by increase in temperature (Figure 5.1), suggesting that the Sagmo ore-body might has experienced a higher metamorphic grade compering to other ore bodies in which pyrite predominates pyrrhotite.

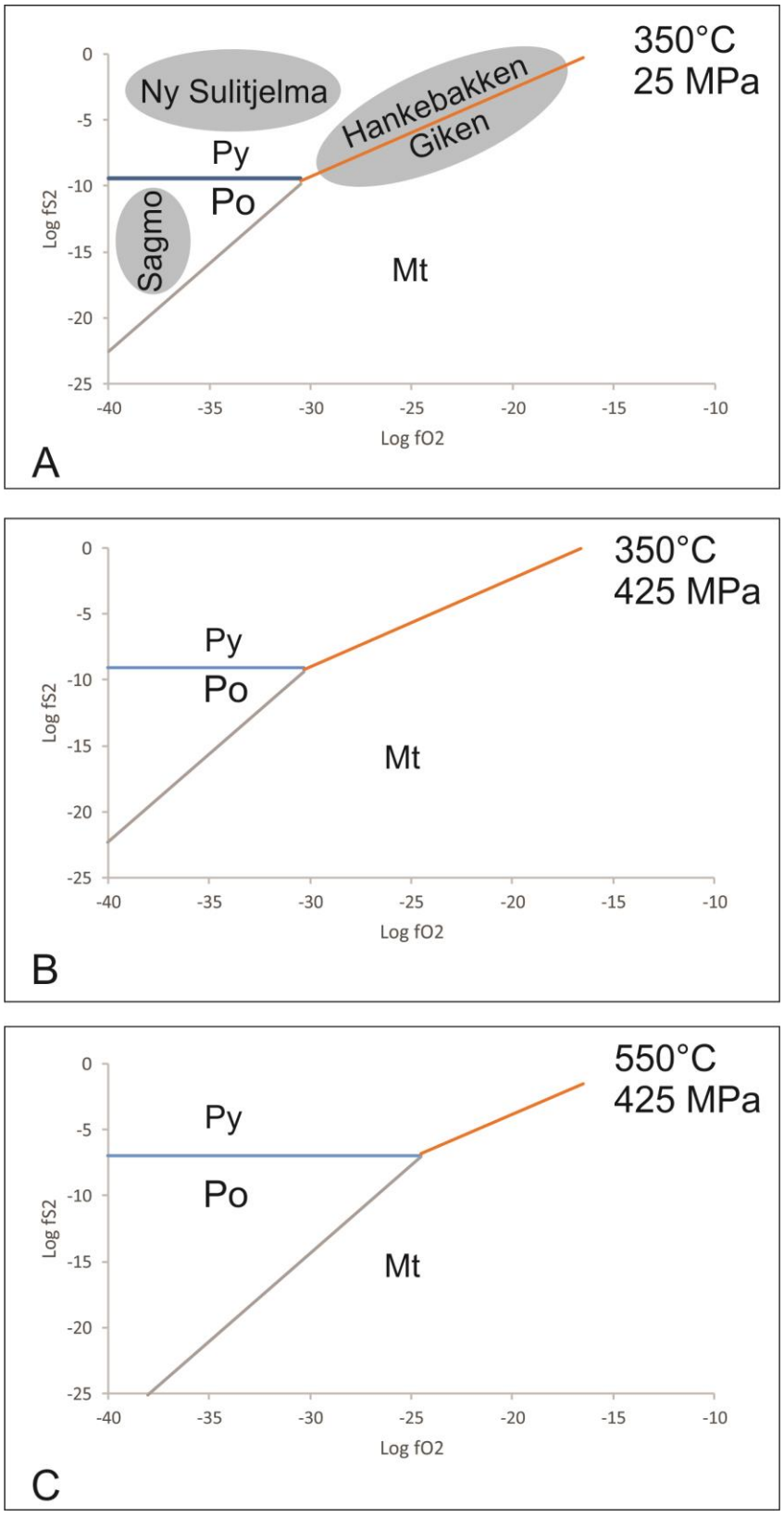

Figure 5.1: Log fO2 vs. Log fS2 diagram for the system Fe-S-O, showing a proposed environment for Fe-sulfide and oxide depositionat the Sultjelma VMS deposits. Stability of pyrite (Py), pyrrhotite (Po) and magnetite (Mt) is constructed using the SUPCRT92 software and associated database (Johnson et al., 1992).

The oxygen fugacity in the Sulitjelma is mostly controlled by abundant organic matter that originates from pelagic sediments and/or syn-depositional microbiological activity. Organic matter, occurring as pyrobitumen and within hydrocarbon-bearing fluid inclusions, is common for VMS deposits worldwide (Maslennikov et al., 2017; Rasmussen, 2000; Reysenbach & Cady, 2001).

In Sulitjelma, the pyrite textures are described as resembling the whole series of deformation and metamorphic events which has affected the deposits (Cook, N. J., 1996). Pyrite, in contrast to more ductile pyrrhotite, chalcopyrite, sphalerite and galena, occurs as a more competent mineral. This study confirm that pyrite in massive sulfide bodies, occur mostly as large rounded grains accompanied by ductile chalcopyrite, sphalerite and low amounts galena. This pyrite texture has been suggested to be formed as a result ductile deformation and rotation of pyrite grains during growth (Cook, N. J., 1996). In other, more disseminated samples, pyrite grains occur as subhedral and euhudral grains. Such grains could indicate a secondary texture formed by recrystallization during annealing during slow cooling (Craig & Vaughan, 1994) and probably reflect the retrograde metamorphic stage at the Sulitjelma deposits.

In several studied samples, Ti-rich phases such as rutile, ilmenite and titanite have been found in various amounts. Rutile appears as the dominant Ti-phase occurring as small disseminated and slightly rounded grains (Figure 4.27). Such grains have been described by (Cook, N. J., 1996) as overgrowing what is thought to be earlier and possibly pre-metamorphic ilmenite (Cook, N. J., 1996). The presence of ilmenite was disclosed through SEM analyses both by EDS and EBSD techniques. The EBDS map generated for sample SJ-02 (Figure 4.28) shows only a minor amount of ilmenite compared to dominating rutile. Titanite also occurs as a common accessory mineral. Among possible alteration processes, weathering of ilmenite to leucoxene is a known possibility (Nesse, 2012). Such a process is dependent on water and occurs due to the leaching of iron at low temperatures (<50 °C) close the surface (Mücke & Bhadra Chaudhuri, 1991).

Lithogeochemical analyses of bulk ore samples from the Sulitjelma deposits reflect a positive correlation of Ti, Sc and V with Al, indicating alumosilicate mineral phases, probably micas and/or biotite, as a major carrier of these elements.

In sample SH1-03 a substantial amount of elongated minerals showing an intergrowth of magnetite, ilmenite and rutile. The sample resembles the texture and mineralogy of a micaschist and the minerals follow the foliation direction. The grains are also usually elongated (included pyrite) which suggests ductile deformation (Figure 4.8). From the line analyses done during the SEM study of the samples, one can clearly see that diffusion from the different "mineral zones" within the grains has occurred. The occurrence of magnetite and ilmenite can be explained due to exolution of ilmenite from Ti-rich magnetite. Due to solid solution to ulvöspinel, titanium is known to often be incorporated to some degree in magnetite. In metamorphic rocks, such a feature is not uncommon and can occur due a decrease of temperature or an increase of oxygen fugacity (Nesse, 2012). With this in mind, it is likely that the exolution of ilmenite in sample SH1-03 is related to the retrograde metamorphic event in Sulitjelma. The presence of rutile is however more difficult to explain as they occur as lines or needle-like structures orientated perpendicular to the elongation of the rest of the grain and hence perpendicular to the foliation. In many cases rutile are seen replacing ilmenite (Figure 4.9) which could indicate either a continued exolution process or a two stage event where rutile as formed due to a later event. The orientation of the ruiles perpendicular to general grain and foliation direction, could suggest a crystallographic control.

A low Ag content in galena and close spatial association of galena and Ag-sulfides/sulfosalts suggest retrograde decomposition of primary Ag-rich galena into two immiscible Pb-S and Ag-S phases (Figure 4.16). Similar textural features have been confirmed in experimental studies of retrograde re-equilibration in the Pb-Ag-Sb-S system (Chutas et al., 2008).

Sphalerite contains significant amount of Fe and Cu, and traces of Mn. The CuS content of sphalerite that occurs in equilibrium with chalcopyrite was used as independent geothermometer after Hutchison & Scott (1981). The CuS-sphalerite geothermometer yielded temperature of 590ºC ± 20ºC, suggesting the equilibration of sphalerite and chalcopyrite under high temperature metamorphic conditions.

Although the Sulitjelma deposits were metamorphosed up to amphibolite grade and recrystallisation evidently took place under dynamic conditions near the peak of the metamorphic cycle, rare primary fluid inclusions hosted by syn-ore quartz have been preserved (Type 1, Type 2 and Type 3). These three types of fluid inclusions reflect pre-metamorphic ore-forming conditions, including temperature and pressure of ore deposition

(Fig. X2). Type 3 is particularly indicative, whereas it contains coexisting L-rich and V-rich inclusions that homogenize into an overlapping temperature interval from 355 to 370ºC, and reflects entrapment pressure of 20-24 MPa or 2000 – 2400 m depth, assuming a bulk salinity of 7.5 wt.% NaCl and a hydrostatic regime (Haas Jr., 1971).

However, primary fluid inclusion assemblages have been overprinted with later, metamorphogenic, fluids (Type 5). The metamorphogenic fluids show variations in their salinities, homogenization temperature and volatile content. The diagram presented in Figure x2 combines isochores constructed for various generations of fluid inclusions from the Sulitjelma ore deposits and previously published P-T-t paths for regional metamorphic conditions (dashed grey curve, Burton et al., 1989; solid grey curve, Boyle and Westhead, 1992). Secondary fluid inclusions found in Ny Sulitjelma samples (NS T5) overlap with prograde metamorphic conditions, whereas secondary inclusions from Giken (G T5) and Jakobsbakken (J T5) rather represented retrograde fluids. The metamorphic conditions at Giken have been estimated by a combination of fluid inclusion isochores and the sphalerite-CuS geothermometer. The estimated temperature and pressure range between 570 and 610ºC and between 350 and 475 MPa, respectively (Figure 5.2).

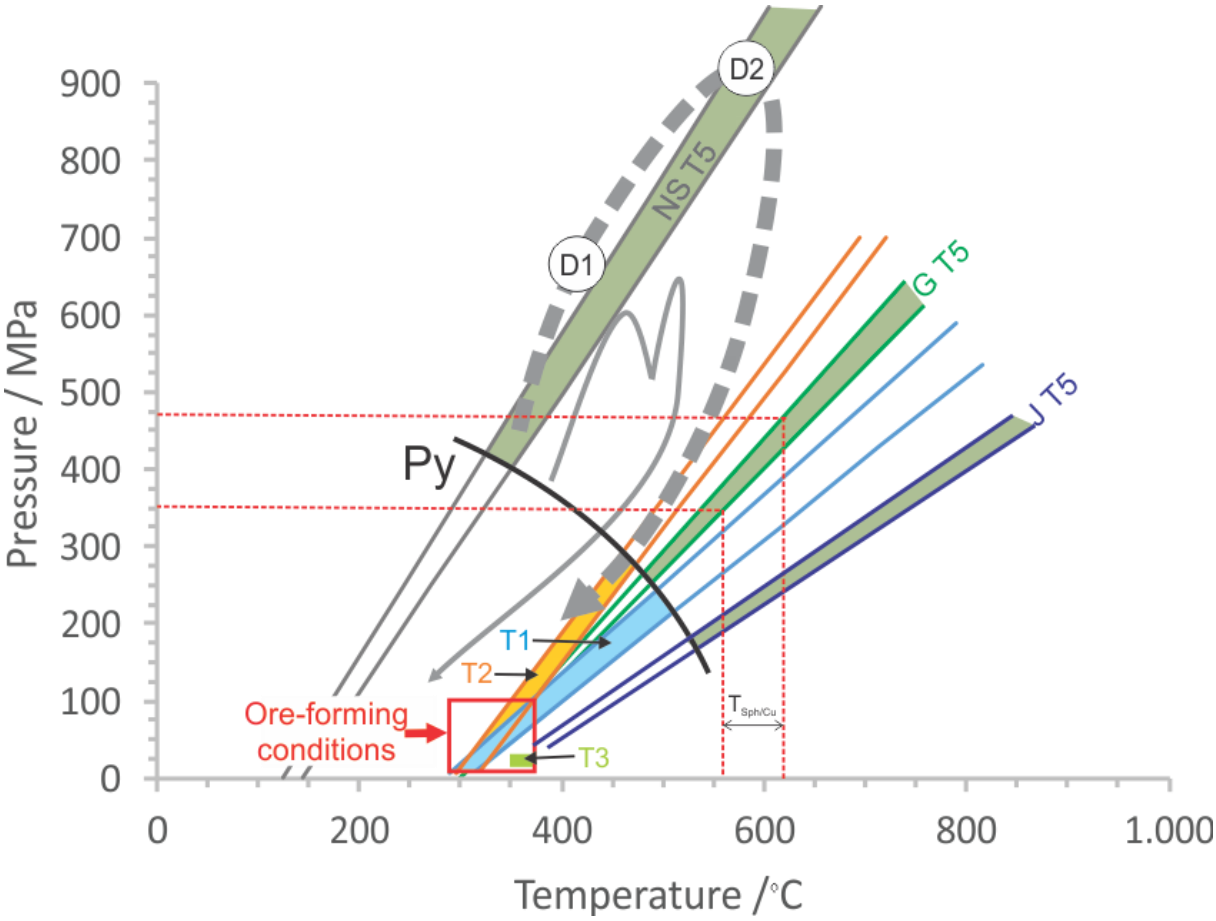

Figure 5.2: Diagram illustrating the P-T evolution of fluids at the Sulitjelma VMS deposits. P-T-t paths for the Furulund Group, eastern samples as a solid line (Burton et al., 1989) *and western samples as a dashed line* (Boyle, A. P. & Westhead, 1992)*. Black curve define pyrite brittle-ductile transition* (Kullerud & Yoder, 1959)*. Representative isochores are constructed for various generations of fluid inclusions (Type 1 (T1) to Type 5 (T5)) from Ny Sulitjelma (NS), Giken (G) and Jakobsbakken (J). The sphalerite-CuS geothermometer is combined with fluid inclusion data from the Giken ore body.*

Classification of the Sulitjelma ore deposits

Although the Sulitjelma ore deposits has been described as a VMS deposit, many classification have been applied. Several authors including (Billett, 1987; Burton et al., 1989; Cook, N. J., 1993; Cook, N. J., 1996; Cook, N. J. et al., 1990) are describing the Sulitjelma mineralization as a part of a Sulitjelma ophiolitic sequence and a classical example of Cyprus-type mineralization. In contrast, (Pedersen et al., 1991) argue that the term ophiolite as inappropriate and suggest using the Sulitjelma igneous complex instead. In contrast, Fox et al. (1988) classified the Sulitjelma deposits as a Besshi-type VMS.

The results this study, including ore mineralogy and base-metals distribution (Cu:Zn:Pb ratios; Figure 4.29), classify the Sulitjelma deposits as a VMS Cu-Zn mafic type of mineralization (Barrie & Hannington, 1999).

6 Conclusion

- Both, ore bodies and their host rocks, were exposed to deformation processes and recrystallization during the cycle of metamorphism and tectonic transport caused by the Scandian Orogeny. These processes has heavily affected ore textures as well as mineral chemistry of ore and gangue minerals.
- The mineralization at the Sulitjelma deposits is characterized by predomination of pyrite over other sulfide minerals. The major ore-bearing phases are chalcopyrite and sphalerite. Galena occurs as a major mineral only in the Jakobsbakken ore body. Pyrrhotite predominates in the Sagmo ore body. Ag-sulfides, Fe-oxides and Ti-oxides are common accessory minerals. The major gangue mineral is quartz.
- Fluid inclusion studies give an insight into P-T-X characteristics of ore-forming fluids but also revealed several generations of metamorphogenic fluids. Ore-forming conditions are estimated from primary boiling fluid inclusion assemblages indicating the formation temperature between 355 and 370ºC and formation pressure of 20-24 MPa, or 2000 – 2400 m depth assuming a bulk salinity of 7.5 wt.% NaCl and a hydrostatic regime.
- Secondary fluid inclusions found in Ny-Sulitjelma samples reflect prograde metamorphic conditions, whereas secondary inclusions from Giken rather represented retrograde fluids. The metamorphic conditions at Giken, estimated by a combination of fluid inclusion data and the sphalerite-CuS geothermometer, suggest metamorphic P-T conditions between 570 and 610ºC and between 350 and 475 MPa, respectively.

References

Barrie, C. T. & Hannington, M. D. (1999) *VOLCANIC-ASSOCIATED MASSIVE SULFIDE DEPOSITS: PROCESSES AND EXAMPLES IN MODERN AND ANCIENT SETTINGS*. SOCIETY OF ECONOMIC GEOLOGISTS, INC.

Billett, M. F. (1987) The Geology of the Northern Sulitjelma Area and Its Relationship to the Sulitjelma Ophiolite (Arctic Circle). *Norsk Geologisk Tidsskrift*, 67 (2), pp. 71–83.

Boyle, A. P., Mason, R. & Hansen, T. (1985) A New Tectonic Perspective of the Sulitjelma Region. In: Gee, D. G. & Sturt, B. A. ed., *The Caledonide Orogen- Scandinavia and Related Areas*. John Wiley & Sons Ltd, pp. 529–542.

Boyle, A. P. & Westhead, K. (1992) Metamorphic Peak Geothermobarometry in the Furulund Group, Sulitjelma. In: *Scandinavian caledonides: Implications for uplift*. pp. 615–626.

Burton, K. W., Boyle, a. P., Kirk, W. L. & Mason, R. (1989) Pressure, Temperature and Structural Evolution of the Sulitjelma Fold-Nappe, Central Scandinavian Caledonides. *Geological Society, London, Special Publications* [Online], 43 (1), pp. 391–411. Available from: <http://sp.lyellcollection.org/cgi/doi/10.1144/GSL.SP.1989.043.01.36>.

Chutas, N. I., Kress, V. C., Ghiorso, M. S. & Sack, R. O. (2008) A Solution Model for High-Temperature PbS-AgSbS2-AgBiS2 Galena. *American Mineralogist*, 93 (10), pp. 1630–1640.

Cook, N. J. (1993) Deformation and Metamorphism of Massive Sulphides at Sulitjelma, Norway. *Mineralogical Magazine*, 57 (386), pp. 67–81.

Cook, N. J. (1996) *Mineralogy of the Sulphide Deposits at Sulitjelma, Northern Norway*. 11.

Cook, N. J., Halls, C. & Kaspersen, P. O. (1990) The Geology of the Sulitjelma Ore Field, Northern Norway - Some New Interpretations. *Economic Geology*, 85 (8), pp. 1720–1737.

Corfu, F., Andersen, T. B. & Gasser, D. (2014) The Scandinavian Caledonides: Main Features, Conceptual Advances and Critical Questions. *Geological Society, London, Special Publications* [Online], 390 (1), pp. 9–43. Available from: <http://sp.lyellcollection.org/lookup/doi/10.1144/SP390.25>.

Craig, J. R. & Vaughan, D. J. (1994) Ore Mineral Textures. In: *ORE MICROSCOPY AND ORE PETROGRAPHY*. 2nd ed. John Wiley & Sons, INC., pp. 120–163.

Deer, W. A., Howie, R. A. & Zussman, J. (1992) *The Rock-Forming Minerals*. Pearson Education Limited.

Fox, J. S., Farquhar, R., Rui, I. & Cook, N. (1988) Genesis of Basalt-Hosted Massive Sulphide Deposits from the Trondheim and Sulitjelma Districts, Norway: Ore Lead Isotopic Considerations. *Mineralium Deposita*, 23 (4), pp. 276–285.

Galley, A. G., Hannington, M. D. & Jonasson, I. R. (2007) Volcanogenic Massive Sulfide Deposits. *Mineral Deposits of Canada: A Synthesis of Major Deposit-Types, District Metallogeny, the Evolution of Geological Provinces, and Exploration Methods*, (5), pp. 141–161.

Goehner, R. P. & Michael, J. R. (1996) Phase Identification in a Scanning Electron Microscope Using Backscattered Electron Kikuchi Patterns. *J. Res. Natl. Inst. Stand. Technol.*, 101 (3), pp. 301–308.

Haas Jr., J. L. (1971) The Effect of Salinity on the Maximun Thermal Gradient of a Hydrothermal

System at Hydrostatic Pressure. *Economic Geology*, 66, pp. 940–946.

Johnson, J. W., Oelkers, E. H. & Helgeson, H. C. (1992) *SUPCRT92: A Software Package for Calculating the Standard Molal Thermodynamic Properties of Minerals, Gases, Aqueous Species, and Reactions from 1 to 5000 Bar and 0 to 1000°C*. 18.

Kullerud, G. & Yoder, S. (1959) Pyrite Stability Relations in the Fe-S System.

Large, R. R. (1992) Australian Massive Sulfide Deposits : 87, pp. 471–510.

Maslennikov, V. V., Maslennikova, S. P., Large, R. R., Danyushevsky, L. V., Herrington, R. J., Ayupova, N. R., Zaykov, V. V., Lein, A. Y., Tseluyko, A. S., Melekestseva, I. Y. & Tessalina, S. G. (2017) Chimneys in Paleozoic Massive Sulfide Mounds of the Urals VMS Deposits: Mineral and Trace Element Comparison with Modern Black, Grey, White and Clear Smokers. *Ore Geology Reviews* [Online], 85, pp. 64–106. Available from: <http://dx.doi.org/10.1016/j.oregeorev.2016.09.012>.

Mcdonough, W. F. & Sun, S. S. (1995) The Composition of the Earth. (January 1995).

Mücke, A. & Bhadra Chaudhuri, J. N. (1991) The Continuous Alteration of Ilmenite through Pseudorutile to Leucoxene. *Ore Geology Reviews*, 6 (1), pp. 25–44.

Nesse, W. D. (2012) *Introduction to Mineralogy*. New York.

Nowell, M. M. & Wright, S. I. (2005) Orientation Effects on Indexing of Electron Backscatter Diffraction Patterns. *Ultramicroscopy*, 103 (1), pp. 41–58.

Ohmoto, H. (1996) Formation of Volcanogenic Massive Sulfide Deposits: The Kuroko Perspective. *Ore Geology Reviews* [Online], 10 (3)–(6), pp. 135–177. Available from: <http://linkinghub.elsevier.com/retrieve/pii/0169136895000216>.

Passchier, C. W. & Trouw, R. a J. (2005) *Microtectonics*.

Pedersen, R. B., Dunning, G. & Furnes, H. (1991) A U/Pb Age for the Sulitjelma Gabbro, North Norway: Further Evidence for the Development of a Caledonian Marginal Basin in Ashgill–Llandovery Time. *Geological Magazine*, 128 (2), pp. 141–153.

Rasmussen, B. (2000) Filamentous Microfossils in a 3, 235-Million-Year-Old Volcanogenic Massive Sulphide Deposit. *Nature*, 405 (8 June), pp. 676–679.

Reysenbach, A. L. & Cady, S. L. (2001) Microbiology of Ancient and Modern Hydrothermal Systems. *Trends in Microbiology*, 9 (2), pp. 79–86.

Robb, L. (2005) *Introduction to ORE FORMING PROCESSES*. Blakwell Science Ltd.

Twiss, R. J. & Moores, E. M. (2007) *Strcural Geology*. W. H. Freeman and Company.

Vokes, F. M. (2012) Caledonian Massive Sulphide Deposits in Scandinavia: A Comparative Review. In: *Handbook of stratabound and stratiform ore deposits*. pp. 79–128.

Appendix I

Table 1: List of studied orebodies and their locations from NGU (2015/2017)

Orebody	**X-coordinate**	**Y-coordinate**
Giken	547233 m.	7446596 m.
Hankabakken	548333 m.	7447146 m.
Jakobsbakken	543479 m.	7442349 m.
Ny-Sulitjelma	549333 m.	7447496 m.
Sagmo	543930 m.	7445099 m.

Definitions and terms

Undulose Extinction
Undulose extinction refers to an observable effect under crossed polars which can been seen as a crystal not going extinct in a homogenously matter. The reason for this is due to a lightly bent crystal lattice due to dislocations. Such an observed feature serve as an unmistakable sign of intracrystalline deformation (Passchier & Trouw, 2005).

Dynamic Recrystallization
Is a process taking place during deformation which results in the formation of new crystal grains originating from older grains (Twiss & Moores, 2007). Controlled by either temperature, flow stress or both, there are three recrystallization processes which can occur; grain boundary migration (GBM), subgrain rotation (SGR) and bulging (BLG) see figure 1-2 (Passchier & Trouw, 2005).

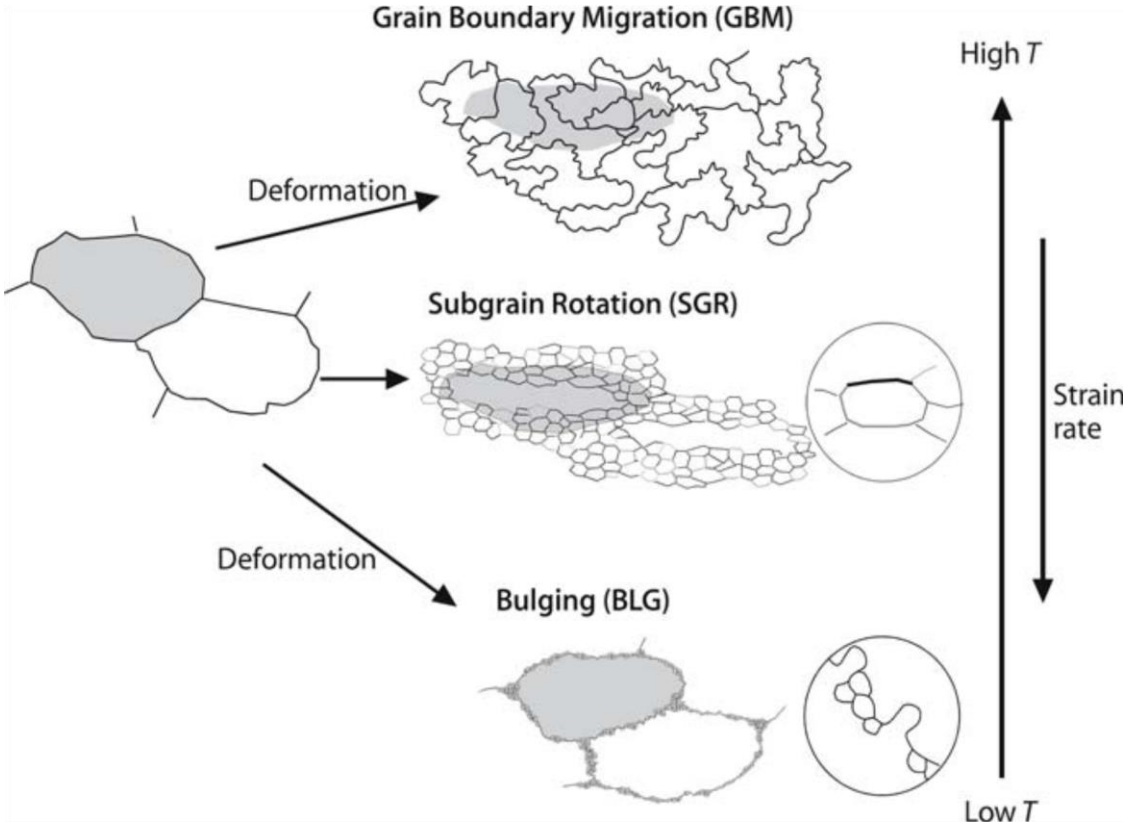

Figure 6.1: Shows the three possible types of dynamic recrystallization resented by two grains. Grey overshadow separates the two large grains as they go through a recrystallization process. From Passchier & Trouw (2005).

Appendix II

Table 6.1 EBSD parameters

Step size	5 µm
Field With	7.98 mm
Field Height	13.5 mm
Hit Rate	81.3 %
Accelerating Voltage	20.00 kV
Working Distance	26.2 mm
Specimen Tilt (degrees)	70.0 °
Number of Bands Detected	6

Table 6.2: Phase fraction

Phase Name	Phase Fraction (%)	Phase Count	Mean Band Contrast	Standard Deviation Band Contrast	Min Band Contrast	Max Band Contrast	Mean MAD	Standard Deviation MAD	Min MAD	Max MAD
Sphalerite	0,21	10536	65.26	30.66	15.00	198.00	1.22	0.45	0.08	2.00
Pyrite	0,04	1863	60.47	26.29	13.00	187.00	1.15	0.42	0.18	2.00
PyrrhoSuper	0,88	44150	116.19	43.68	17.00	211.00	0.65	0.39	0.05	2.00
Quartz-new	58,01	2895941	122.78	21.45	15.00	195.00	0.48	0.22	0.02	2.00
Biotite	1,56	77812	71.18	31.05	14.00	173.00	1.08	0.48	0.03	2.00
Muscovite	3,37	168086	69.83	28.49	13.00	175.00	1.03	0.48	0.03	2.00
Rutile	0,47	23350	119.10	45.03	16.00	201.00	0.64	0.49	0.03	2.00
Ilmenite	0,98	48980	72.77	33.94	14.00	210.00	1.17	0.47	0.07	2.00
Titanite	1,42	70926	62.76	29.11	13.00	210.00	1.33	0.39	0.05	2.00
Apatite	0,76	37948	69.96	31.46	14.00	186.00	1.00	0.50	0.02	2.00
Albite - mon	9,92	495004	80.39	21.31	14.00	233.00	0.78	0.37	0.02	2.00

Calcite	0,40	20112	72.19	31.51	15.00	190.00	1.17	0.42	0.05	2.00
Clinozoisite	2,72	135920	63.15	27.10	14.00	184.00	1.26	0.40	0.07	2.00
chalcopyrite	0,48	23960	68.17	28.52	13.00	183.00	1.18	0.43	0.08	2.00
Galena	0,07	3523	73.27	26.35	17.00	184.00	1.08	0.41	0.11	2.00
Zero Solutions	18,71	934135	57.60	31.43	0.00	255.00				